THE DERIVATION OF TROPOSPHERIC COLUMN OZONE USING THE TOR APPROACH AND MAPPING TECHNIQUE

A Dissertation
Presented to
The Academic Faculty

by

Qing Yang

In Partial Fulfillment
of the Requirements for the Degree
Doctor of Philosophy in the
School of Earth and Atmospheric Sciences

Georgia Institute of Technology
December, 2007

THE DERIVATION OF TROPOSPHERIC COLUMN OZONE USING THE TOR APPROACH AND MAPPING TECHNIQUE

Approved by:

Dr. Derek M. Cunnold, Advisor
School of Earth and Atmospheric Sciences
Georgia Institute of Technology

Dr. Ray Wang
School of Earth and Atmospheric Sciences
Georgia Institute of Technology

Dr. Michael Bergin
School of Civil and Environmental Engineering
Georgia Institute of Technology

Dr. Yuhang Wang
Earth and Atmospheric Sciences
Georgia Institute of Technology

Dr. Robert Black
School of Earth and Atmospheric Sciences
Georgia Institute of Technology

Date Approved: [Month dd, yyyy]

To my grandma and my mother!

ACKNOWLEDGEMENTS

I would like to express my sincere gratitude to my advisor, Dr. Derek M. Cunnold. His persistent guidance, encouragement, and understanding in the past years have made it possible for me to finish my Ph.D study. His scientific knowledge, strict scientific attitude, and keen insight have made my graduate study a fulfilled and invaluable experience.

My thanks also go to the rest of my thesis committee members, Dr. Michael Bergin, Dr. Robert Black, Dr. Ray Wang, and Dr. Yuhang Wang for their valuable comments and suggestions. A special thank you must also go to Dr. Ray Wang for the useful research discussions and technical assistance.

I would like to thank Dr. Yuhang Wang's group for proving model data used in this thesis. Many thanks go to Yunsoo Choi and Chun Zao for providing the REAM data and the EPA surface ozone data, respectively.

In addition, I appreciate Dr. Robert Dickinson for supporting my trip to the NCAR Ninth Annual Community Climate System Model (CCSM) Workshop at Santa Fe, New Mexico, in June 2004. It was a great experience to gain knowledge on boundary layer and climate modeling from him.

Supports from family and friends are precious to me in my graduate study. I would like to thank the big family I have from my grandma to my nephews especially my parents and my husband. I am truly grateful to my good friends for their friendship and support.

TABLE OF CONTENTS

LIST OF TABLES

Page

LIST OF FIGURES

Page

LIST OF SYMBOLS AND ABBREVIATIONS

AVDC	Aura Validation Data Center
CCD	Convective Cloud Differential
DOAS	Differential Optical Absorption Spectroscopy
DU	Dobson Unit
HALOE	Halogen Occultation Experiment
MLS	Microwave Limb Sounder
NCEP	National Center for Environmental Prediction
OMI	Ozone Monitoring Instrument
OMI/MLS	OMI-MLS tropospheric ozone columns
PV	Potential Vorticity
REAM	Regional chEmistry trAnsport Model
SBUV	Solar Backscatter Ultraviolet
SCO	Stratospheric Ozone Column
TOMS	Total Ozone Mapping Spectrometer
TCO	Total Ozone Column
TOR	Tropospheric Ozone Residual
TES	Tropospheric Emission Spectrometer
UARS	Upper Atmosphere Research Satellite
VMR	Volume Mixing Ratio
Z	Geopotential height
χ	ozone mixing ratio

SUMMARY

Tropospheric ozone columns (TCOs) derived from differences between the Dutch-Finnish Aura Ozone Monitoring Instrument (OMI) measurements of the total atmospheric ozone column and the Aura Microwave Limb Sounder (MLS) measurements of stratospheric ozone columns are discussed. Because the measurements by these two instruments are not spatially coincident, interpolation techniques, with emphasis on mapping the stratospheric columns in space and time using the relationships between lower stratospheric ozone and potential vorticity (PV) and geopotential heights (Z), are evaluated at mid-latitudes. It is shown that this PV mapping procedure produces somewhat better agreement in comparisons with ozonesonde measurements, particularly in winter, than does simple linear interpolation of the MLS stratospheric columns or the use of typical coincidence criteria at mid-latitudes. The OMI/MLS derived tropospheric columns are calculated to be 4 Dobson units (DU) smaller than the sonde measured columns at mid-latitudes. This mean difference is consistent with the MLS (version 1.5) stratospheric ozone columns being high relative to Stratospheric Aerosol and Gas Experiment (SAGE II) columns by 3 DU. Standard deviations between the derived tropospheric columns and those measured by ozonesondes are 9 DU (30%) annually but they are just 6 DU (15%) in summer. Uncertainties in the interpolated MLS stratospheric columns are likely to be the primary cause of these standard deviations. An important advantage of the PV mapping approach is that it works well when MLS data are missing (e.g., when an orbit of measurements is missing). In the comparisons against ozonesonde measurements, it provides up to twice as many comparisons compared to the other

techniques. The OMI/MLS derived tropospheric ozone columns have been compared with corresponding columns based on the Tropospheric Emission Spectrometer (TES) measurements, and Regional chEmical trAnsport Model (REAM) simulations. The variability of tropospheric ozone columns has been examined for spring and summer 2005 over North America and the surrounding oceans. Comparisons of monthly mean distributions show good agreements between OMI/MLS tropospheric ozone columns, REAM columns, and TES columns. Two six-day periods in March have been selected to study the periodic TCO enhancements in two regions, around the Baja peninsula (Mexico) and over the West Coast of California. Thirteen-day back trajectories and daily maps of carbon monoxide (CO) and ozone from GEOS-CHEM and OMI/MLS have been used to investigate the influence of cross-Pacific transport. It is concluded that in the first period of the case study, the high ozone concentrations in mid and lower troposphere over the West Coast of California have been under the influence of cross-Pacific transport. Meteorological fields indicate that the high ozone concentrations in the upper troposphere over the West Coast of California and the high TCOs over the Baja peninsula are associated with stratospheric intrusions through a deep Rossby wave breaking event. The correlations between REAM TCOs and surface ozone from Environmental Protection Agency ground network measurements indicate that the TCO enhancement over the West Coast is associated with an increase of surface ozone. The correlations of REAM TCOs with geopotential height, wind fields, and tropopause height during the case study period suggest that TCO enhancement is best characterized in springtime by decreases of geopotential height on the 500 mb surface.

CHAPTER 1

INTRODUCTION

Although ozone is a trace gas, it plays an important role in atmospheric chemistry and climate variability. In the upper troposphere and stratosphere, ozone is a green-house gas which has important implications for climate change through radiative forcing. Ozone is also a secondary pollutant in the lower troposphere. High ground ozone concentrations have been known to cause human health problems, low crop yields, forest damage, break down of certain materials, and increased oxidation of the atmosphere. The lifetime of ozone in the troposphere is in the order of one month, though it varies from only a few days in the boundary layer of the tropics to close to a year in the upper troposphere [Kley, 1997].

Tropospheric ozone has two major sources, transport from the stratosphere and formation via photochemical processes. The transport of ozone from the stratosphere down to the troposphere is associated with large-scale wave-induced forcing, synoptic scale mechanisms, and small-scale mechanisms such as extratropical cyclones (cyclogenesis) and tropopause folding (Holton, 1995; Mahlman, 1997; Zanis, 2003). Model studies from Roelofs and Lelieveld [1997] suggested that, on average, 40% of the tropospheric ozone is stratospheric in origin and 10-60% of the surface ozone comes from the stratosphere.

The formation of ozone in the troposphere via complex photochemical oxidation processes involves precursor species such as volatile organic compounds (VOC), carbon

monoxide (CO), and nitric oxides (NO_X, the sum of NO and NO_2). Ozone formation is often coupled with the transport of trace gases within the troposphere. Because of the rapid economic development in East Asia, large amounts of ozone and ozone precursors are produced or emitted in this region. Trans-Pacific transport of Asian pollution has been found to influence the ozone and aerosol air quality in the United States during spring [Heald et al., 2006; Hudman et al., 2004; Yienger et al., 2000]. Trans-Pacific transport of ozone pollution mostly takes place in the free troposphere where winds are strong and the ozone lifetime is long [Hudman et al., 2004, and reference therein]. After the pollutants have been mixed into the free troposphere, it takes about 5-10 days for the pollution to cross Pacific [Heald et al, 2003, and references therein]. Using CO as a tracer of the trans-Pacific transport, model simulations and air campaign studies suggest that trans-Pacific transport episodes often peak in spring with three to five large Asian pollution events reaching the Western United States [Liang 2004; Yienger et al., 2000]. CO originates from biomass burning and anthropogenic pollution, and has a lifetime of approximately 2 months [e.g., Heald et al., 2003]. Studies have shown that trace gases generated from biomass burning are usually transported over the Pacific at lower latitudes than anthropogenic pollutants due to the relatively lower latitudes of the biomass burning locations [Heald et al, 2003]. During the TRACE-P study, significant ozone production was found to be limited to biomass plumes originating from low latitudes [Tang et al., 2003]. Ozone production in anthropogenic plumes is generally insignificant due to the weak photochemical activities in spring; however, significant ozone production due to the peroxyacetylnitrate (PAN) deposition over northeast Pacific has been found in dry

sinking air under the condition of strong solar radiation [Heald et al., 2003; Hudman et al., 2004].

Detailed knowledge of the tropospheric ozone distribution is crucial for understanding the chemical and dynamical processes which determine the budgets of many trace gases in both the troposphere and the stratosphere [Fishman et al., 1990].

Ozone measurements using ozonesondes have been offering important information on tropospheric ozone climatology over the past several decades including at mid-latitudes [Logan, 1999] and in the tropics [Thompson et al., 2003]. Restricted by the limited and uneven spatial distribution of their measuring locations, it is, however, difficult for ozonesondes to provide detailed horizontal ozone distribution information globally for non-climatological studies. Satellite instruments, on the other hand, despite the increasing advancement in measurement and retrieval techniques, still have difficulty measuring tropospheric ozone with high accuracy and precision. The combination of satellite measurements from several instruments, however, increasingly offers a good alternative to obtain tropospheric ozone column information with better horizontal resolution. Such measurements could, for example, provide useful information on ozone production resulting from the movement of air pollution from one country to another.

Tropospheric ozone columns have already proved valuable for the study of ozone enhancements associated with dynamical and chemical processes such as biomass burning and El Nino events [e.g., Fishman et al., 1990; Ziemke et al., 1998]. An effective way to derive tropospheric ozone columns from satellite data has been the tropospheric ozone residual method which calculates the tropospheric ozone residual by subtracting the stratospheric ozone column from the total ozone column [e.g., Fishman and Larsen,

1987; Fishman and Brackett, 1997; Chandra et al., 2003]. The Total Ozone Mapping Spectrometer (TOMS) has been providing the total ozone data necessary for this calculation of the ozone residuals for more than two decades. The limitation of the technique primarily has been that the necessary stratospheric column measurements all the way down to the tropopause have not been available with sufficient regularity and/or accuracy. Most of the early work therefore focused on the tropical regions where reasonable assumptions could be made about relatively small or relatively persistent variations in the stratospheric ozone columns (e.g., a longitudinal stationary wave one) [Hudson et al., 1995; Kim et al., 1996; Hudson and Thompson, 1998]. Ozone residual methods have evolved with improvements in satellite measurement techniques especially for ozone in the lower stratosphere.

Using stratospheric ozone columns calculated from the Stratospheric Aerosol and Gas Experiment (SAGE) measurements, Fishman et al. [1990] used the residual method to study the climatological distribution and seasonal cycle of tropospheric ozone columns in the region between 50^{o}N and 50^{o}S for a nine-year period between 1979 and 1987. According to their study, biomass burning is speculated as the cause of the high tropospheric column ozone in the tropics. The major shortcoming of the residuals obtained using SAGE measurements was relatively poor spatial and temporal coverage, since, each day, SAGE measured only 15 sunrise and 15 sunset events in two narrow bands each approximately two degrees of latitude wide.

In an attempt to increase the coverage, the SAGE/TOMS TOR method was modified by replacing SAGE data with Solar Backscatter Ultraviolet (SBUV) measurements [Fishman et al., 1996; Vukovich et al., 1996]. Daily maps of

TOMS/SBUV2 (both version 6) TCO values were produced by Fishman et al. [1996] as a part of the Transport and Atmospheric Chemistry Experiment near the Equator, the Atlantic (TRACE A) campaign. The TOMS/SBUV technique successfully captured large-scale gradients and the derived tropospheric ozone columns were generally within ~15% of the observed values [Fishman et al., 1996]. Nevertheless, Ziemke and Chandra [1998] pointed out that SBUV provides little information on the vertical distribution of ozone below the ozone number density peak, and the SBUV profiles below approximately 25 km altitude are primarily based on the climatological distribution of ozone. Therefore, the TCO values derived from the TOMS/SBUV combination are likely to have persistent errors originating from the reported SBUV profiles in the lower stratosphere [Ziemke and Chandra, 1998].

More recently, Chandra et al. [2003] used the Upper Atmosphere Research Satellite (UARS) Microwave Limb Sounder (MLS) version_5 algorithm ozone retrievals to derive daily and monthly stratospheric ozone columns. The resulting tropospheric ozone columns then obtained by the residual method agree well with the output of a three-dimensional model of chemistry in the tropics south of the equator for 1996-1997, showing similar zonal and seasonal characteristics. The ozone residuals derived by Chandra et al. [2003] were limited to latitudes within $\pm 30^{o}$ because the UARS MLS stratospheric retrievals only extended to 100 mb and thus not to the tropopause at mid-latitudes.

The Convective Cloud Differential (CCD) technique is a variant of the tropospheric ozone residual technique that has also played a useful role in the characterization of tropospheric ozone columns in recent years [e.g., in the tropics,

Ziemke et al., 1998; Ziemke and Chandra, 1999; Chandra, et al., 2002]. Relying on the existence of high convective clouds near the tropopause, the technique calculates tropospheric ozone columns directly from TOMS measurements by taking the difference between the total ozone columns with TOMS reflectivities < 0.2 and a nearby minimum in above cloud top ozone columns (determined from TOMS reflectivities > 0.9) [Ziemke et al., 1998]. The CCD technique has been applied to latitudes as high as 60^{o} over the Pacific Ocean where there are frequent occurrences of deep convective clouds [Ziemke et al., 2005]. Due to the sparseness of high reflectivity and nearby low reflectivity events, the CCD technique is likely to have difficulty producing a high resolution global tropospheric ozone map on a daily or weekly basis.

The implementation of the aforementioned methods offered some insights into the distribution and variability of the tropospheric ozone. However, due to the limitations of the methods including a general assumption of zonally invariant stratospheric column ozone and/or a constant tropopause pressure level of about 100 hPa [e.g., Ziemke et al., 1998; Chandra et al., 2003], most of these studies have been limited to the tropical regions. A more generalized CCD method has been extended to extratropical region [Ziemke et al., 2005]. However, relying on the occurrences of tropopause height clouds, the CCD method is difficult to be applied to a global extent on daily or weekly basis. The distribution of tropospheric column at mid-latitude regions on small time and spatial scale is still uncertain and the question of how accurate could we estimate TCOs from satellite data is still to be answered.

In the ongoing Aura project, with the MLS profiles successfully retrieved down to 215 mb, the subtraction of MLS stratospheric ozone from Ozone Monitoring Instrument

(OMI) total ozone promises the application of the OMI/MLS TOR techniques to extratropical regions to produce daily TCOs with relatively high spatial resolution. The Aura TCO is still in need of cross validations to access its relative accuracy globally.

The objectives of this research are listed below.

- To estimate the tropospheric ozone columns with improved spatial resolutions at the mid-latitudes using OMI and MLS data.
- To assess the accuracy of the derived OMI/MLS tropospheric ozone columns by comparisons against ozonesonde measured columns.
- To examine the TCO distributions over North America using OMI/MLS derived TCOs, TES measurements, and simulations from a regional chemical transport model.
- To identify the mechanisms associated with the TCO enhancements through the study of a spring TCO enhancement event.

The rest of the thesis has been organized into three chapters. Chapter 2 addresses the derivation of OMI/MLS tropospheric ozone columns and the validation of the derived OMI/MLS TCOs using ozonesonde data. Chapter 3 examines the variability of tropospheric ozone columns using regional model simulations and Aura satellite data with the focus on a spring TCO enhancement event. Chapter 4 summarizes the major findings of this research and discusses future plans.

CHAPTER 2

MID-LATITUDE TROPOSPHERIC OZONE COLUMNS DERIVED FROM THE AURA OZONE MONITORING INSTRUMENT AND MICROWAVE LIMB SOUNDER MEASUREMENTS

The recent launch of the Aura satellite has provided improved lower stratospheric and tropospheric ozone measurements. In particular, Aura carries two instruments which are resulting in improved global coverage of tropospheric ozone columns by the residual method. A new MLS instrument is providing good global coverage with improved ozone measurements in the lower stratosphere. Aura also carries a total ozone measuring instrument, the Dutch-Finnish Aura Ozone Monitoring Instrument (OMI), which is similar to the TOMS instruments but with much higher spectral resolution. OMI provides almost global coverage in a single day by observing in the nadir direction and scanning back and forth across the orbit track. MLS is looking forward along the orbit track, thus resulting in almost spatially coincident OMI and MLS measurements with time differences of less than 10 minutes. The most straightforward way to calculate tropospheric ozone columns is to subtract these MLS stratospheric ozone columns from the corresponding nadir OMI total ozone column measurements. A daily map of tropospheric ozone columns produced in this way, however, will have very large data gaps both because of the Aura orbit ground track separation of approximately 24.7^{o} in longitude and because of cloud effects on the OMI measurements.

Daily maps of tropospheric columns may be produced with smaller data gaps by interpolating the MLS derived stratospheric columns to the cross track locations of the OMI measurements. This may be accomplished, for example, by linear interpolation of MLS stratospheric ozone columns between consecutive orbits. However, in this chapter we explore an alternate potential vorticity mapping approach to MLS interpolation at mid-latitudes. This chapter presents an assessment of the quality of the resulting OMI/MLS derived tropospheric ozone columns.

2.1 Data and Methodology

2.1.1 Data from Aura Instruments

The Aura spacecraft was launched in July 2004 for the study of atmospheric dynamics and chemistry. Its sun-synchronous orbit has a 16-day repeat cycle. OMI is the newest version of total ozone measurement instruments on the satellite platform. The Dutch-Finnish OMI is a nadir viewing, near-UV and visible spectrograph; it provides daily global maps of total column ozone with a pixel size of 13×24 km^2 at nadir and a swath width of 2600 km [Levelt et al., 2006a and 2006b].

Along with aerosols, clouds, surface UV irradiance, and several gas species measurements, total ozone was retrieved with daily global coverage. OMI total ozone columns have been retrieved by two methods: using a Differential Optical Absorption Spectroscopy (DOAS) algorithm [Veefkind et al., 2006] and using an enhancement of the TOMS Version 8 algorithm [Bhartia and Wellemeyer, 2004], respectively. Using TOMS algorithm, total ozone information is retrieved primarily from 317.5 and 331.2nm wavelength with the exception that under high ozone and high solar angle condition

331.2 and 360nm are used in the retrieval [Bhartia, 2002, ATBD II]. The OMI total ozone (OMTO3) products retrieved using the TOMS algorithm (available at http://disc.gsfc.nasa.gov/data/datapool/OMI/Level2/OMTO3/) were used in this paper. Under cloudy conditions, variations in cloud height with respect to climatology are estimated to produce a root–mean squared error (rms) of ~2% in OMI TOMS total ozone products; however, errors may reach up to 10%, typically associated with the presence of very bright low clouds [Bhartia, 2006]. In additional, OMI has a weakness of the general inability to resolve the boundary layer ozone for typical atmosphere conditions [Worden et al., 2007].

The MLS is a forward looking limb sounding instrument which measures microwave thermal emission. Its wavelength characteristics allow the instrument to measure during both day and night, as well as to provide reliable measurements even in the presence of aerosols, thin cirrus or polar stratospheric clouds [Waters et al., 2006]. The Aura MLS has been enhanced significantly from UARS MLS providing better upper tropospheric and lower stratospheric measurements. The Aura MLS consists of heterodyne radiometers in five spectral regions with wider spectral range and bandwidth [Waters et al, 2006]. The antenna reflector surfaces degrade with time; however Aura MLS antenna system is expected to perform as good as the UARS MLS antenna by offering long-term stability of the reflectivity [Waters et al., 2006]. MLS performs 240 limb scans per orbit, which provides coverage from 82^{o}S to 82^{o}N in latitude over a time span of 98.8 minutes (Figure 2.1). The ozone measurements for the standard product (which are based on the 240 GHz data) are performed along the sub-orbital track with a

single profile spatial resolution of 6 km cross-track and approximately 200 km along track.

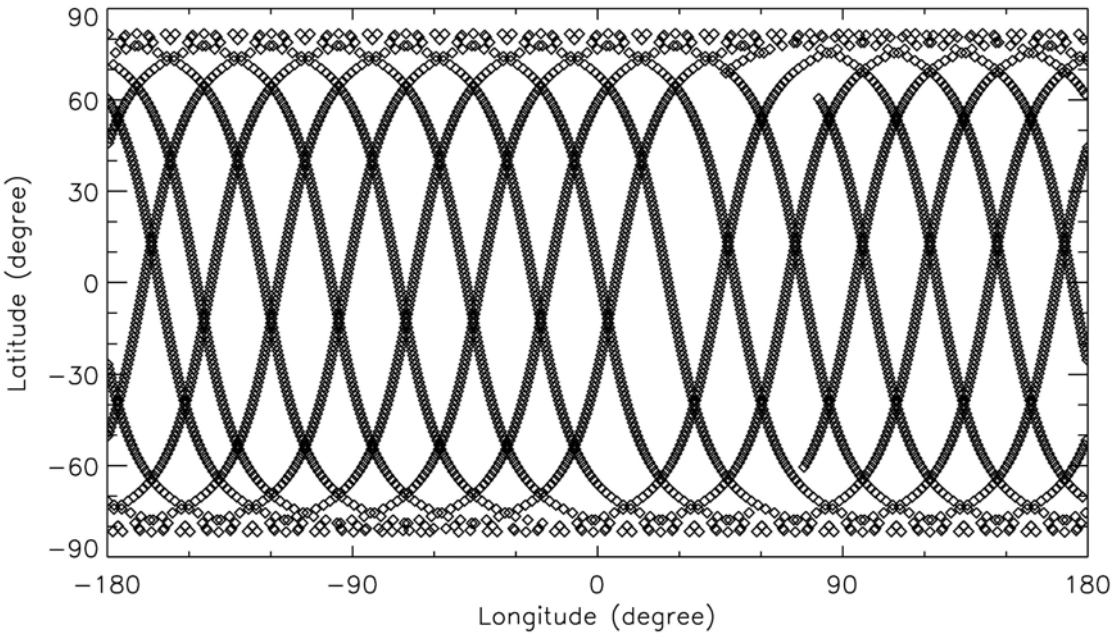

Figure 2.1: The Aura MLS data coverage in a day. The plot is based on the data on a random chosen day, Feb 1, 2005. Each diamond represents the measurement location of one MLS profile.

Temperature, geopotential height, and a number of stratospheric species including ozone data are retrieved in the processing of MLS level 2 data. The retrieval algorithms employ the approach of the standard optimal estimation which involves the nonlinear weighted least squares optimization with the use of *a priori* constraint [Livesey et al., 2006]. Based on the MLS ozone vertical averaging kernels (full width at half maximum), the MLS version 1.5 ozone profiles have a vertical resolution ~3 km in the lower stratosphere [Livesey et al., 2005]. MLS level 2, version 1.5, retrievals, which are reported on pressure levels which differ by $10^{1/6}$ in pressure, have been used for this

study. The MLS ozone profiles possess their best accuracy from 146 mb to 0.46 mb, but there is evidence that the 146 mb measurements are biased high by approximately 10% [Froidevaux et al., 2006]. The expected result of updating to the newer MLS version 2.2 dataset is discussed in section 8, based on a limited number of provisional v2.2 MLS profiles.

2.1.2 SAGE Data

SAGE measurements were used in this study for the evaluation of relative data quality of MLS measurements and for the estimation of stratospheric ozone amounts below 215mb. The Stratospheric Aerosol and Gas Experiment II is a solar occultation space borne instrument which measures the attenuation of solar radiation after the radiation travels through the earth's atmosphere during sunrise or sunset events. The instrument operates in seven spectral channels with center wavelengths ranging from 0.385 to 1.02 micrometers (http://www-sage2.larc.nasa.gov/introduction/). The ozone information is retrieved from the channel centered at 0.6 um wavelength which is located at the center of the Chappuis band, the strong ozone absorption band in the visible wavelength range. The instrument recalibrates during each measurement event by measuring the unattenuated solar radiation at the top of the atmosphere. The orbital plane of SAGE inclines at 57^{o}. Associated with this orbital characteristic, SAGE measurements cover a seasonally dependent latitude range of approximately 70^{o}S to 70^{o}N during each about one month period [Cunnold et al., 1989]. The daily spatial coverage of SAGE II is limited to about a 2 degree latitude band since the instrument measures only 15 sunrise and 15 sunset events in a day.

The retrievals of SAGE profiles consist of two steps. At the first step, the radiometric measurements in the form of binary counts from different channels are converted into slant path transmittance [Cunnold and McCormick, 2002]. In the second step, the slant path transmittance is inverted into vertical profiles of ozone, aerosol, and other gases. The detailed inversion algorithm was explained by Chu et al. [1989]. In this second step, the species separation algorithm is utilized to separate the overlapped contribution from different species. A Twomey modification of Chahine method is employed to retrieve the molecular number density profiles for each species [Chu et al., 1989]. The retrieved profiles are reported on 70 height levels from the ground up with 1 km seperation between consecutive levels.

SAGE II data was compared with Halogen Occultation Experiment (HALOE), ozonesonde, SBUV, and MLS measurements, and it was indicated that SAGE data have an accuracy of 5% (or better) from 25 km to 50 km altitude [e.g., Cunnold et al., 1989, 2000; Wang et al., 1996, 2002]. SAGE II version 6.1 ozone data were found to have approximately 10% accuracy down to the tropopause and approximately 5% overestimation between 15 and 20 km altitude compared with ozonesonde measurements [Wang et al., 2002]. The SAGE II version 6.2 data were used for this study, and the new version is close to version 6.1 with a slight improvement from the correction of an altitude registration problem which has essentially no effect on the ozone retrievals. Due to the difficulty in separating ozone absorption and aerosol scattering effects in SAGE II retrievals, the eruption of Mount Pinatubo impacted SAGE data over a 2 – 3 year extend through high stratospheric aerosol concentrations and an evolving aerosol size

distribution [Cunnold, et al. 2000; Wang et al., 2002]. Data filters were suggested by Wang et al. [2002] to remove the biased data under the high aerosol conditions.

SAGE II provides data from October 1984 to August 2005 with only a few months of missing data from August to October in 2000. The availability of long-term stable measurements and the inherently self-calibrating accurate measurements of stratospheric ozone make SAGE data invaluable for different types of ozone studies.

2.1.3 Ozonesonde Data

The ozonesonde data were used as ground truth to compare against the satellite measurements. The ozonesonde data were obtained from World Ozone and Ultraviolet Radiation Data Center (WOUDC) and Aura Validation Data Center (AVDC). The data for Hohenpeissenberg, Payerne, Uccle, and Churchill stations were obtained from WOUDC, and the ozonesonde data for Boulder, Huntsville, University of Rhode Island, and Trinidad Head station were from AVDC. A summary of the ozonesonde information is presented in Table 2.1.

Table 2.1: Ozonesonde Station Information

Name	ID	Latitude (^{o})	Longitude (^{o})	altitude (m)
Boulder	67	40.00	-105.25	1743
Huntsville	418	35.28	-86.59	196
Narragansett*		41.49	-71.42	21
Trinidad Head	445	40.80	-124.16	20
Hohenpeissenberg	99	47.80	11.02	975
Payerne	156	46.49	6.57	491
Uccle	53	50.80	4.35	100
Churchill	77	58.74	-94.07	30

*University of Rhode Island

2.1.4 Meteorology Data

The meteorological data were from National Center for Environmental Prediction/ National Center for Atmospheric Research (NCEP/NCAR) reanalysis 1 dataset. NCEP/NCAR data are available on 17 pressure surfaces from 1000mb to 10mb for every 6 hours. The spatial resolution is 2.5 × 2.5 degree longitude by latitude. The tropopause pressure and temperature were obtained directly from NCEP tropopause level dataset.

The meteorological data were interpolated onto 19 isentropic surfaces with potential temperatures (θ) being 300, 310, 320, 330, 340, 360, 380, 400, 420, 440, 460, 480, 500, 550, 600, 650, 700, 750, and 800 K, respectively. The vertical interpolation scheme followed Edouard et al. [1997]; the two pressure levels bracketing an isentropic surface were found by scanning a vertical profile from top down. Based on the logarithm of θ being approximately proportional to the logarithm of pressure (p), a parameter (such as wind, temperature, etc.) was interpolated to the isentropic levels by assuming a linear relationship between $\ln(\theta)$ and the parameter. Potential vorticity (PV) was computed in the form of Ertel's potential vorticity. The estimation of PV is very sensitive to the thickness ($\partial\theta/\partial p$) values; therefore as suggested by Edouard et al. [1997], the thickness ($\partial\theta/\partial p$) was calculated at each pressure level first, and then interpolated onto isentropic surfaces. For the best estimation, the isentropic potential vorticity (PV) was calculated directly on isentropic surfaces.

2.2 Methodology Used to Derive Tropospheric Ozone Columns

2.2.1 Coincident Profiles

Tropospheric ozone columns were first derived from coincident OMI and MLS measurements using the residual method. Except where otherwise stated, coincidence in this paper is defined as ±12 hours, and ±1^{o} of latitude and ±8^{o} of longitude for MLS, and ±1.25^{o} × 1.25^{o} longitude and latitude for OMI measurements. Thus, for example, for comparisons of coincident tropospheric columns against ozonesonde measurements both the OMI and the MLS measurements would have to satisfy their respective coincidence criteria with the ozonesonde measurements.

Since the OMI only makes measurements during daytime and the MLS measures both day and night, it might be expected that tropospheric ozone columns with the best accuracy would be produced by combining the OMI data and only the nearby MLS profiles with measurement time differences of less than 10 minutes. Although the tropospheric ozone columns produced with this more strict time coincidence criterion produce a reduction of approximately one Dobson unit (DU) in the mean differences versus ozonesonde data, these tropospheric ozone columns are not statistically different from the tropospheric ozone columns produced when nighttime MLS measurements are also included. Therefore the tighter temporal restriction has not been applied in our reported comparisons.

A code provided by the MLS team was used for the computation of ozone columns from the MLS profile measurements. The routine incorporates the MLS retrieval assumption that the ozone mixing ratio varies linearly in log (pressure) between the reported levels. The column ozone amount (Y) between two adjacent MLS pressure levels is:

$$Y = const \times \left[-\chi_2 P_2 (1 - \ln(\frac{P_1}{P_2})) - \chi_1 P_1 (1 + \ln(\frac{P_1}{P_2})) + \frac{(\chi_1 P_2 + \chi_2 P_1)}{\ln(P_1 / P_2)} \right] \quad (1)$$

where χ_1, P_1 and χ_2, P_2 are the ozone mixing ratios (χ) and the pressures (P) at the lower and upper levels, respectively. For ozone mixing ratios in ppmv and pressures in mb, const = 0.789352 results in Y in Dobson units. This algorithm is recommended for calculations of MLS ozone columns because it is consistent with the assumptions made in the MLS retrieval algorithm.

Two other stratospheric ozone column computation approaches are:

$$Y = \int \chi P d(\ln P) = const \times \frac{(\chi_1 P_1 + \chi_2 P_2)}{2} \ln(\frac{P_1}{P_2}) \quad (2)$$

$$Y = \int \chi dP = const \times \frac{(\chi_1 + \chi_2)}{2} (P_1 - P_2) \quad (3)$$

where the integration symbol here indicates integration over an MLS layer. These two equations are based on the assumptions that χP (equation 2) and χ (equation 3) vary linearly between MLS layers with $\ln P$ and with P, respectively. Compared to equation 1, applying equations 2 and 3 to the vertically gridded MLS profiles yield mean differences of ±1% in the stratospheric ozone columns: the use of equation 2 underestimates individual columns by 1.0±0.1%, and the use of equation 3 overestimates columns by an equal amount. The sensitivity of the MLS stratospheric ozone column amounts to the different integration approaches is due to the large vertical spacing (a factor of $10^{1/6}$ in pressure or ~2.7 km) between two adjacent MLS vertical levels.

MLS profile data have been used down to 215 mb in altitude unless the tropopause is located above this; in that case the tropopause pressure is used as the lowest level for the stratospheric column. When the tropopause is below 215 mb, ozone

measurements by the SAGE II have been used to fill in the region between 215 mb and the tropopause (more details are provided in the mapping section). To avoid the influence of corrections for clouds on OMI total column retrievals, we used only total ozone columns from OMI obtained under clear sky conditions because OMI contains climatologically-based adjustments for the ozone that lies below the clouds. The clear sky condition was defined here by a reflectivity of less than 10% based on the OMI 360 nm reflectivity provided in the level 2 dataset, but results were compared against other reflectivity conditions. The possibility of a scan angle effect in the OMI measurements on the tropospheric ozone column derivation were investigated by grouping the derived tropospheric ozone columns into three groups according to the OMI scan angles. No noticeable scan angle effects were detected.

2.2.2 Non-coincident Profiles

Instead of requiring a coincident MLS profile within $\pm 8^{o}$ of longitude, tropospheric ozone columns also have been derived from the combination of OMI total ozone columns and potential vorticity (PV) mapped MLS stratospheric ozone columns. Potential vorticity mapping is capable of constructing a high resolution stratospheric ozone field, and it has the potential to simulate the small scale spatial structure in the stratospheric ozone columns up to about 250 km resolution (which is roughly the horizontal resolution of most of the meteorological assimilation models).

Potential vorticity is a conserved quantity on isentropic surfaces during adiabatic transport. Using empirical relationships between PV and ozone to predict ozone on isentropic surfaces is one approach that has been used to study lower stratospheric dynamics [e.g., Morgenstern and Marenco, 2000; Jing et al., 2004]. In our study, a two-

predictor (PV and geopotential height (Z)) mapping was applied to the MLS ozone measurements on isentropic surfaces. As shown in Figure 2.2, PV is highly correlated with ozone mixing ratio with the correlations changing from positive to negative at the height of the 550K potential temperature surface at mid-latitudes. Geopotential height (Z) shows lower correlations with ozone mixing ratio than with ozone number density, but on the lowest isentropic surfaces geopotential height is fairly well anti-correlated with ozone mixing ratio. The correlation coefficients of PV with ozone mixing ratio change with latitude, and they are fairly large for latitudes higher than 20^o.

MLS ozone has been mapped on the 19 isentropic surfaces which are approximately 1-2 km apart vertically. To be consistent with the assumption of the MLS retrievals, ozone mixing ratio (χ) was linearly interpolated on a logarithmic pressure scale. An isentropic ozone mapping relationship, expressed as in equation 4 below, was determined using linear regression of the interpolated natural logarithm of the MLS ozone mixing ratio ($\ln \chi$) and the corresponding PV and geopotential height (Z) data on each of the isentropic surfaces :

$$\ln(\chi) = \alpha + \beta_1 \cdot PV + \beta_2 \cdot Z \tag{4}$$

Separate α, β_1, and β_2 coefficients were determined from linear regressions for each 10^o latitude band and using all the MLS measurements within $\pm 60^o$ longitude and ±1.5 days of the desired location and time. Obtaining separate coefficients for different regions and different time periods was found to produce better mapping results particularly in winter. The meteorological data used in the mapping were either calculated or directly obtained from NCEP/NCAR reanalysis 1 data. Having determined the coefficients, the ozone mixing ratio for any location on each isentropic surface and any time was then

determined using equation 4. The mapped ozone fields have a spatial resolution of $2.5^{o} \times 2.5^{o}$ (longitude by latitude) and a six-hour temporal resolution (i.e., the same as the NCEP/NCAR reanalysis data).

Stratospheric ozone columns were obtained by adding up the column amounts in three regions: between the tropopause and 215 mb, between 215 mb (or the tropopause pressure if it is less than 215 mb) and 700 K potential temperature (~ 18 mb), and above 700 K. The 700 K isentropic surface were chosen to be the upper boundary of the middle region because the NCEP meteorological data are sometimes missing at higher potential temperatures and because of the reduced validity of the mapping procedure in the upper stratosphere. The 215 mb lowest boundary for the middle region was chosen because it is the lowest level that has typically been used to calculate MLS stratospheric columns [e.g., Ziemke et al., 2006]. Note that because potential temperature and pressure coordinates are being mixed here, the stratospheric column integrations involve conversions between two sets of levels and vertical interpolation.

The stratospheric ozone column amounts in the uppermost layer were calculated from MLS profiles satisfying the coincidence criteria given in section 2.2.1. For the cases when the tropopause is below 215 mb the column amounts in the lowest layer (tropopause to 215 mb) were estimated by applying mapping to the Stratospheric Aerosol and Gas Experiment II (SAGE II) data. The necessary SAGE II ozone mapping relationships (in the form of equation 4) were derived for each of the 12 months of the year based on the SAGE II data from 1995-2005 (since the annual trend of stratospheric ozone has been small over that period); thus, for example, the January mapping relationships were derived using 11 years of January data.

In the mapping approach, before subtracting the stratospheric ozone columns, the clear sky Level 2 OMI total ozone columns on the same day were averaged over an area of $2.5^{o} \times 2.5^{o}$ latitude by longitude in order to match the spatial resolution of the NCEP data.

A more straightforward approach to obtaining stratospheric ozone columns as close as possible to the locations of the low reflectivity OMI total column measurements is to employ linear interpolation in longitude and latitude and to use only daytime MLS measurements. Tropospheric ozone columns obtained in this way were compared against those obtained by the coincidence and mapping procedures.

2.3 MLS Data Precision and Accuracy

Because tropospheric ozone residuals represent small differences between two large numbers it is important to study the MLS ozone profile precisions and the accuracy of the MLS data. The MLS profile precisions based on the reported single-profile precisions, are presented in Figure 2.3 by season in the mid-latitudes and tropics. In the upper stratosphere, the precisions are 2-3%. The precisions deteriorate with decreasing height in the lower stratosphere reaching 10-15% at 200 mb at mid-latitudes. The precisions expressed in percentage are smallest in winter and spring mostly because of higher mixing ratios in the lower stratosphere in those seasons.

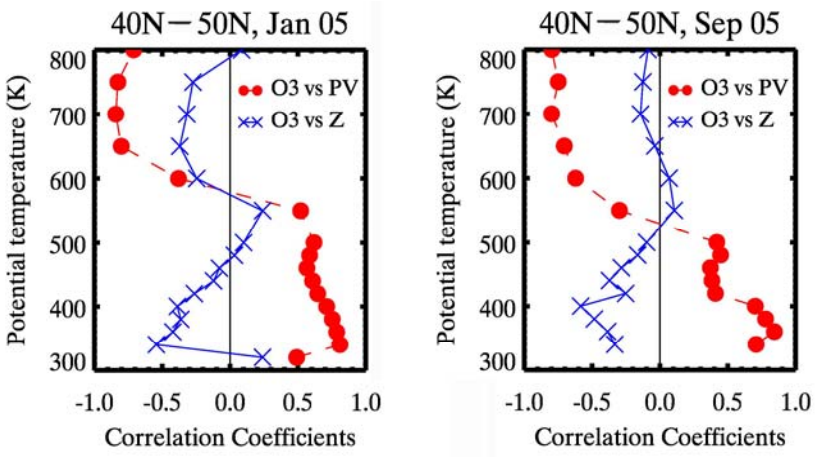

Figure 2.2: Correlations between potential vorticity (PV)/geopotential heights (Z) and MLS ozone mixing ratios at mid-latitudes of the Northern Hemisphere on isentropic surfaces. The correlations shown are for 40-50^{o}N for the months of January (left panel) and September (right panel) 2005.

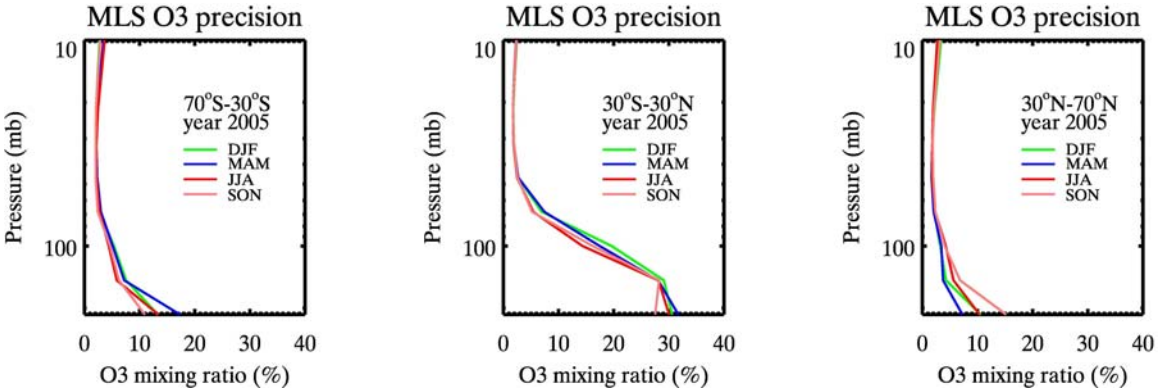

Figure 2.3: The MLS ozone measurement precisions between 215mb and 10mb in 2005 estimated by season at 30^{o}N-30^{o}S and at mid-latitudes in the two hemispheres. Questionable profiles (MLS status flag $\neq$ 0 or precision $\leq$ 0) are not included. The precisions are based on the single profile precision reported by the MLS ozone (version 1.5) level 2 software.

We compared the MLS data against coincident SAGE II (version 6.2), SAGE III (version 3.0), and UARS HALOE, version 19) satellite data, as well as against the Southern Hemisphere Additional Ozonesonde (SHADOZ), the Climate Monitoring and Diagnostics Laboratory (CMDL), and the WOUDC ozonesonde data at a total of 22 ozonesonde sites. The coincident measurements all possess a vertical resolution superior to that of the MLS measurements. The coincident measurements were therefore first interpolated to vertical levels differing by a factor of $10^{1/18}$ in pressure such that every third level coincides with an MLS retrieval level. The three mixing ratios closest to an MLS level were then averaged with log (pressure) weighting to provide the coincident profile values on the MLS vertical grid. This procedure was designed to be consistent with the MLS retrieval algorithm assumption that the ozone mixing ratio varies as log (pressure) between the MLS levels. The same vertical summation procedures were used for all the data sets.

Figure 2.4 shows the mean ozone differences in percentage between MLS and coincident data for mid-latitudes and the tropics from August 2004 to July 2005. There is some indication that MLS is biased low between 1 and 3 mb. However, these levels contribute little to the stratospheric ozone columns. From 3 mb to approximately 100 mb, the agreement between all the instruments is better than approximately 5%. Significant disagreement occurs below 100mb; however, the sondes suggest the MLS measurements are good to 10% at 146 mb, and SAGE II measurements suggest differences larger than that only in the tropics where SAGE II values are known to be low in the troposphere [Wang et al., 2002]. Based on ozonesonde comparisons, Wang et al. [2006] have shown that HALOE version 19 measurements are biased low below about two MLS layers

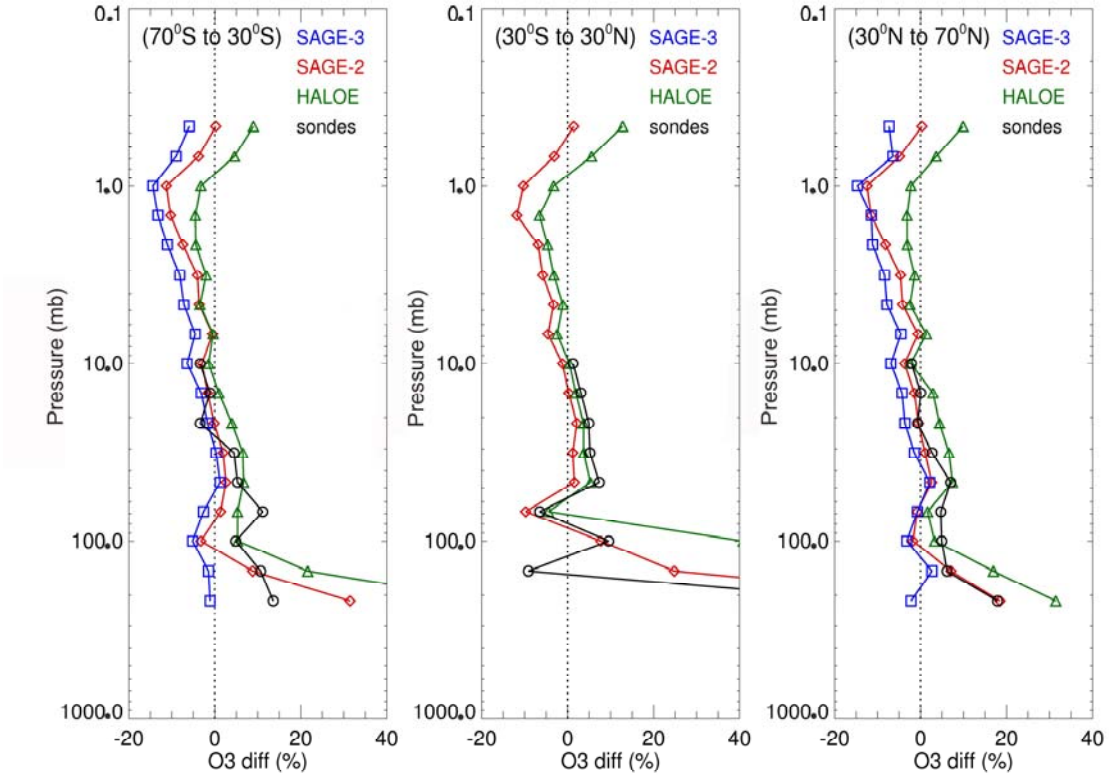

Figure 2.4: Mean ozone differences between MLS measurements and ozonesondes and SAGE II, SAGE III, and HALOE satellite measurements (MLS-coincident, expressed in % of the MLS values) in three latitude bands. The coincidence criteria are $\pm 1^{o}$ in latitude, $\pm 8^{o}$ in longitude, and ±12 hours. The data cover the period from August 2004 to July 2005. Ozonesonde data include measurements from 22 ozonesonde stations. This figure is referenced to Wang et al. [2006] and Yang et al. [2007].

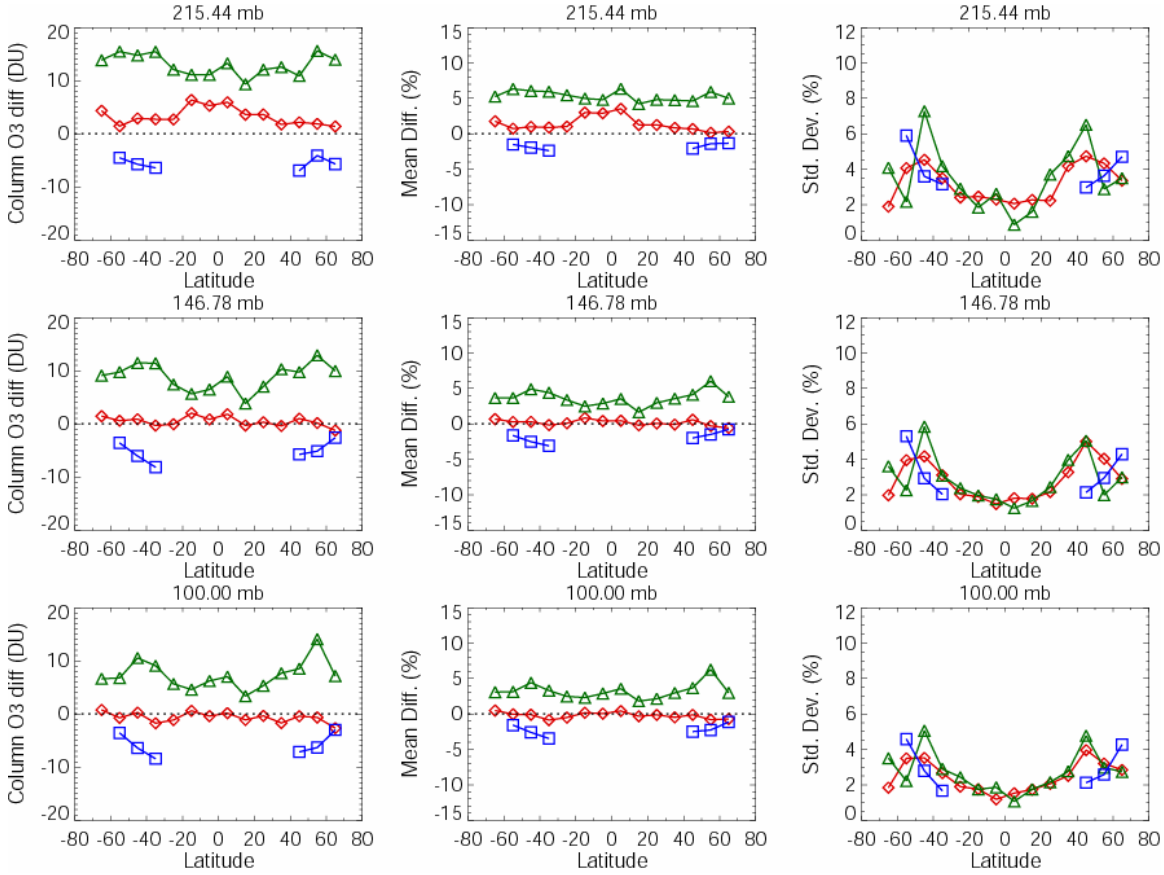

Figure 2.5: Mean differences (in Dobson units and %) and standard deviations of the differences (in %) of stratospheric ozone columns, in 10^{o} latitude bands, calculated from MLS and coincident SAGE II (red), SAGE III (blue), and HALOE (green) measurements from August 2004 to July 2005. The lower boundaries of the columns are the bottoms of the MLS layers centered at 215.4, 146.8, and 100 mb respectively. As in Figure 3 the sign of the differences is MLS – other satellite measurements. This figure is referenced to Wang et al. [2006] and Yang et al. [2007].

above the tropopause, whereas SAGE II measurements are good to about 10% down to the tropopause. SAGE III measurements are less extensive in latitude than SAGE II and HALOE measurements, and Wang et al. [2006] have shown them to be biased high relative to SAGE II by 2-10%, depending on altitude. The most reliable ozone comparisons below 100 mb for the selected latitude ranges should be against ozonesondes and against SAGE II at mid-latitudes. On this basis, it seems that MLS measurements at 215 mb are biased high by approximately 10-15% at mid-latitudes.

The MLS stratospheric ozone columns obtained by upward summation from the bottom of the 215, 146, and 100 mb layers, respectively, are next compared against those from coincident SAGE II, SAGE III, and HALOE measurements. The means and standard deviations of the stratospheric ozone column differences are presented in Figure 2.5. The MLS column means are seen to be very consistent with the SAGE II measurements, and even the known tropospheric bias of the SAGE II measurements only significantly impacts the tropical columns when the 215 mb layer is included. Excluding this layer the agreement is approximately 1 DU (about 0.4%). At mid-latitudes when the 215 mb layer is included the MLS columns are approximately 1% (2-3 DU) higher than the SAGE II columns. This difference reflects the bias of the MLS measurements at 215 mb. Although the MLS mean differences with respect to SAGE III and HALOE measurements are significantly more variable, the standard deviations of the differences in the columns with respect to all three sets of measurements are $\leq$ 7% at mid-latitudes (and less than 5% with respect to SAGE II).

The excellent agreement between the SAGE II and the MLS stratospheric columns suggests, among other things, that a consistent long-term record of the

stratospheric ozone columns might be produced by extending the OMI/MLS derived tropospheric column time series backward in time using the combination of SAGE II stratospheric columns obtained since 1984 and TOMS total columns.

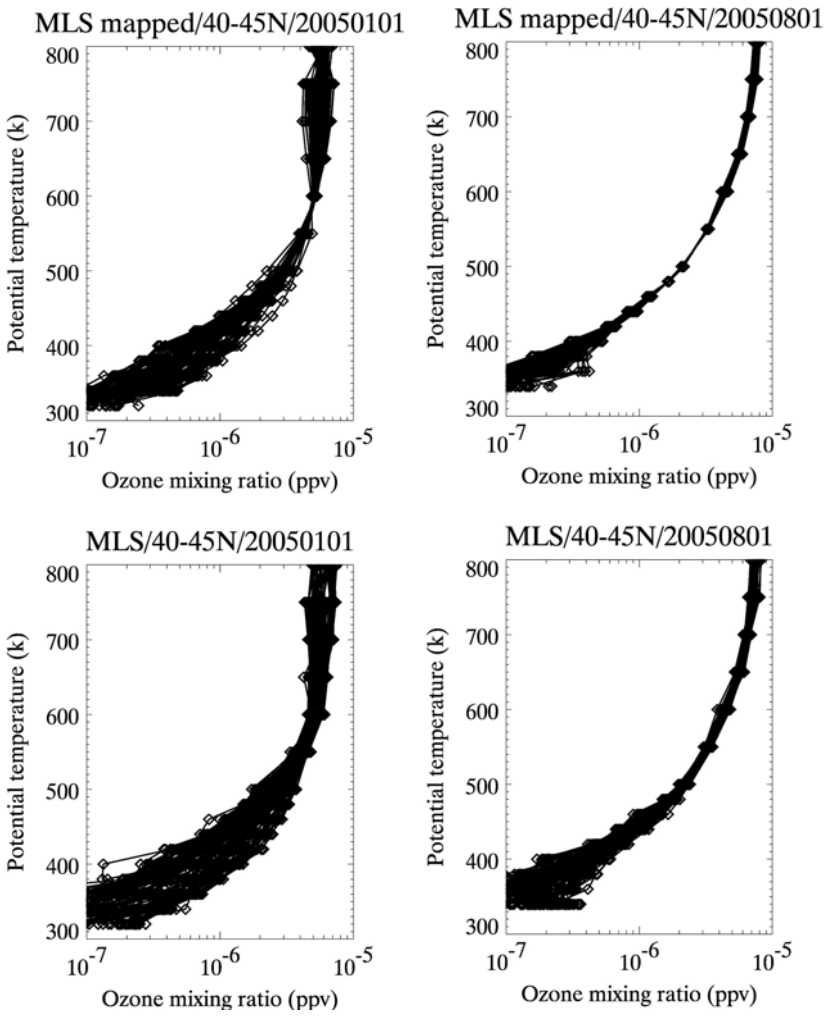

Figure 2.6: Mapped and observed MLS profiles for 40°-45°N on a randomly selected day in winter (January 01, 2005) and a randomly selected day in summer (August 1, 2005). A mapped profile was calculated at the location and time of each measurement profile.

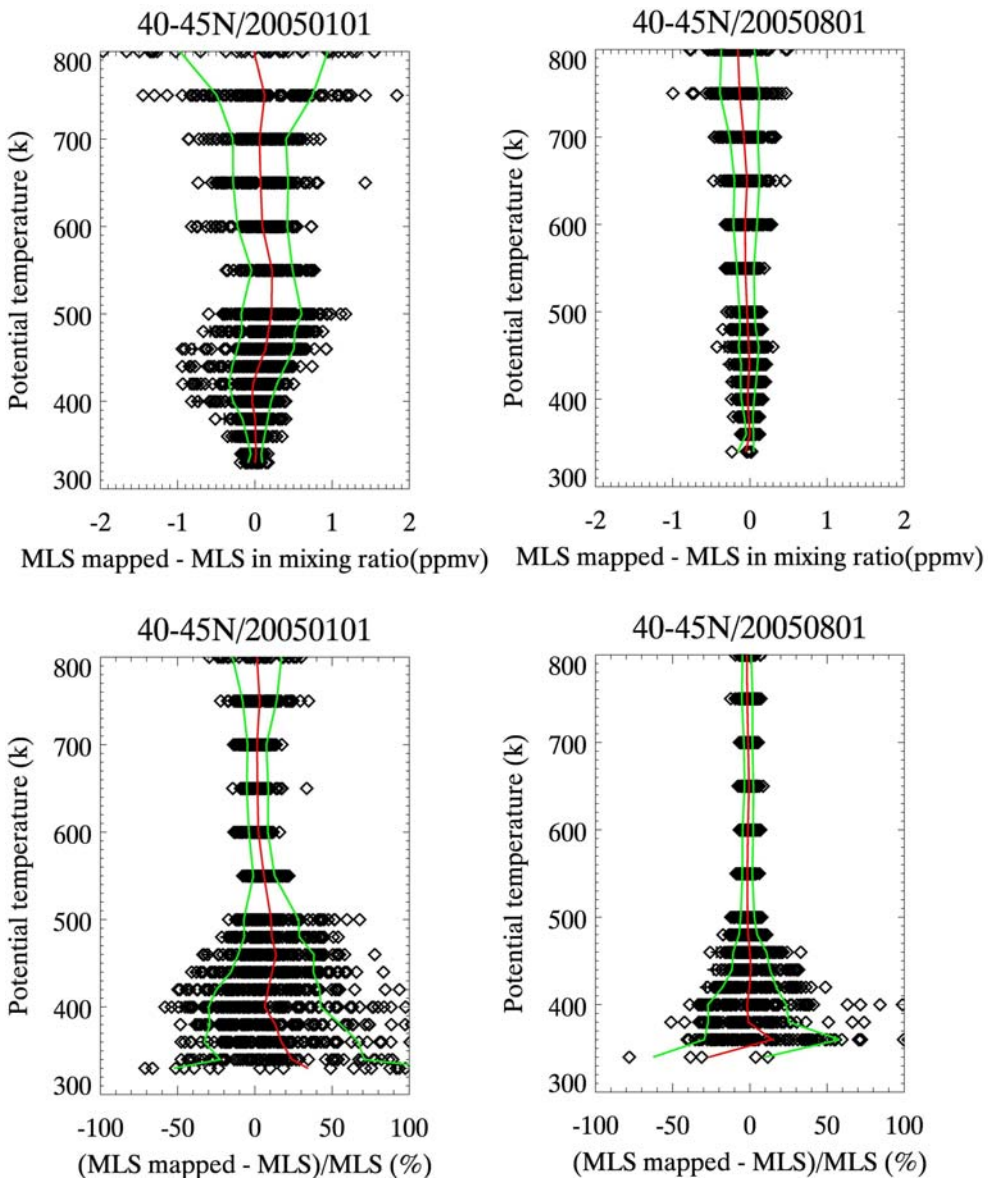

Figure 2.7: Vertical profile differences between mapped and observed MLS profiles as those in Figure 2.6. The red lines represent mean differences and the green lines represent one standard deviation (±σ) away from the mean differences in either direction.

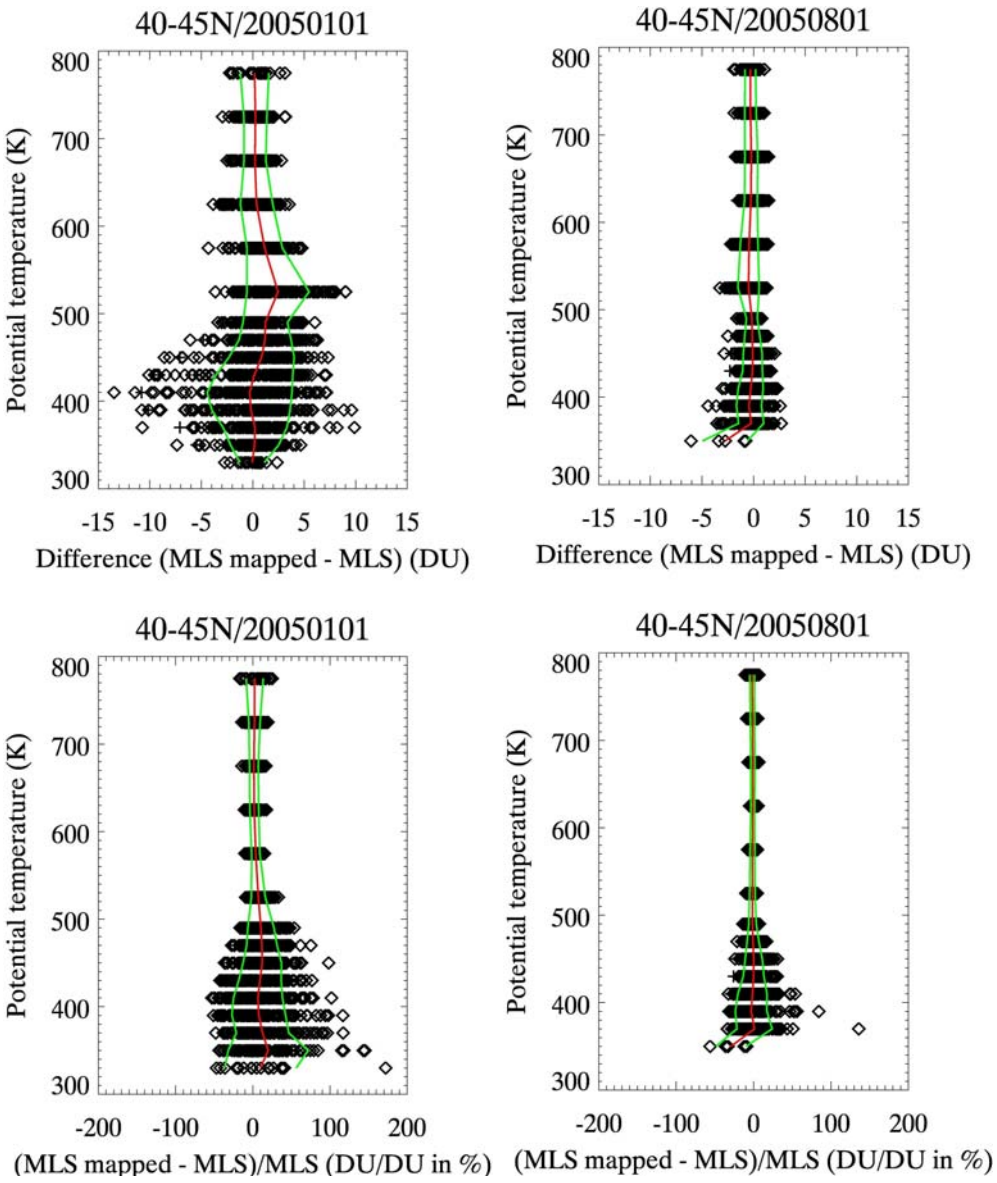

Figure 2.8: Layer ozone differences between mapped and observed MLS profiles as those in Figure 2.6. The red lines represent mean differences and the green lines represent one standard deviation (±σ) away from the mean differences in either direction.

2.4 Mapped Ozone Precision and Accuracy

For the purpose of evaluating the mapping procedures, the observed MLS ozone profiles were compared against the mapped profiles which correspond to the same times and locations. Figures 2.6, 2.7, and 2.8 show those comparisons for 40^{o}-45^{o}N on a randomly selected summer day and a randomly selected winter day. Figure 2.6 shows the mapped and observed profiles. Figure 2.7 shows the means and standard deviations of the differences in mixing ratios on isentropic surfaces, while Figure 2.8 shows the means and standard deviations of the column ozone differences in each layer blanketed by two isentropic surfaces. Figure 2.6 indicates that mapping slightly reduces the variations in the MLS profiles in a day, and this is more noticeable in the region around 550 K where the correlations between PV and ozone are relatively weak. As shown in Figures 2.7 and 2.8, the relatively small standard deviations of the differences and the approximately zero mean differences at most levels in summer indicate the good accuracy of mapping results during summer. In winter, as shown in Figures 2.7 and 2.8, the largest mean differences are at around 550 K in ppv (or DU/layer), and at below 400 K in percentage. The standard deviations of the differences increase downwards below 400 K. Therefore, the performance of mapping varies with altitudes and seasons, and the relatively low quality mapping results have been at the levels around ~500 K and below ~400 K in winter.

The prediction error of the ozone mapping were estimated more extensively by comparing an ensemble of individually predicted profiles against observed MLS profiles using the mean square root of $press_p$ (predicted residual sums of squares):

$$press_p = \sqrt{\sum_{i=1}^{n} (y_i - \hat{y}_{i(i)})^2 / (n-1)} \ , \tag{5}$$

where y_i is the ith case of the n-1 observed responses, and $\hat{y}_{i(i)}$ is the fitted value by deleting the ith case from n-1 cases, and then using the fitted regression function to obtain the predicted value $\hat{y}_{i(i)}$. The standard prediction error is calculated as one standard deviation of $press_p$ for all n cases. The solid lines in Figure 2.9 represent those prediction errors for two months of data in 40-50^{o}N. The standard prediction error in each approximately 2.7 km thick layer (right panel) is typically less than 3 DU in summer and fall. However, for winter and early spring, the prediction errors are larger, mostly less than 5 DU on and above 50 mb, and they increase downwards reaching a maximum of approximately 7 DU at around 82 mb. The green and red dashed lines in Figure 2.9 represent, for March and September, respectively, the standard deviations of the differences between MLS measured profiles and the profiles obtained by averaging profiles measured on the previous and on the succeeding orbits at the same latitude. Because the solid line points are almost a factor of two less in standard deviation than the dashed line points, and because the MLS measurement errors are small (Figure 2.3), significant improvements are indicated by using mapping as opposed to using spatial linear interpolation to fill in for a missing orbit of MLS measurements. This indicates that mapping is clearly advantageous when interpolation is required over 24^o of longitude.

The mapped and the coincident ozone measurements from MLS were next compared with ozonesondes (Figure 2.10) between 35^{o}N and 60^{o}N over the period of August 2004 to July 2005. MLS ozone is indicated to be unbiased relative to the sondes from 600 K to 700 K (approximately 29-18 mb or 24-28 km), it is approximately 5% larger than the sondes from 460 K to 600 K (approximately 70-29 mb or 19-24 km), and

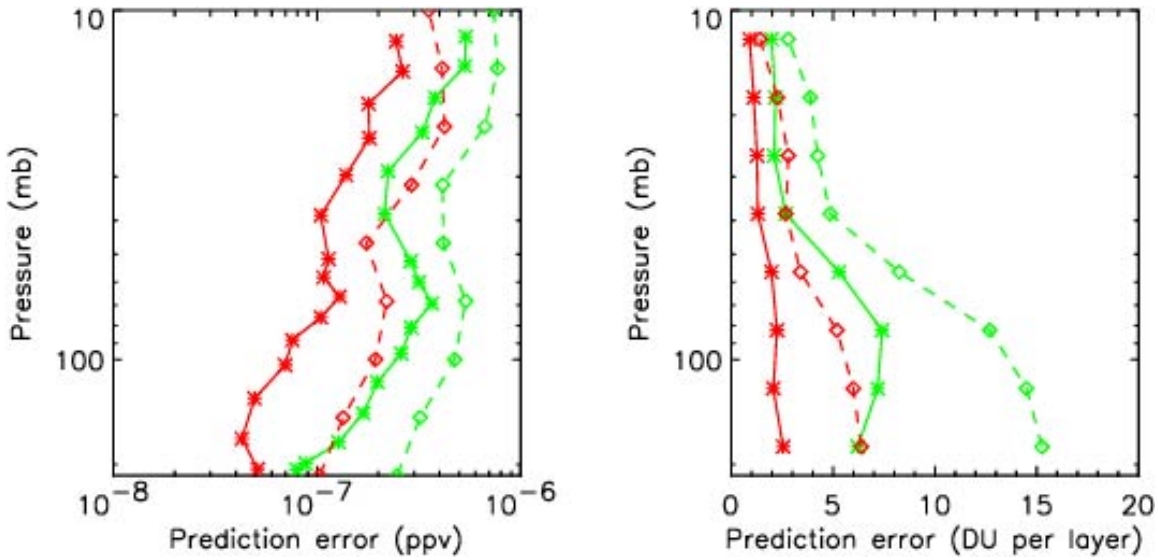

Figure 2.9: Mean prediction errors of ozone mapping for 40°- 50°N in March (green lines) and September (red lines) 2005. The solid lines show standard deviations of the differences between measured MLS profiles and profiles which have been mapped to the locations of the measured profiles. The dashed lines (March in green and September in red) represent standard deviations of the differences between MLS measured profiles and the profiles averaged from measurements on the previous and succeeding orbits at the same latitude. The solid lines in the left panel were calculated on isentropic surfaces, and the average pressures of those surfaces have been used in the ordinate. The right panel shows the prediction errors in Dobson units per layer between by two adjacent MLS pressure surfaces.

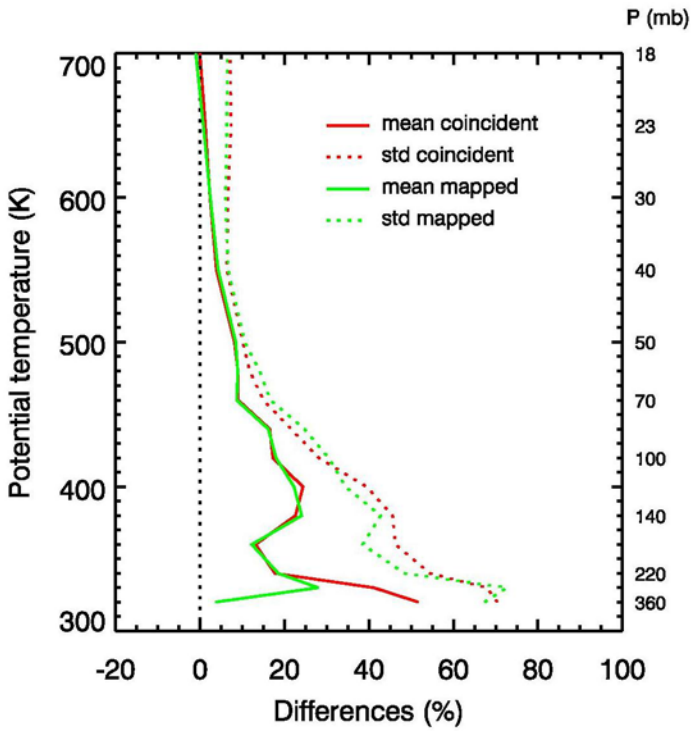

Figure 2.10: Mean and standard deviations of lower stratospheric differences (%) between mapped and coincident MLS and ozonesonde profiles at eight ozonesonde stations between 35^{o} and 60^{o}N over the period of December 2004 to November 2005. The coincidence criteria are ±12 hours in time, ±8^{o} in longitude, and ±1^{o} in latitude. The mapped ozone is predicted at the time and location of the ozonesonde measurements. The ozonesonde sites include Boulder, Huntsville, Narragansett, Trinidad Head, Uccle, Churchill, Hohenpeissenberg, and Payerne. The approximate pressures on selected isentropic surfaces corresponding to the potential temperatures are shown on the right hand ordinate.

it is approximately 15% larger below this, down to the tropopause which is located at approximately 340 K (approximately 220 mb or 11 km). These results are similar to the direct MLS/ozonesonde comparisons shown in Figure 2.4 for 30-70^{o}N.

The standard deviations of the differences shown in Figure 2.10 are approximately 5% above 600 K; this is consistent with the MLS measurement precisions shown in Figure 3 when combined with ozonesonde precisions of approximately 5%. Below 600 K the standard deviations increase to approximately 40% at the tropopause. This occurs not only because of the reduction in the precision of the MLS measurements (Figure 2.3) but equally, and probably more, importantly because of small scale (less than 500 km) atmospheric variability in the lower stratosphere. This affects the comparisons through the lack of complete coincidence between the profiles being measured. Similar standard deviations of the differences have been reported in SAGE II/ozonesonde comparisons in the lower stratosphere [Wang et al., 2002].

Figure 2.10 suggests that mapping produces no more than a small annually-averaged reduction in the standard deviations of the differences (e.g., around 360 K (160 mb)) compared to directly using MLS profiles within 8^{o} of longitude. Mapping produces smaller mean differences only around 330K (250 mb). It may be that the nominal spatial resolution of the NCEP reanalysis data of approximately 250 km is not sufficient to allow mapping to provide more clearly superior results for this coincidence criterion. Secondly, these small scale effects are the principle cause of the differences between the mapped and measured profiles. The small scale effects are most distinct in spring, since changing the coincident MLS profiles criterion to within 4^{o} in longitude produces ~ 2 DU reduction in the standard deviations of the differences for TCOs and SCOs satellite/sonde

comparisons in Tables 2.2 and 2.3 for spring, while other seasons only result in a slightly reduction of the standard deviations of the differences.

2.5 Column Ozone between the Tropopause and 215 mb

The small mid-latitude lower stratospheric ozone column contributions from the layer between the lowest utilized level of the MLS data (215 mb) and the tropopause are obtained using SAGE II ozone profile measurements. It has been shown that SAGE II version 6.2 ozone data and ozonesonde agreement in the mean is approximately 10% down to the tropopause and better than 5% between 15 (~ 120 mb) and 20 km (~ 55 mb) [Wang et al., 2002, 2006]. Jing et al. [2004] have shown that mapped lower stratospheric SAGE II profiles have standard deviations of differences from Hohenpeissenberg ozonesondes of less than 30%. Estimated column amounts in this layer, when the tropopause is below 215 mb, have been calculated four times daily, with the same spatial and temporal resolutions as the meteorological dataset, using mapped SAGE II measurements. Figure 2.11 shows that the resulting seasonal mean ozone columns in this layer for December 2004 to November 2005 have a strong latitudinal and seasonal dependence. In mid-latitude regions, the mean column decreases from ~ 9 DU at about 55^{o} latitude to ~ 3 DU at about 35^{o} latitude. The SAGE II column amounts in this layer differ from the corresponding columns measured by ozonesondes (at the Figure 6 sites) from August 2004 to November 2005 by -0.3 DU in the mean, with a standard deviation of the differences of 2.5 DU (32%). In all the calculations the tropopause pressure was obtained from the NCEP reanalysis data set.

In 2005, for 21% of the tropospheric ozone columns derived using OMI/MLS coincidences the tropopause was located at a higher pressure than 215 mb. The fraction

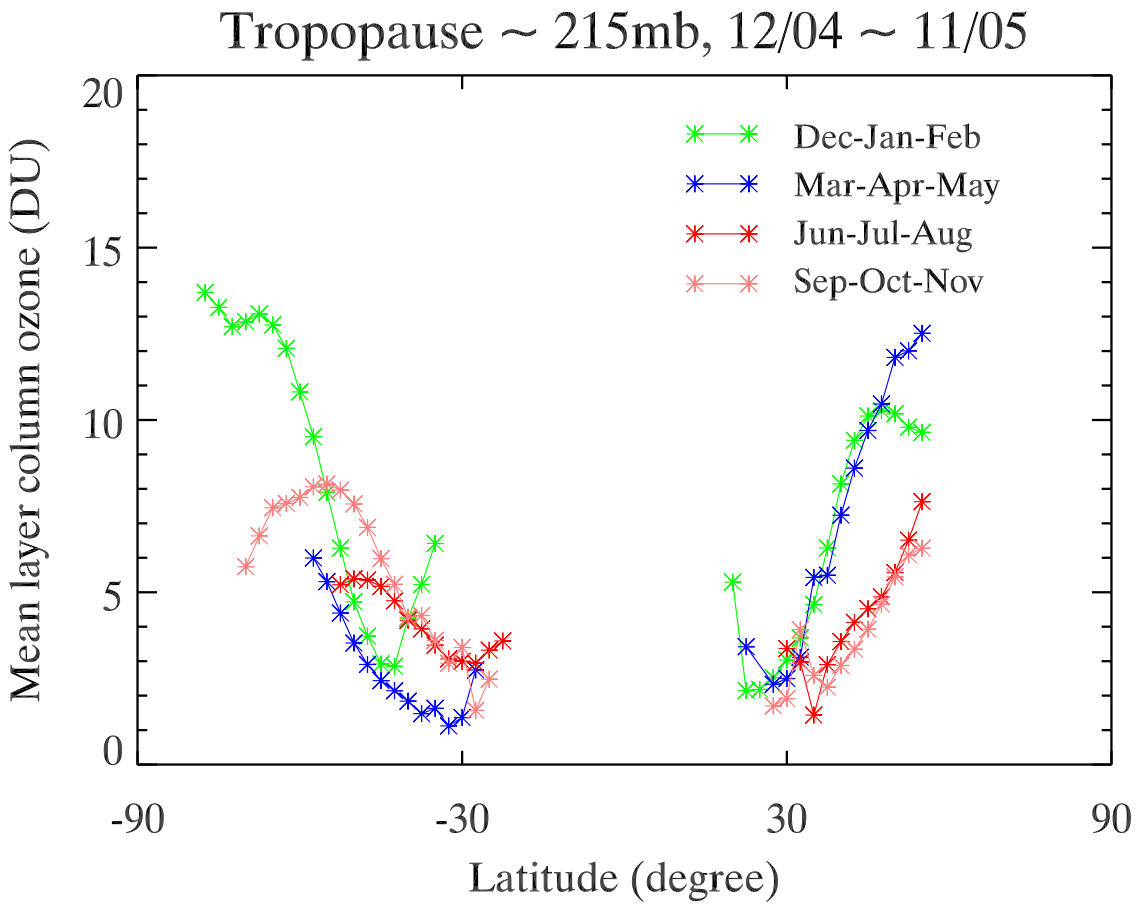

Figure 2.11: Seasonal mean ozone columns (DU) between the tropopause and 215 mb over the time period from December 2004 to November 2005. These were calculated using equation 4 with the monthly mean coefficients at each isentropic level for each calendar month, having been derived using SAGE II measurements from January 1995 to August 2005. Only data when the tropopause was at a higher pressure than 215 mb were included in the calculations of the seasonal means.

of tropospheric ozone columns for which SAGE II mapping were used (still referred to as OMI/MLS tropospheric columns) had a strong latitude dependence, increasing from 1.5% for the 20-30^{o} latitude band to approximately 45% for the 40-50^{o} latitude band and to 95% for the 70-80^{o} latitude band.2.6 MLS Lower Stratospheric Columns and Derived Tropospheric Columns

2.6 MLS Lower Stratospheric Columns and Derived Tropospheric Columns

The MLS lower stratospheric ozone columns between 700 K (~ 18 mb) and 215 mb (or the tropopause if this is above the 215 mb level) and the derived tropospheric ozone columns were compared separately against corresponding columns measured by ozonesondes at eight Northern Hemisphere mid-latitude sites (the same sites as those used to make Figure 2.10) for the period from August 2004 to November 2005. The comparisons against the time series of lower stratospheric columns and tropospheric ozone columns measured by Hohenpeissenberg ozonesondes are presented in Figure 2.12. It is clear that the lower stratospheric ozone columns from the satellites have captured most of the variability seen by the ozonesondes. It is also clear that the most divergent comparisons in lower stratospheric columns occur in winter months (November to March) and that mapping produces improvements in the comparisons on several occasions (e.g., January 31 and March 4).

A few data with large discrepancy between sonde and OMI/MLS TCOs in the time series in Figure 2.12 were investigated by comparing the corresponding ozone and temperature profiles, and one of the examples is given in the left panels of Figure 2.13. The lower stratospheric ozone columns are 140.8, 178.5, and 184.0 DU, respectively, for

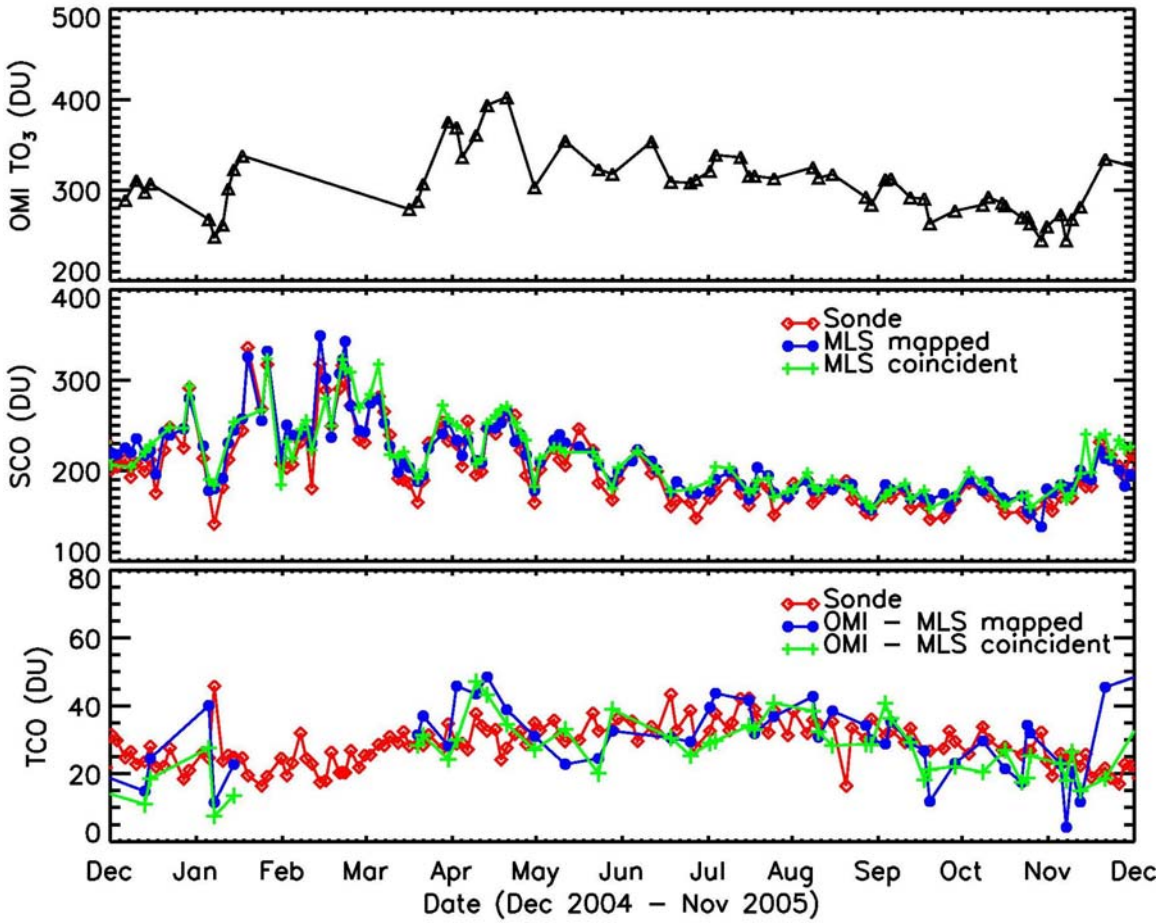

Figure 2.12: Time series comparisons of MLS stratospheric ozone columns (SCOs) between 215 mb (or the tropopause if it is located above the 215 mb level) and 700 K (~18 mb), middle panel, and resulting derived tropospheric ozone columns (TCOs), lower panel, against columns measured by Hohenpeissenberg (47.80°N, 11.02°E) ozonesondes from December 2004 to November 2005. Both coincident columns and columns mapped to the times and the location of the ozonesondes are shown. For reference the uppermost panel shows clear sky OMI total ozone columns (TO_3) coincident with the ozonesonde measurements.

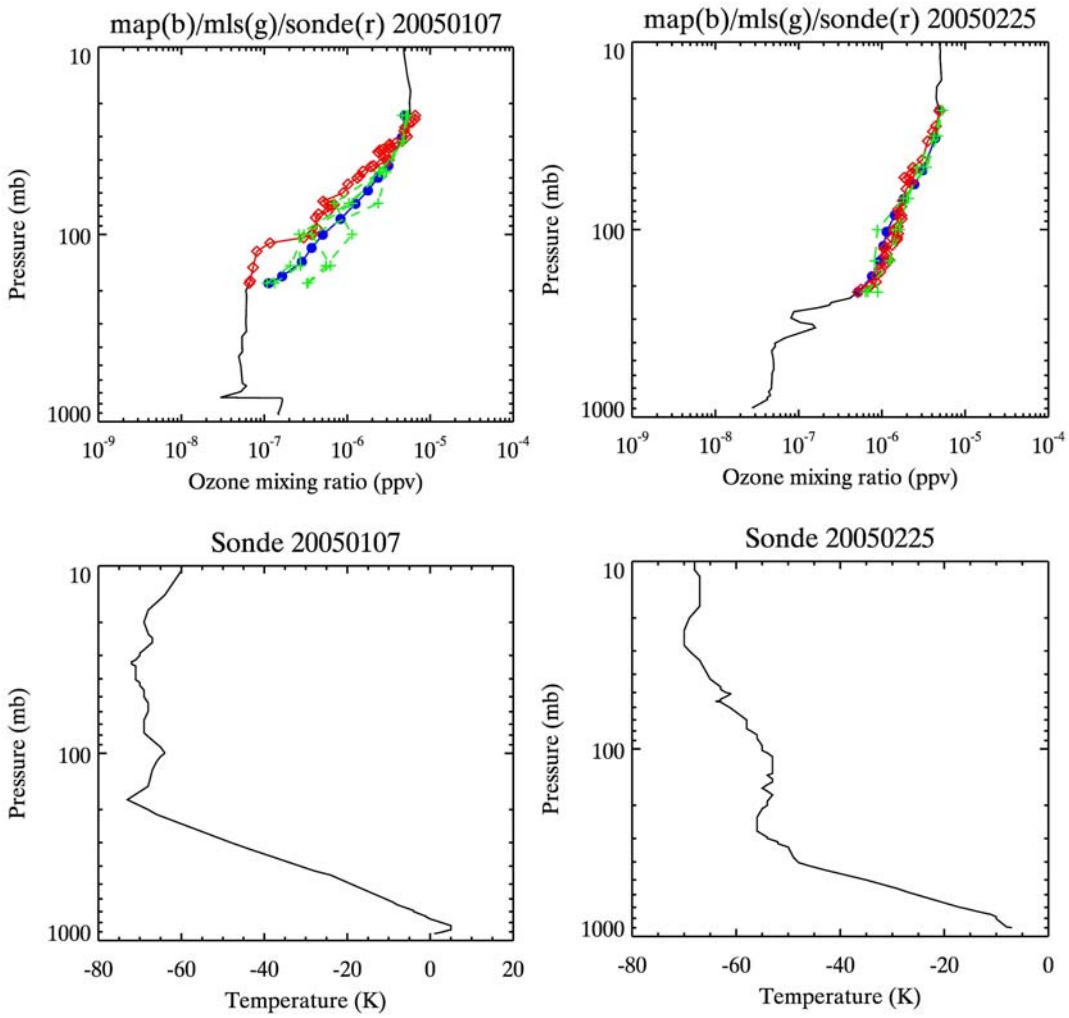

Figure 2.13: Ozone profiles from ozonesondes (red diamonds, red and black lines), PV mapped MLS (blue circles and blue lines) data, and individual coincident MLS measurements (green crosses and green lines) on January 7, 2005 and on February 25, 2005. The ozonesonde temperature profiles for both days are presented as black lines in the bottom panels).

ozonesonde, mapped MLS, and coincident MLS on January 07, 2005, and the resulting TCOs are 45.80, 12.96, and 7.43 DU, respectively. As shown in upper left panel of Figure 2.13, on this day the mapped MLS profile overestimates compared with the ozonesonde at pressures > 30 mb with a more significant overestimation at 100-200 mb due to a sudden decrease in ozone mixing ratio in this region even though the temperature measured by profile still indicate within stratosphere. The four coincident MLS profiles have a relatively large variation among them, and have an overestimation tendency similar to that of the mapped profile. In addition, the ozonesonde profiles on this day indicate a dramatic ozone enhancement in near surface layer, which is probably due to an ozone pollution event occurring within the surface inversion layer. For comparison purposes, right panels of Figure 2.12 show ozone and temperature profiles on February 25, 2005. Relatively good agreements were found among ozone profiles in the stratosphere and among the corresponding TCOs on February 25. Therefore, the presence of small scale dynamic in the lower stratosphere (near tropopause in particular) could lead to disagreement in the stratospheric column comparisons between satellite and ozonesondes. In addition, OMI has difficulty measuring ozone below boundary layers, air pollution events occurring near surface could also add to the occasional, large discrepancy between OMI/MLS and sonde measurements.

Based on the data from all eight stations, the lower stratospheric ozone columns have approximately 0.8 correlation coefficients with coincident total ozone column data, but the tropospheric ozone columns from ozonesondes and the satellite products have correlation coefficients of approximately 0.14 and 0.4 with total ozone. The high

Table 2.2: Means and standard deviations of differences between mapped and coincident MLS lower stratospheric ozone column measurements (from 215 mb, or the tropopause if it is above the 215 mb level, to 700 K (approximately 18 mb)), and similar columns at eight ozonesonde stations located between 35° and 60°N. In these calculations the differences were first expressed separately in percentages of the sonde columns and in Dobson units (DU) respectively. Annually-averaged differences are also shown for Lauder (-45.04°S, 169.68°E) ozonesondes. The period of comparison was August 2004 to November 2005.

months	Sonde (DU)	Diff. (MLS_Mapped - Sonde)			Diff. (MLS_Coinc. - Sonde)		
		data #	DU, (%)	std [DU, (%)]	data #	DU, (%)	std [DU, (%)]
DJF	215.5	89	10.7 DU (5.6%)	13.0 DU (7.0%)	62	-9.5 DU (-5.1%)	17.7 DU (8.4%)
MAM	210.2	90	8.7 DU (4.9%)	13.8 DU (7.1%)	72	14.5 DU (7.2%)	13.4 DU (6.7%)
JJA	167.0	131	11.0 DU (6.9%)	7.7 DU (4.9%)	109	9.4DU (5.9%)	8.2 DU (5.1%)
SON	164.8	242	10.9 DU (7.1%)	9.5 DU (5.9%)	73	11.3 DU (7.1%)	11.7 DU (6.8%)
ALL NH	180.9	553	10.5 DU (6.4%)	10.6 DU (6.1%)	427	11.1 DU (6.5%)	12.4 DU (6.7%)
Lauder	196.3	46	9.5 DU (5.2%)	9.6 DU (4.8%)	35	8.5DU (4.6%)	9.4 DU (4.8%)

Table 2.3: Means and standard deviations of the differences between tropospheric column ozone values calculated from clear sky OMI minus mapped or coincident MLS measurements (with the addition of mapped SAGE II measurements when the tropopause was below the 215 mb level) and similar columns at eight ozonesonde stations between 35^{o} and 60^{o}N. Separate differences are shown for mapped and for coincident MLS stratospheric ozone columns. As for Table 1, separate calculations were made using DU and percentage differences. Annually-averaged differences are also shown for Lauder ozonesondes.

months	Sonde (DU)	Diff. (MLS_Mapped - Sonde)			Diff. (MLS_Coinc. - Sonde)		
		data #	DU, (%)	std [DU, (%)]	data #	DU, (%)	std [DU, (%)]
DJF	29.1	27	-3.9 DU (-12.0%)	12.8 DU (37.9%)	27	-7.5 DU (-24.3%)	11.3 DU (35.0%)
MAM	36.3	40	-1.9 DU (-4.8%)	11.5 DU (33.4%)	40	-5.1 DU (-15.7%)	11.8 DU (35.9%)
JJA	39.9	48	-3.8 DU (-9.0%)	5.4 DU (13.6%)	48	-4.2 DU (-10.4%)	5.9 DU (15.1%)
SON	30.6	73	-4.1 DU (-12.8%)	8.0 DU (29.1%)	73	-3.1 DU (-10.0%)	8.2 DU (30.3%)
ALL NH	34.0	188	-3.5 DU (-10.0%)	9.1 DU (28.5%)	188	-4.4 DU (-13.3%)	9.2 DU (29.6%)
Lauder	23.9	20	-6.1 DU (-24.9%)	5.6 DU (22.6%)	20	-2.8 DU (-12.5%)	6.8 DU (30.8%)

correlations between lower stratospheric ozone and total ozone are not surprising since the lower stratosphere contributes most of the ozone in the total column, but the variations in the total column explain a relatively small proportion of the variations in tropospheric ozone columns at mid-latitudes.

Summaries of the statistics based on the eight ozonesonde station comparisons (reflectivity ≤ 10%) are presented in Tables 2.2 and 2.3. They indicate that both mapped and coincident MLS lower stratospheric ozone columns are larger by about 11 DU than the sonde measured columns. This is consistent with the mean differences shown in Figure 2.10, which also indicates that most of the offset arises from the region between 50 mb (500 K) and the tropopause. Only during the spring are the mean differences, with respect to the sondes, between the mapped (8.7 DU) and the coincident (14.5 DU) MLS lower stratospheric columns significant at the 95% confidence level. Note, however, that the standard deviations of the differences between sondes and the mapped and coincident MLS columns in spring are similar. Mapping results in somewhat smaller standard deviations in winter and a more consistent bias in the tropospheric columns relative to the other seasons. Constraining the coincidence criteria to ± 4^o of longitude instead of ± 8^o reduces the mean tropospheric column offset in winter to -4.6 DU, but there are no other improvements in the comparisons.

Linear interpolation in longitude and latitude produces annually averaged differences versus the ozonesondes over the August 2004 to November 2005 period of 12.0 ± 11.3 (standard deviation) for the lower stratosphere and -5.0 ± 10.1 in the troposphere. This is slightly worse than the mapped results, but it is in winter that the mapped results are definitely superior because the linear interpolation approach yields

differences versus sondes of 17.8 ± 16.1 (versus 10.7 ± 13.0 using mapping) in the lower stratosphere and -9.5 ± 16.0 (versus -3.9 ± 12.8 using mapping) in the troposphere. A particular strength of the mapping technique compared to using linear interpolation or coincidence is that mapping is much less affected by missing MLS measurements. For example, in the comparisons with the sondes there were often twice as many comparisons that could be made using mapping than by using linear interpolation.

The derived tropospheric columns are, in the mean, 4 DU smaller than the ozonesonde column measurements. Figure 2.8 showed that the MLS stratospheric columns are larger than SAGE II columns by approximately 3 DU. In the study of Ziemke et al. [2006], MLS columns were also shown to be ~ 4 DU high relative to OMI columns above convective clouds. Jing et al. [2006], however, reported an OMI/MLS tropospheric ozone column versus sonde column difference of 1 ± 9 DU (1 standard deviation), but this is because the MLS columns in their work were calculated using equation 2 for the column integration which, as was pointed out earlier, produces smaller stratospheric ozone column amounts by approximately 1%.

The lower stratospheric mean offset of +11 DU relative to the sondes, combined with the -4 DU offset of the derived tropospheric columns, implies that the upper portion of the MLS stratospheric columns is low by approximately 7 DU. Relative to SAGE II (and SAGE III and HALOE), MLS indeed has shown smaller values of ozone above approximately 10 mb (Figure 2.4; see also Froidevaux et al., 2006).

The standard deviations of the derived tropospheric ozone column differences are significantly larger in the winter/spring seasons because of greater dynamical and hence stratospheric column variability at that time of year. Note that the tropospheric ozone

column statistics in Table 2.3 are based upon a subset of the columns that are coincident with the ozonesonde measurements because of the OMI total ozone measurement requirement of clear skies. For direct comparison purposes, essentially the same subset has been used for the mapped samples. As an additional check on the statistics, differences between the coincident and the mapped column results were directly calculated. These mean differences were exactly equal to the differences to be expected from Tables 2.2 and 2.3, and the standard deviations were somewhat larger than those shown in the two Tables. The latter result indicates that there is considerable variability in the differences between the individual coincident and the mapped columns.

Tables 2.2 and 2.3 also show mean annual differences against a relatively small number of Lauder ozonesondes. The results are not significantly different from the combined annual results from the eight northern hemisphere sites (labeled ALL). It is concluded that the overall conclusions of this paper based on the mostly northern hemisphere analysis are probably also applicable to the southern hemisphere.

The clear sky condition is defined in this chapter by a reflectivity less than 10%. Results have also been calculated for reflectivity values of up to 30% (Table 2.4). Changing reflectivity thresholds from 10% to 30% produced 40% more tropospheric ozone column data in the NH, but the overall mean and standard deviation of the differences with ozonesondes remained about the same for the eight mid-latitude NH ozonesonde stations. Specifically, there was an about 0.7 DU (~3%) increase in the magnitude of the mean differences and an about 0.7 DU (~4%) increase in the standard deviation of the differences. The TCO values produced with clear sky reflectivity thresholds of 20% and 30% are shown in Figure 2.14 for a comparison with those

generated with a threshold value of 10% (bottom panel of Figure 2.12). Despite the increased number of available TCO data and relatively stable statistics presented previous based on comparisons at the eight ozonesonde stations (Table 2.4), sporadic extreme high and low TCO values appear in the time series with the increase of the reflectivity threshold at Hohenpenssenberg station.

Comparisons between OMI total columns and ground based total column measurements (e.g., by the Dobson instruments) show OMI values are higher by 0.4±0.5% (Yang et al., 2007). In Visconti et al. [2007] the accuracy and precision of OMI columns are given as 2% and 1%, respectively. Therefore the low bias (with respect to tropospheric ozonesonde measurements) in the derived tropospheric ozone columns almost certainly is related to the high bias in the MLS v1.5 stratospheric columns. In addition, the indicated precision of the OMI columns of approximately 1% suggests that the relatively large standard deviations (~ 10 DU) in the derived tropospheric ozone columns relative to the ozonesondes are associated with variations in the differences between the interpolated MLS lower stratospheric columns and the sonde columns. This is consistent with the standard deviations in the SAGE II/MLS column comparisons shown in Figure 2.5. However, there also may be some contributions to the differences produced by differing spatial resolutions of the satellite and sonde measurements and by non-exact coincidence between the MLS and the ozonesonde measurements.

Table 2.4: Means and standard deviations of differences between OMI/MLS mapped and coincident TCOs, and similar columns at eight ozonesonde stations located between 35^{o} and 60^{o}N with the use of different reflectivity thresholds to define clear sky condition.

OMI refls	stn ID	MLS mapped			MLS coincident		
		data #	mean (DU)	std (DU)	data #	mean (DU)	std (DU)
≤10%	8 stns	206	-2.1 (-5.8%)	12.1 (38.8%)	198	-5.1 (-15.3%)	10.1 (31.9%)
	67	23	-3.3 (-11.8%)	13.2 (43.6%)	23	-10.9 (-38.4%)	10.7 (40.0%)
	418	16	0.3 (-1.5%)	12.6 (38.6%)	15	-7.4 (-23.1%)	11.4 (33.3%)
	0	13	-3.4 (-15.8%)	14.6 (51.5%)	10	-0.8 (-3.2%)	8.3 (25.8%)
	445	18	1.8 (8.3%)	17.6 (48.5%)	16	-3.5 (-9.1%)	9.9 (29.6%)
	53	17	-9.0 (-26.5%)	11.9 (38.0%)	17	-8.6 (-26.2%)	9.5 (30.4%)
	77	3	1.4 (3.9%)	8.2 (28.5%)	2	-4.3 (-13.9%)	
	99	54	-0.2 (0.7%)	10.9 (37.9%)	57	-2.8 (-7.9%)	9.9 (31.4%)
	156	62	-2.9 (-7.1%)	9.7 (30.2%)	58	-4.8 (-12.2%)	9.6 (26.3%)
≤20%	8 stns	268	-2.2 (-6.1%)	12.9 (42.3%)	251	-5.9 (-17.8%)	10.6 (34.9%)
	67	24	-4.2 (-14.7%)	13.4 (44.0%)	24	-12.3 (-42.6%)	11.1 (40.9%)
	418	19	0.7 (-0.5%)	12.0 (35.4%)	17	-7.1 (-22.0%)	10.8 (32.4%)
	0	15	-2.2 (-11.6%)	14.7 (49.1%)	12	-2.1 (-5.6%)	8.2 (23.6%)
	445	20	0.8 (3.3%)	15.7 (39.8%)	18	-1.3 (-3.9%)	13.1 (35.5%)
	53	24	-9.6 (-28.8%)	15.5 (48.7%)	23	-8.1 (-25.3%)	8.6 (27.8%)
	77	4	-0.8 (-3.7%)	6.9 (23.6%)	3	-3.5 (-11.6%)	3.8 (13.4%)
	99	77	0.3 (2.7%)	11.6 (43.3%)	76	-5.3 (-17.6%)	10.9 (37.3%)
	156	85	-3.2 (-7.9%)	11.8 (38.6%)	78	-5.2 (-12.7%)	9.9 (31.6%)
≤30%	8 stns	85	-2.0 (-5.1%)	13.2 (45.6%)	263	-6.0 (-18.0%)	11.8 (44.9%)
	67	25	-4.9 (-16.8%)	13.0 (42.4%)	25	-13.0 (-44.3%)	10.9 (40.0%)
	418	18	1.8 (2.5%)	11.9 (34.9%)	16	-5.4 (-17.4%)	10.5 (30.8%)
	0	16	-1.4 (-8.5%)	14.0 (45.3%)	13	-0.5 (-0.9%)	9.3 (24.6%)
	445	14	-1.4 (-1.9%)	15.3 (39.3%)	12	-6.0 (-16.1%)	8.7 (26.3%)
	53	24	-9.7 (-29.2%)	15.6 (49.1%)	23	-8.2 (-25.7%)	8.7 (27.8%)
	77	5	-6.5 (-29.1%)	11.6 (51.3%)	3	-4.5 (-14.9%)	2.8 (10.5%)
	99	97	1.2 (6.1%)	13.1 (51.5%)	93	-4.8 (-15.5%)	14.5 (61.9%)
	156	88	-3.2 (-7.6%)	11.7 (37.9%)	78	-5.6 (-13.7%)	9.5 (29.4%)

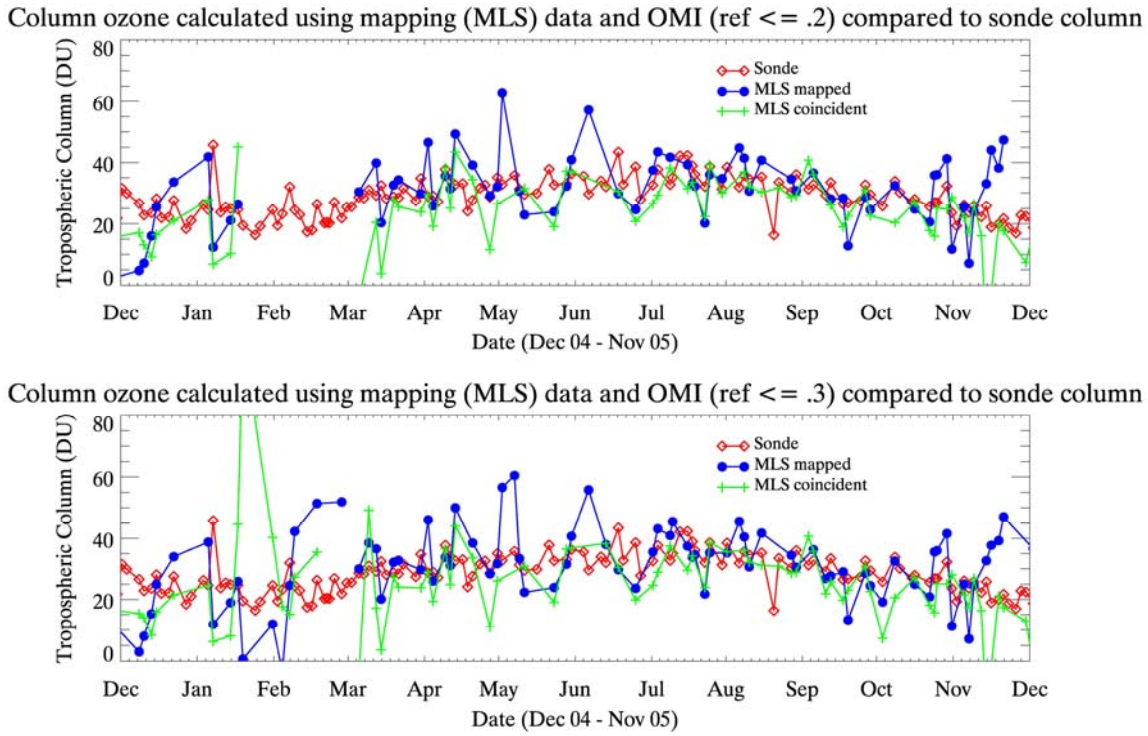

Figure 2.14: The same as the bottom panel of Figure 2.12 with the clear sky OMI reflectivity threshold being 20% for upper panel and 30% for lower panel.

2.7 The Use of Total Column Ozone as a Mapping Constraint

It is well known that there is a close relationship between total ozone and synoptic conditions in the troposphere and lower stratosphere; troughs and crests of the upper troposphere are often temporally associated with high or low ozone concentration [Shalamyanskiy and Romanshkina, 1980]. In addition, the locations of arctic air, tropical air, and the mid-latitude air are found to be, respectively, coincident with high, low, and intermediate total column ozone values [Hudson et al., 2003, and references therein]. It has been noted that the passage of the upper tropospheric fronts is associated with a sharp increase or decrease of the total ozone value [Hudson et al., 2003, and references therein].

On the basis of these well established relationships, we tested the use of total ozone columns as a third predictor in the relationship (equation 4). So far this was only tested in the mapping of SAGE II stratospheric ozone measurements. As shown in Figure 2.14, correlations between ozone and total ozone are higher than those between ozone with PV on isentropic surfaces below ~420 K. Using TOMS total columns as the third predictor was found to reduce the standard deviations of the stratospheric ozone column and tropospheric ozone column differences during winter relative to the ozone columns at Hohenpeissenberg in 1998 by about 4 DU (Figure 2.15). The addition of total ozone as a third predictor is expected to improve the winter period prediction for Aura MLS mapping as well, but such an approach needs further testing and careful application.

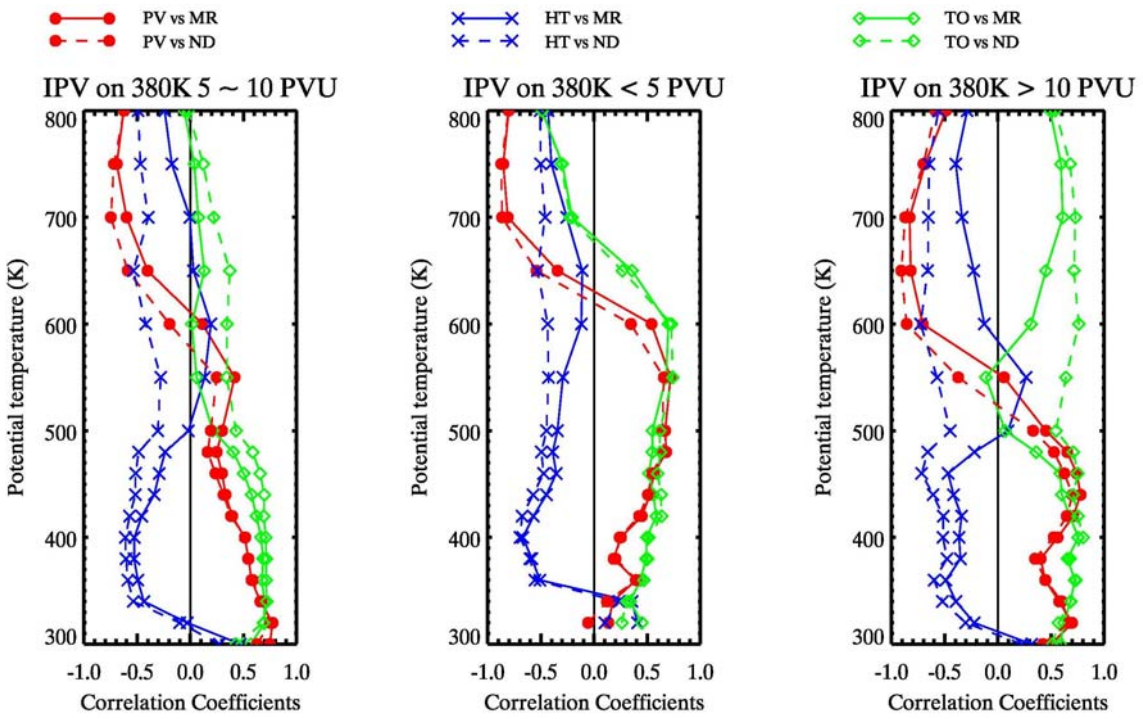

Figure 2.14: Correlation coefficients of ozone with PV (red), Geopotential height (HT, blue), and TOM total ozone (TO, green) for January 1998. PV on 380 K were used to partition the data in the Northern Hemisphere. The partition criteria are PV values on 380 K between 5 and 10 PVU (left), < 5 PVU (middle), and > 10 PVU (right), respectively. The correlations with ozone mixing ratio are represented by solid lines and the correlations with ozone number density are represented by dash lines.

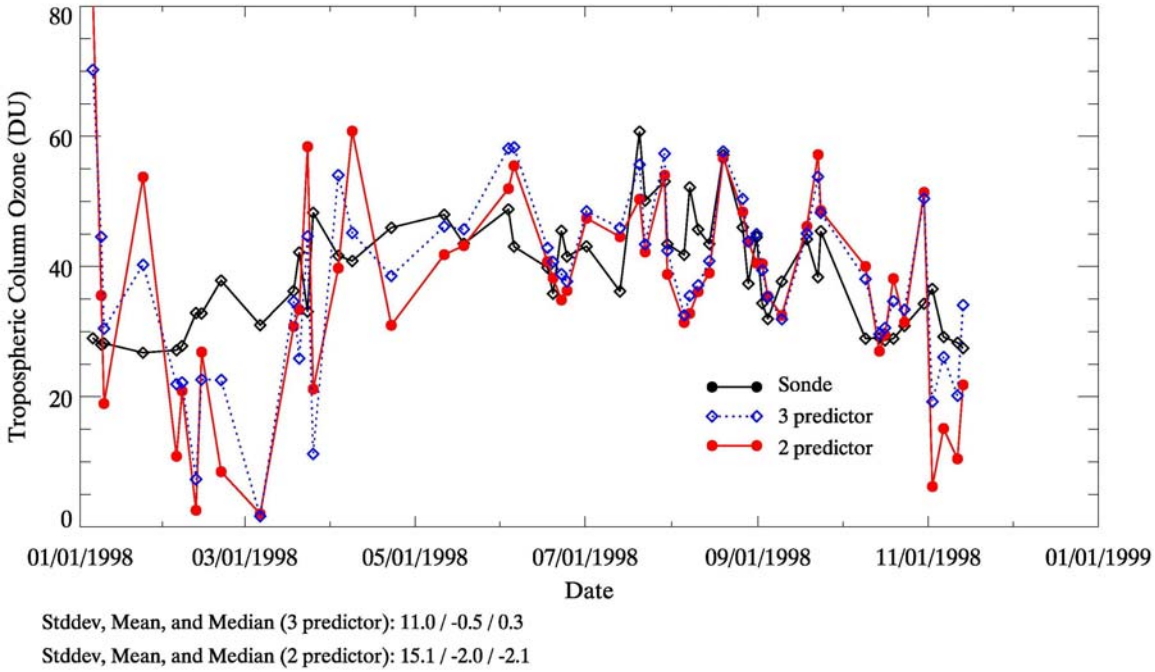

Figure 2.15: Comparisons of tropospheric ozone columns derived using two-predictor (PV and geopotential height, red circles) and three-predictor (total ozone column as third predictor, blue diamonds) ozone mappings with ozonesonde columns (black circles) at Hohenpenssenberg station during 1998. SAGE II ozone data were used for the ozone mapping in the lower stratosphere. Ozone columns above 25 mb ($P \leq 25$ mb) were obtained from SBUV data. The total ozone data were from TOMS measurements.

2.8 A Preliminary Estimate of MLS Version 2.2 Retrieval Results

MLS version 2.2 provisional profiles were used for 15 days in 2004 and 2005 for comparisons versus mid-latitude ozonesonde measurements. Using $\pm 1.25^{O} \times \pm 1.25^{O}$ longitude by latitude and the same day as coincidence criteria, 17 coincident profiles were found at 6 (out of 8) ozonesonde stations: Boulder, Narragansett, Trinidad Head, Uccle, Hohenpeissenberg, and Payerne. The comparison based on the 17 coincident profiles indicates that the MLS lower stratospheric columns (tropopause, or 215 mb, to 700 K) produced from version 2.2 data have a mean offset of 9.4 DU relative to the ozonesonde columns. This offset is about 2 DU less than the mean offset (11.5 DU) calculated for the version 1.5 data using the same ozonesonde profiles.

A more extensive evaluation of stratospheric ozone columns from MLS v2.2 retrievals has been made by directly comparing the columns obtained using the two versions of MLS retrievals from the 15 days of measurements. The v2.2 total stratospheric columns are calculated to be a few DU less on average than the v1.5 columns. The standard deviations of the differences in these stratospheric columns between the two versions are approximately 4-5 % [Froidevaux et al., 2007]. Therefore use of the new version 2.2 MLS retrievals will probably result in OMI/MLS tropospheric ozone columns (which for MLS v1.5 were biased by 4 DU relative to the sondes) which are essentially unbiased with respect to tropospheric columns measured by ozonesondes, but the standard deviations of the differences are unlikely to change significantly except perhaps in summer.

2.9 Conclusions

Procedures for combining Microwave Limb Sounder (MLS) stratospheric ozone column (above 215 mb) measurements with Dutch-Finnish Ozone Monitoring Instrument (OMI) total atmospheric column ozone measurements to produce tropospheric ozone columns have been discussed. The mapping (referred to here as PV mapping) of the MLS stratospheric columns to the locations and times of the OMI measurements using relationships between ozone, potential vorticities (PV), and geopotential heights on isentropic surfaces over three day periods has been emphasized. Using this procedure with the NCEP/NCAR reanalysis meteorological data set, we find that the resulting tropospheric ozone columns are 4 DU low on average from August 2004 to November 2005 relative to measurements from eight northern hemisphere mid-latitude ozonesonde sites. This has been shown to be consistent with the MLS (version 1.5) stratospheric columns above 215 mb being high relative to Stratospheric Aerosol and Gas Experiment (SAGE II) columns by approximately 3 DU.

In the lower stratosphere mapped MLS ozone columns between approximately 18 and 215 mb (or the tropopause if it is above the 215 mb level) have a standard deviation in the differences of approximately 11 DU from the sonde measurements over one year period. Based on comparisons against other satellite measurements, as well as differences between mapped and individual coincident MLS profiles, uncertainties in the interpolated MLS measurements are most likely the principal contributors to these standard deviations. The standard deviations in the lower stratospheric column differences are mirrored in standard deviations in the differences between ozonesondes and OMI/MLS

derived tropospheric columns of, for example, 12 DU in winter/spring and 6 DU in summer.

Preliminary indications are that the 4 DU offset of the OMI/MLS derived tropospheric columns relative to ozonesondes will essentially disappear when version 2.2 MLS retrievals become generally available. The vertical integration procedure supplied by the MLS team should be used for obtaining stratospheric ozone columns from the MLS measurements. Other integration algorithms which are often used for the vertical integration result in column differences of approximately ±1% because of the MLS layer thickness of approximately 2.7 km.

PV mapping of MLS columns has been shown to be especially effective for spatially interpolating over 24^{o} of longitude, and it reduces the standard deviations of the lower stratospheric differences from ozonesonde measurements somewhat during winter compared to linear interpolation between MLS measurements or just using the nearest MLS measurement to the sonde location.

The uncertainties (one sigma) in the individual OMI/MLS derived tropospheric columns, based on the ozonesonde comparisons, are approximately 35% and 15% in winter and summer, respectively. Therefore, for many applications, it may be best to use spatially or temporally averaged columns [e.g., Jing et al., 2006]. A significant advantage of the mapping procedures is that it produces an increased number of averagable observations especially when there is missing MLS data. In addition, using a 30%, instead of a 10%, reflectivity as the condition for clear sky OMI measurements produced approximately 40% more tropospheric ozone column measurements without any

significant increase in their mean differences and their standard deviations relative to the sondes.

CHAPTER 3

THE STUDY OF TROPOSPHERIC OZONE COLUMN ENHANCEMENTS OVER NORTH AMERICA USING A REGIONAL MODEL AND SATELLITE DATA

The coupling of dynamics and chemistry makes it challenging to understand ozone variability in the troposphere. The integration of satellite measurements and model simulations is a promising approach to provide some insights into the study of tropospheric ozone.

Jing et al. (2004) compared OMI/MLS TCOs (tropospheric columns below 147mb) with a 3-D Regional chEmical trAnsport Model (REAM) over the U.S. and its surrounding oceans during the summer of 2005. Some large changes in TCOs were found to be associated with near-surface ozone changes and geopotential height changes at 147 mb. Compared with summer time, in spring the upper troposphere and lower stratosphere are dynamically more active, and the cross-Pacific transport of air pollutants is most intense. This study examined the variability of the tropospheric ozone columns using Aura satellite data as well REAM regional model simulations for both the spring and summer 2005 over the North America and its surrounding oceans. A spring TCO enhancement event was investigated.

3.1 Models and Measurement Data

3.1.1 Model Descriptions

REAM and GEOS-CHEM simulations were integrated in this study to investigate TCO enhancements over North America. GEOS-CHEM, a 3-D global model of tropospheric chemistry, has been widely used to study the meteorology and chemistry in the Asian outflow over the Pacific [e.g., Heald et al, 2003].

REAM is a 3-D regional chemical transport model whose chemistry and deposition modules are based on the same modules used in GEOS-CHEM [Wang et al., 2006]. Its initial and boundary conditions of the tracer concentrations are also obtained from GEOS-CHEM. The model is driven by meteorological data from the NCAR/Penn State MM5 simulations. REAM simulations have been archived every hour. The domain of REAM covers most part of the North America with a horizontal resolution of 70 km × 70 km, and has 23 vertical layers between surface and the model upper boundary (10mb). REAM is characterized with improvements in lightning schemes, mixing depth estimation, surface NOx emission, and so on. A number of studies [e.g., Choi et al., 2005; Wang et al., 2006; Zeng et al., 2003] on effects of lightning and convection, trans-Pacific transport, and polar tropospheric chemistry have been based on REAM simulations [Choi et al., 2007]. The detailed description of the model, the comparisons with GEOS-CHEM, and REAM's validation against surface, aircraft, and satellite measurements can be found in Choi et al. [2007].

3.1.2 Surface Ozone

Hourly archived surface ozone data were obtained from the United State (U.S.) Environmental Protection Agency (EPA) ground network measurements, which can be directly downloaded from www.epa.gov/ttnairs1/airsaqs/detaildata/downloadaqsdata.htm.

3.1.3 TES

The Tropospheric Emission Spectrometer (TES) is an infrared, high-resolution, Fourier transform spectrometer, which is on board the Aura satellite providing ozone measurements in the troposphere [Beer, 2006]. TES operates in global survey and special observation modes. This study used the standard TES products produced from the global survey mode. Nadir viewing level-2 (version 002) ozone data were used due to their better spectral resolutions and data precisions compared to limb viewing data. The 'master flag' provided along with the TES data were used to filter out the ozone profiles with retrieval problems. Two conditions suggested by [Osterman, 2007] were used to filter out the questionable data retrieved during nighttime over continents under conditions of poor surface and lower atmosphere temperature contrast. When comparing TES tropospheric ozone columns against OMI/MLS columns, the TES averaging kernels are not needed and thus have not been used.

3.1.4 OMI/MLS TCOs

Based on the tropospheric ozone residual (TOR) approach, three types of tropospheric ozone columns were computed using OMI and MLS data. They are called

OMI/MLS coincident, OMI/MLS 2-D interpolated, and OMI/MLS mapped TCOs, respectively. Following similar logistics on the derivation of OMI/MLS at sonde locations and times as described in Chapter 2, a new set of OMI/MLS were calculated with OMI clear sky reflectivity threshold being 30%. The following paragraphs briefly summarize the derivation of OMI/MLS TCOs (sometimes briefed as OMI/MLS) used in this chapter.

OMI/MLS mapped TCOs were derived from the ungridded level-2 (L2_V002) total ozone data that are at the full instrument resolution. While OMI/MLS coincident and OMI/MLS 2-D interpolated TCOs were computed using the gridded level-2 clear sky total ozone, which was obtained by binning the ungridded clear sky total ozone into $1^{o}\times1.25^{o}$ (latitude by longitude) regular grids.

OMI/MLS coincident TCOs were computed using a straightforward approach. Coincident MLS profiles with respect to each gridded total ozone measurement were defined by being measured in the same day and within ±1.25 in longitude and latitude relative to the center of the total ozone grid. Applying the TOR approach to the gridded total ozone and the averaged coincident MLS profile yields a tropospheric ozone residual with a resolution of $1^{o}\times1.25^{o}$ (latitude by longitude).

The OMI/MLS 2-D interpolated TCOs are characterized by the interpolation of MLS ozone profiles from two adjacent orbits (daytime MLS measurements only) to the between-orbit locations using simple spatial 2-D interpolation. No temporal interpolation was considered. If no MLS measured profiles were found within a total ozone grid, 2-D spatial interpolations were implemented to obtain an interpolated profile provided that MLS profiles from two adjacent orbits on the same day as the OMI measurements were

available. The resulting OMI/MLS 2-D interpolated TCOs have a spatial resolution of $1^o \times 1.25^o$ (latitude by longitude), which is the same as that of the gridded clear sky total ozone.

A potential vorticity/geopotential height (PV/Z) mapping approach was used as another approach to increasing the spatial and temporal resolutions of the MLS measurements. A mapping relationship for each $2.5^o \times 2.5^o$ (longitude by latitude) grid on certain isentropic surface on certain day was determined based on the MLS measurements within $\pm 60^o$ in longitude, $\pm 5^o$ in latitude and ±1.5 days. A mapped profile was generated followed by the residual calculation at the time and location of each clear sky OMI measurement (ungridded). The OMI/MLS mapped TCOs were then binned to $0.5^o \times 0.5^o$ (latitude by longitude) or coarser grids (specified in the text or figure captions).

In summary, the three types of OMI/MLS TCOs differ from each other by the different approaches applied to the MLS profiles: simple coincidence criteria, 2-D interpolation, and ozone mapping. The last two types of TCOs have the advantage of supplying increased spatial resolution. The mapping approach has a particular strength of being less affected by the missing MLS measurements.

The TCOs were calculated both in DU and in volume mixing ratio (VMR). The conversion of TCOs from DU to VMR can be achieved by dividing by the pressure difference (in mb) between surface and the tropopause, followed by multiplication by a constant (0.7889). The TCO expressed in VMR has the advantage of eliminating the TCO variations caused by changes in the amount (weight more specifically) of air in the tropospheric columns associated with, for example, the topography effects. The daily mean pressure differences between surface and tropopause were used to convert TCOs

from DU to VMR units, since the coincident and 2-D interpolated TCOs were derived from OMI and MLS data corresponding to different (measurement) times. However, the accuracy of the TCOs expressed in VMR may inevitably be slightly compromised when the surface and tropopause pressures have large variations in a day. Therefore, unless specified, this study focused on the TCOs in DU (although the contour maps in VMR are presented as well).

3.2 Model and Satellite Data Inter-comparisons

Inter-comparisons of the model and observations are necessary to determine the relative quality of each dataset. In Chapter 2, three different types of OMI/MLS TCOs were compared with the corresponding ozonesonde columns obtained at eight Northern Hemisphere mid-latitude sites for the period from August 2004 to November 2005. It was found that the OMI/MLS TCOs have an annual average difference of ~-4 ± 11 DU relative to ozonesonde columns. A similar standard deviation of the differences is found for the lower stratospheric columns. Considering that OMI values are higher by only 0.4 ±0.5% [Yang et al., 2007] relative to ground based total column Dobson measurements, it was concluded that the low bias in the tropospheric ozone columns is related to the high bias in the MLS v1.5 stratospheric columns (biased high by about 11 ± 11 DU in the lower stratosphere and possibly biased low by about 7 DU in the middle and upper stratosphere). The largest variations of the mean differences in tropospheric ozone columns with respect to ozonesondes occurred in winter and spring. During the spring, the mean differences of tropospheric columns with respect to the sondes were -1.9 ± 11.5

DU, -5.1 ± 11.8 DU, and -5.9 ± 10.2 DU for coincident, mapped, and 2-D interpolated TCOs, respectively, at mid latitudes.

With the emphasis on the validations with ozonesonde, the OMI/MLS in Chapter 2 used OMI (ungridded) and MLS data which were coincident with ozonesonde measurements in locations and time (or mapped to sonde locations and time). However, with slight differences, in this chapter the gridded clear sky OMI data were used in the derivation of OMI/MLS coincident and 2D interpolated TCOs, while OMI/MLS mapped TCOs were still calculated from OMI level-2 ungridded data. Along with the REAM tropospheric ozone columns, the new set of OMI/MLS TCOs were compared against the corresponding ozonesonde columns at the four Aura ozonesonde validation stations over the North America (between 35^{o}-42^{o}N) during spring and summer 2005. The mapped TCOs at OMI measurement locations and times were averaged over a $1^{o} \times 1.25^{o}$ (latitude by longitude) box centered at the ozonesonde locations for this comparison. The regular gridded OMI/MLS 2-D interpolated and coincident TCOs were spatially interpolated to the ozonesonde locations using data in the nearest four grids.

Figure 3.1 shows the time series of the tropospheric ozone columns at four AVDC sonde stations (Boulder, Huntsville, Rhode Island, and Trinidad Head). In general, OMI/MLS and REAM TCOs follow with the general trend of sonde TCOs but with REAM values being slightly lower. The low REAM TCO values with respect to sondes in spring are consistent with the results of Choi et al. [2007] in which it was indicated that REAM underestimates ozone concentration relative to sondes at pressures≥600 mb in March and at pressures ≥400 mb in April and May 2005 for the stations between 30-45^{o}N (Boulder, Huntsville, Trinidad Head, and Wallops Island).

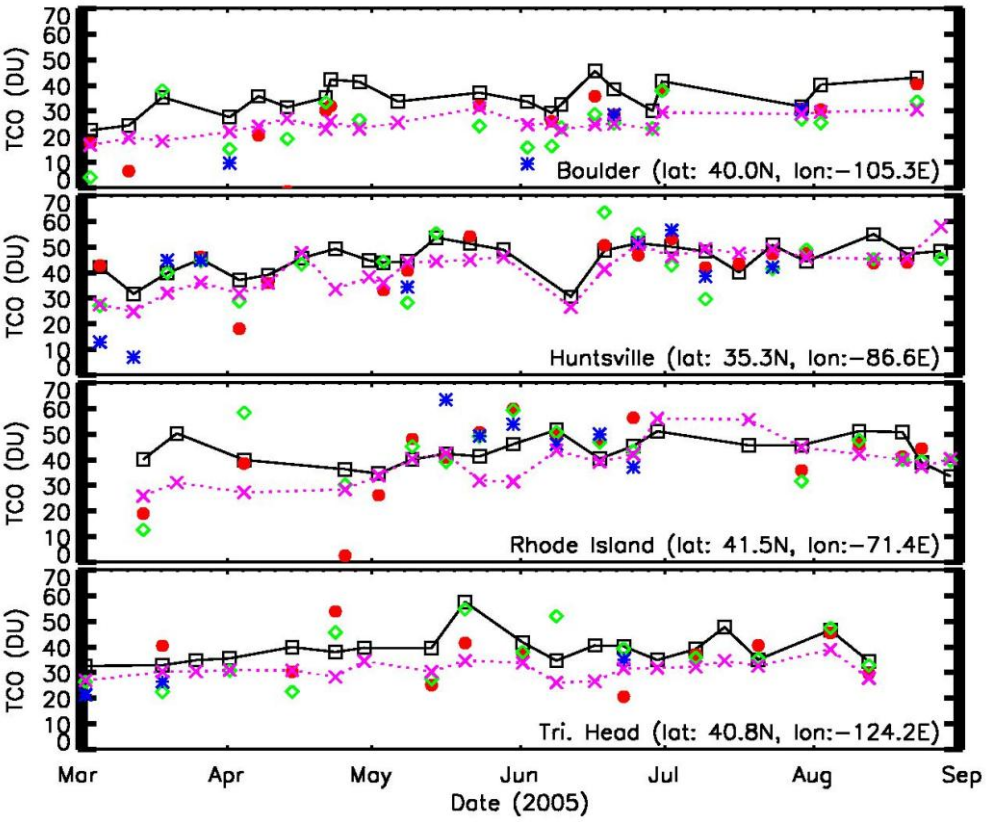

Figure 3.1: The tropospheric ozone columns calculated from ozonesonde (black squares), REAM (magenta crosses), OMI/MLS mapped (red circles), OMI/MLS 2D-interpolated (green diamonds), and OMI/MLS coincident (blue stars) data at four AVDC ozonesonde stations over North America during spring and summer 2005. The four sonde stations are Boulder, Huntsville, Rhode Island, and Trinidad Head (from top down). The OMI/MLS mapped TCOs used in this comparison were computed by averaging the ungridded OMI/MLS mapped over a $1^{o} \times 1.25^{o}$ (latitude by longitude) area centered at the ozonesonde locations. The OMI/MLS 2D-interpolated and coincident TCOs were spatially interpolated to the ozonesonde locations using data in the nearest four grids; in case only one datum was available in the four grids, this datum was used to represent the value at the sonde location.

Table 3.1: Inter-comparisons of tropospheric ozone columns from OMI/MLS, REAM, and ozonesonde at four ozonesonde stations, Boulder, Huntsville, Rhode Island, and Trinidad Head, for spring and summer 2005.

	type of comparisons	data #	correlation	mean diff	stddev diff
spring+summer	mapped vs. sonde	56	0.66	-4.7DU (-12.5%)	9.9DU (27.3%)
	2D interpolated vs. sonde	63	0.64	-5.5DU (-15.0%)	11.3DU (30.6%)
	coincident vs. sonde	22	0.71	-5.2DU (-15.3%)	12.3DU (33.3%)
	ream vs. sonde	84	0.72	-6.7DU (-16.6%)	6.4DU (14.9%)
	mapped vs. ream	56	0.63	2.2DU (6.4%)	10.1DU (34.3%)
	2D interpolated vs. ream	63	0.56	1.6DU (5.0%)	12.0DU (43.1%)
	coincident vs. ream	22	0.70	0.6DU (-1.0%)	11.9DU (38.5%)
spring	mapped vs. sonde	27	0.64	-6.5DU (-18.7%)	12.5DU (35.2%)
	2D interpolated vs. sonde	30	0.64	-6.8DU (-19.8%)	13.6DU (37.8%)
	coincident vs. sonde	11	0.72	-5.3DU (-17.5%)	15.3DU (41.5%)
	ream vs. sonde	43	0.70	-8.3DU (-20.8%)	5.7DU (12.7%)
	mapped vs. ream	27	0.55	1.7DU (4.1%)	13.3DU (46.4%)
	2D interpolated vs. ream	30	0.50	1.7DU (4.7%)	14.8DU (56.7%)
	coincident vs. ream	11	0.72	1.6DU (0.1%)	15.1DU (49.8%)
summer	mapped vs. sonde	29	0.65	-3.0DU (-6.7%)	6.5DU (15.4%)
	2D interpolated vs. sonde	33	0.63	-4.3DU (-10.6%)	8.6DU (21.8%)
	coincident vs. sonde	11	0.75	-5.1DU (-13.1%)	9.1DU (24.6%)
	ream vs. sonde	41	0.74	-5.0DU (-12.2%)	6.7DU (15.9%)
	mapped vs. ream	29	0.73	2.7DU (8.6%)	6.1DU (17.2%)
	2D interpolated vs. ream	33	0.64	1.4DU (5.3%)	8.9DU (26.1%)
	coincident vs. ream	11	0.78	-0.5DU (-2.1%)	8.2DU (25.1%)

Table 3.1 summarizes the comparisons between OMI/MLS and REAM TCOs and their comparisons with ozonesondes in spring and summer 2005. Similar to the results in Chapter 2, the OMI/MLS TCOs have mean differences of approximately -5 ±11 DU compared with sondes with springtime having a more negative offset (~-6 DU) and a larger standard deviation of the differences (~14 DU) than those of summer 2005 (~-4 ± 8 DU). Compared with the comparisons between OMI/MLS and sonde TCOs, comparisons between REAM and sondes yield a more negative offset of -6.7 (-8.3 DU in spring and -5.0 DU in summer) and a significantly smaller standard deviation of the differences of 6.4 DU (5.7 DU for spring and 6.7 DU for summer). The correlation coefficients between OMI/MLS and sondes TCOs range from 0.64 for OMI/MLS 2D interpolated TCOs to 0.71 for OMI/MLS coincident TCOs during March-August 2005. The correlation coefficients between REAM and sonde TCOs are ~0.72 for the same period. The fairly large correlations between sonde TCOs and OMI/MLS and REAM TCOs indicate the relatively good quality of both REAM and OMI/MLS TCOs relative to ozonesonde measurements.

At the four ozonesonde stations, relative to REAM, OMI/MLS have offsets of ~2 ± 15 DU in spring and ~1 ± 8 DU in summer with OMI/MLS mapped TCOs having slightly smaller standard deviations of the differences in both seasons. The correlation coefficients between OMI/MLS and REAM TCOs range from 0.50 to 0.78 with highest coefficients in summer (~0.7) at the four stations. According to Table 3.1, using mappings and 2-D interpolations produces nearly three times more TCO data than using simple coincidence criteria. Mapped TCOs show a slightly smaller number of data than 2-D interpolated TCOs in Table 3.1. This is because the interpolation of OMI/MLS 2-D

interpolated TCOs to the sonde location includes data from an area larger than $1^o \times 1.25^o$ (averaging area size of the OMI/MLS mapped in this comparison). The relatively high correlation coefficients between REAM and OMI/MLS values justify the integration of REAM and OMI/MLS data for the study of TCO enhancements.

Figure 3.2 shows the vertical profile comparisons between TES and REAM for March, July, and August 2005, and TES averaging kernels have been applied to the REAM data. Based on Figure 3.2, TES and model ozone profiles have the best agreement at pressures > 300 mb. The difference between TES and REAM data is less than 15% at pressures ≥ 400 mb; however, the mean differences and standard deviations of the differences increase dramatically with altitude at pressures < ~300 mb. In August, the mean differences between 300 and 100 mb are within 100 ppb which is the best among the three months.

TES TCOs were compared with those from REAM and OMI/MLS TCOs for spring and summer 2005 (Table 3.2). The correlation coefficients between REAM and TES TCOs are about 0.6, while those between OMI/MLS TCOs and TES are around 0.5. REAM TCOs are lower than TES TCOs by 10.5 DU ± 8.9 DU, while OMI/MLS are lower by ~ 6 ± 10 DU during spring and summer. The large offset between model and TES could be explained by the overestimation in TES measurement in the upper part of the troposphere, in addition to the underestimation of REAM TCOs relative to sondes. Inter-comparisons of OMI/MLS and REAM TCOs at TES measurement locations indicate a mean difference of ~4±11DU which is higher than the similar comparison obtained at the four sonde locations because this comparison covers a larger latitude range of ~20^oN-60^oN.

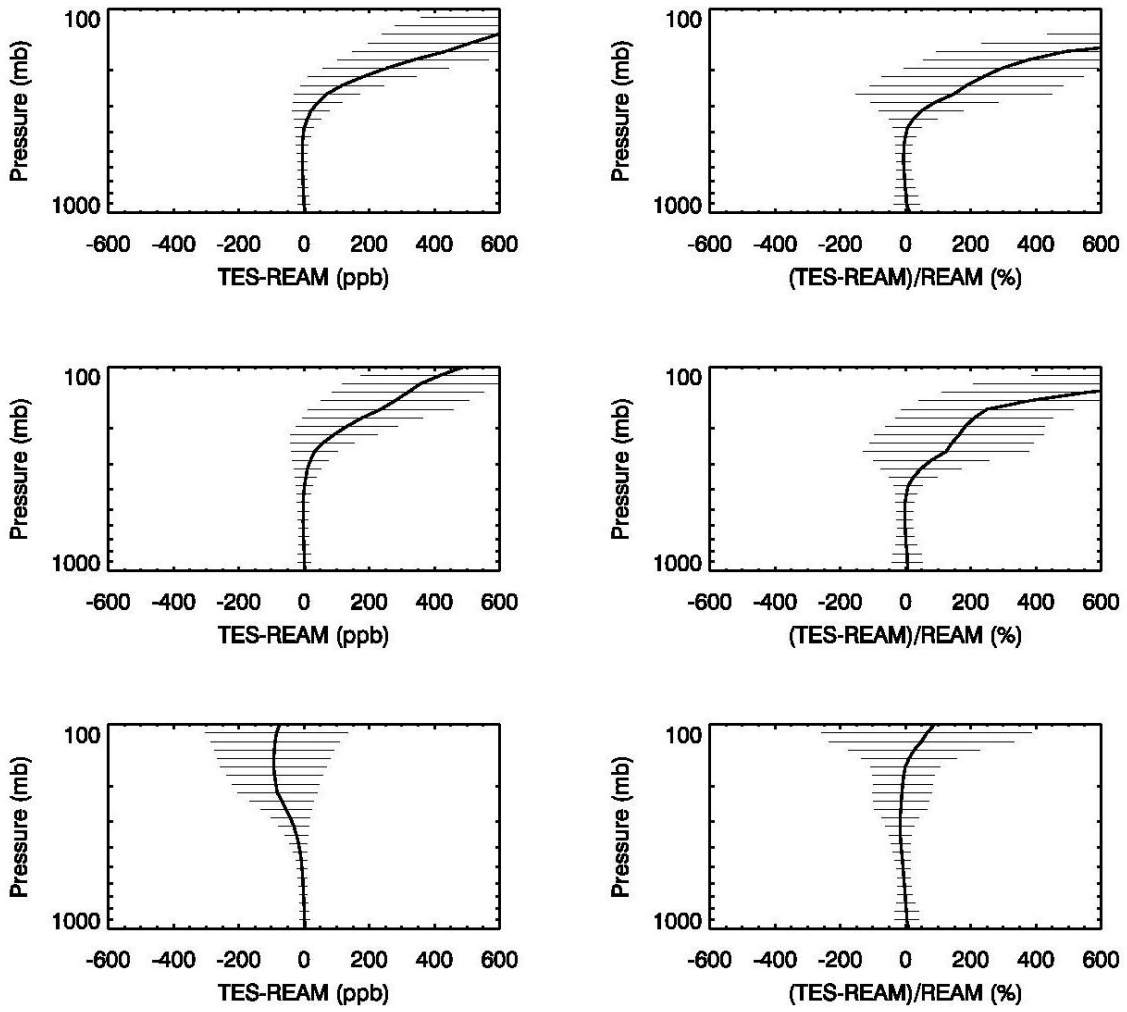

Figure 3.2: The vertical profile comparisons between TES and REAM (TES – REAM) for March (top panels), July (middle panels), and August (bottom panels) 2005. The thin lines indicate one standard deviation away from the means at both directions. TES averaging kernels were applied to the REAM data before the comparisons.

Table 3.2: Comparisons of OMI/MLS and REAM TCOs with TES TCOs at TES measurement locations and times.

period	TCOs	data #	correlation	Differences (OMI/MLS or REAM - TES)	
				mean [DU, (%)]	std [DU, (%)]
Mar.-Aug	mapped	3223	0.54	-6.2DU (-12.7%)	9.2DU (20.2%)
	2D interpolated	3297	0.51	-5.9DU (-12.4%)	10.0DU (22.8%)
	coincident	2834	0.47	-5.6DU (-11.4%)	11.0DU (25.3%)
	ream	3935	0.59	-10.5DU (-23.8%)	8.9DU (18.4%)
spring	mapped	728	0.46	-3.9DU (-7.3%)	11.8DU (27.7%)
	2D interpolated	833	0.51	-5.4DU (-11.6%)	11.6DU (27.6%)
	coincident	696	0.37	-5.7DU (-11.9%)	14.8DU (34.8%)
	ream	1010	0.57	-11.4DU (-26.6%)	8.7DU (18.0%)
summer	mapped	2495	0.59	-6.8DU (-14.2%)	8.2DU (17.0%)
	2D interpolated	2464	0.51	-6.1DU (-12.7%)	9.4DU (21.0%)
	coincident	2138	0.54	-5.5DU (-11.2%)	9.4DU (21.3%)
	ream	2925	0.6	-10.2DU (-22.9%)	9.0DU (18.4%)

The differences between OMI/MLS and REAM TCOs are latitude dependant and they are approximately 1 DU, 3 DU, 5 DU, and 7DU, respectively, for 20-30^{o}N, 30-40^{o}N, 40-50^{o}N, and 50-60^{o}N for spring and summer, 2005. The TCO values calculated from GEOS-CHEM are highly correlated with REAM TCOs with a typical correlation coefficient of 0.9 within each 10-degree latitude band during March - June 2005.

3.3 Monthly Average Distributions

3.3.1 Spring

The monthly mean TCO distributions based on REAM and OMI/MLS are shown in Figures 3.3 (in DU) and 3.4 (in VMR) for spring 2005. A band of TCO enhancement occurred in the extra-tropical region over North America and the adjacent oceans in spring. The band of TCO enhancement (in DU) is divided into one high over the Eastern North Pacific near the Baja Peninsula and the other over the Gulf of Mexico, Eastern United States and the adjacent North Atlantic (Figure 3.3). The TCO enhancements increased from March to May. The enhancement band (>35 DU in REAM data) was relative narrow in south-north direction in March. This band gradually widened and covered more Northeastern States and the adjacent North Atlantic Ocean from April to May. The model and satellite monthly mean TCOs agree reasonably well in these main distribution features, with satellite data showing more small-scale variations. Compared with the coincident products, mapping and 2-D interpolated products generally have a better agreement with model data in terms of locations and intensities of the TCO enhancements. Since the OMI/MLS coincident TCOs are not homogenously distributed in time and location, it is not unexpected that they show more small patchy highs

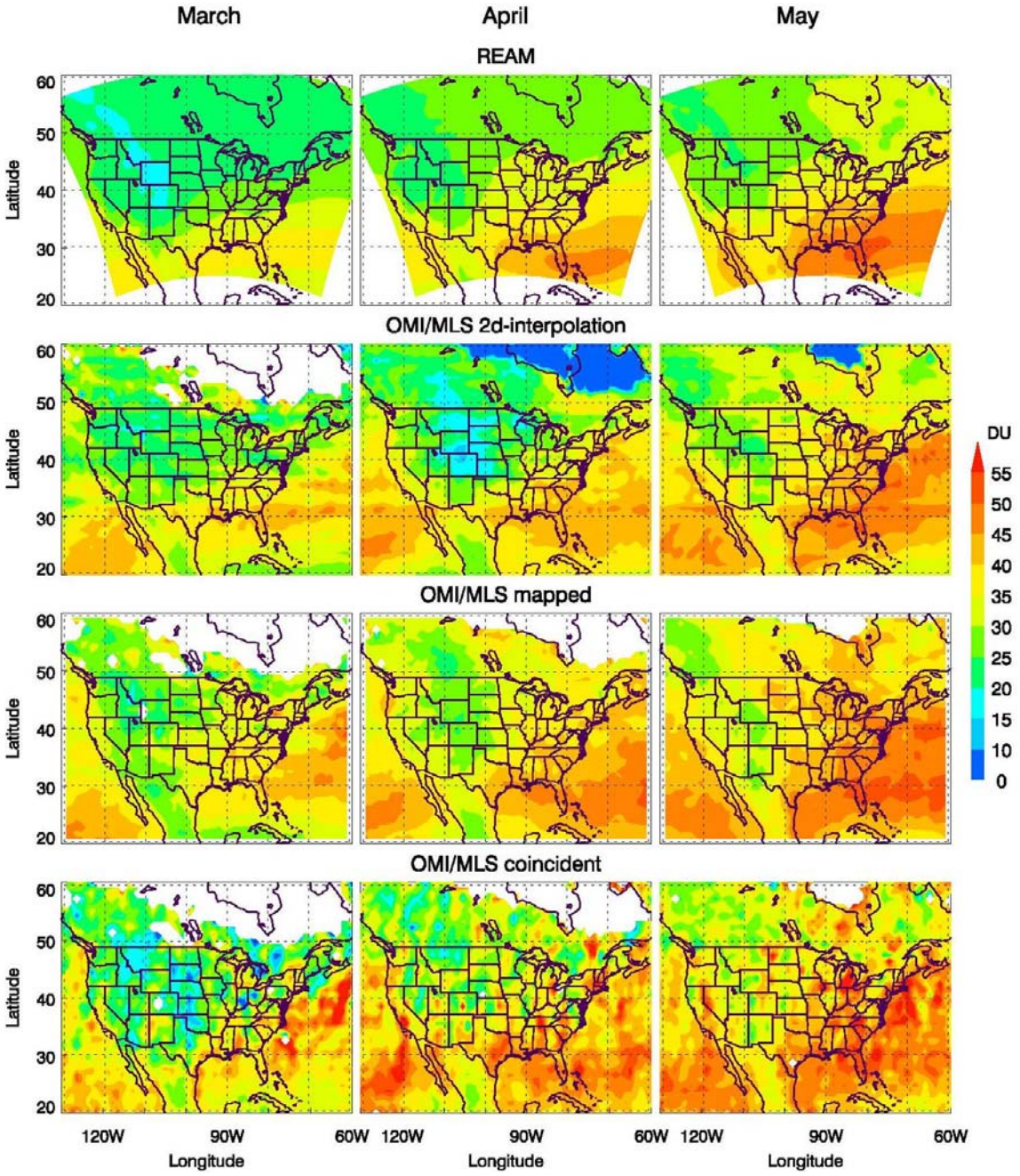

Figure 3.3: Monthly mean tropospheric ozone columns (in DU) based on REAM and OMI/MLS 2D interpolated, OMI/MLS mapped, and OMI-MLS coincident columns (left to right) for March to May (top down) 2005. REAM data are in their original model grids of 70 km × 70 km, and OMI/MLS residuals are in $1.25^{o} \times 1.25^{o}$ (latitude by longitude) grids.

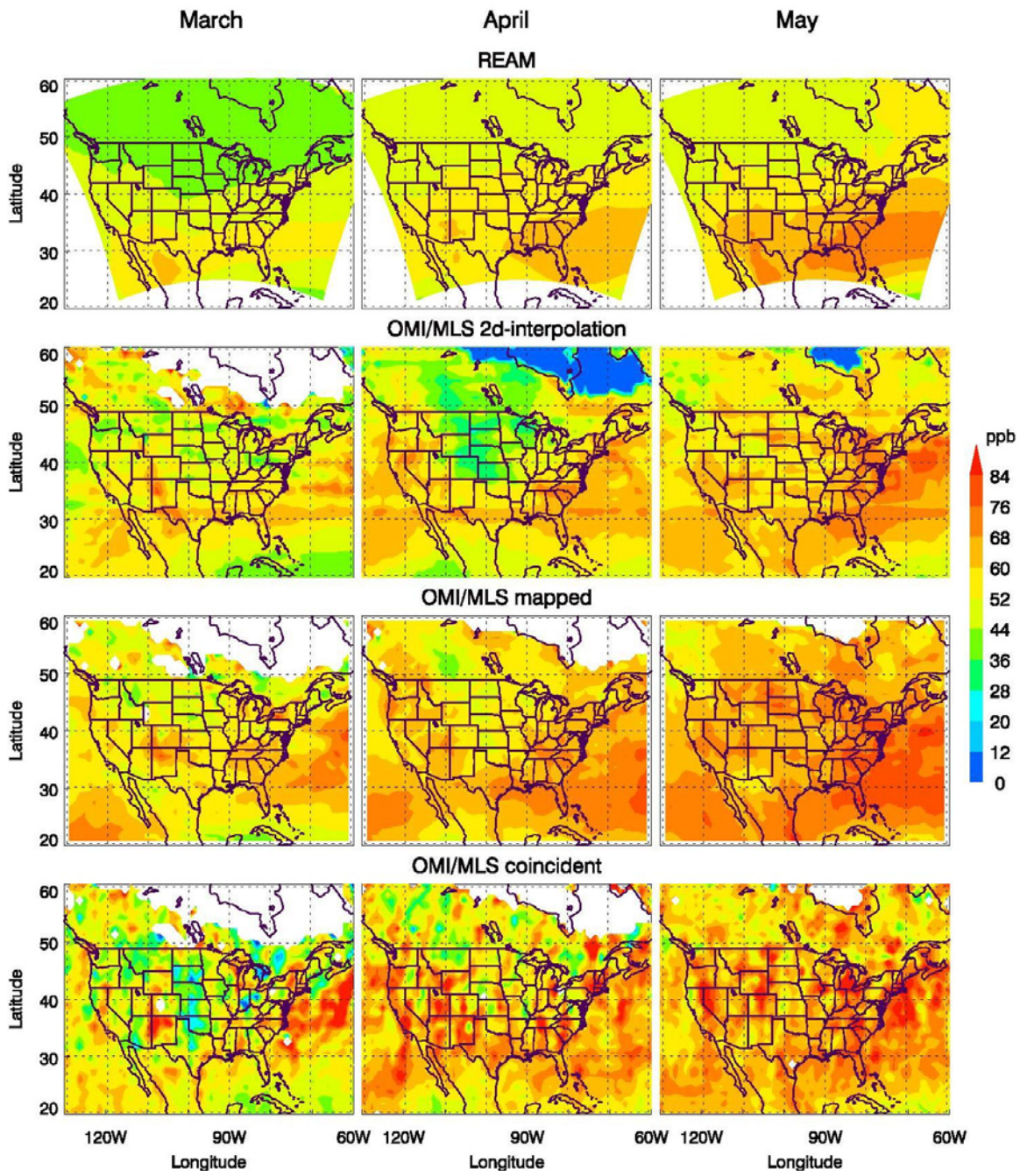

Figure 3.4: Monthly mean tropospheric ozone columns (in VMR) distributions based on REAM and OMI/MLS 2D interpolated, OMI/MLS mapped, and OMI-MLS coincident columns (left to right) for March to May (top down) 2005. REAM data are in their original model grids of 70 km × 70 km, and OMI/MLS residuals are in $1.25^{o} \times 1.25^{o}$ (latitude by longitude) grids.

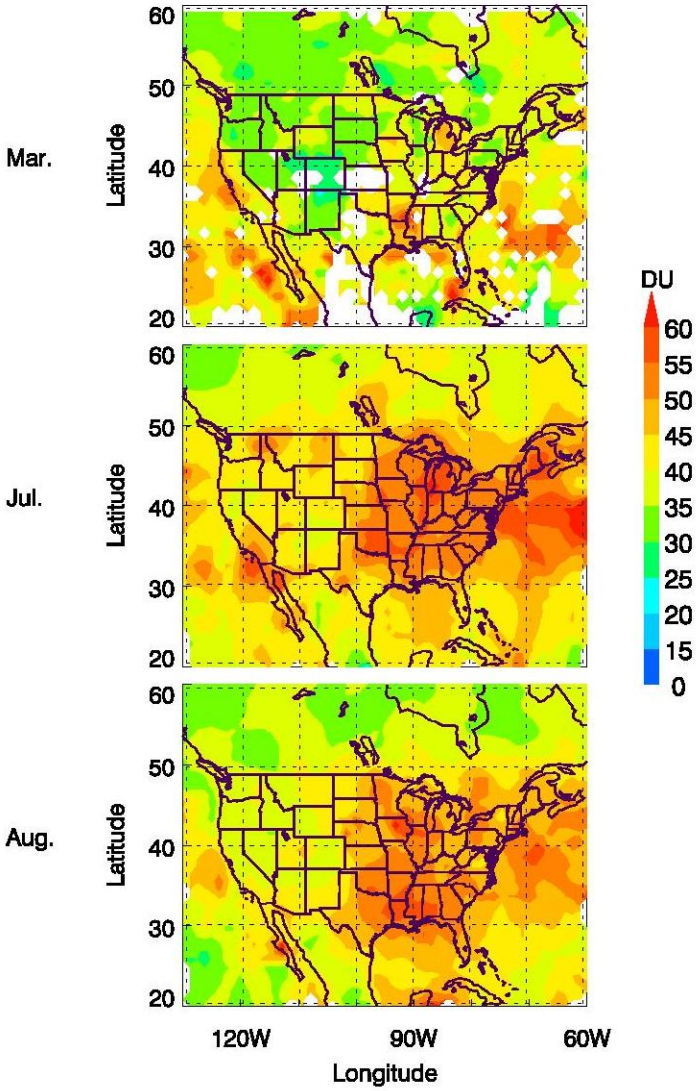

Figure 3.5: Monthly mean TES tropospheric ozone columns (in DU) over North America for March (top), July (middle), and August (bottom) 2005. A Barnes smoothing routine with a 250 km influencing distance was used to bin the data into $1^{o}\times1.25^{o}$ latitude by longitude grids. Note that there is no enough data to produce monthly mean TCO maps for April and May 2005.

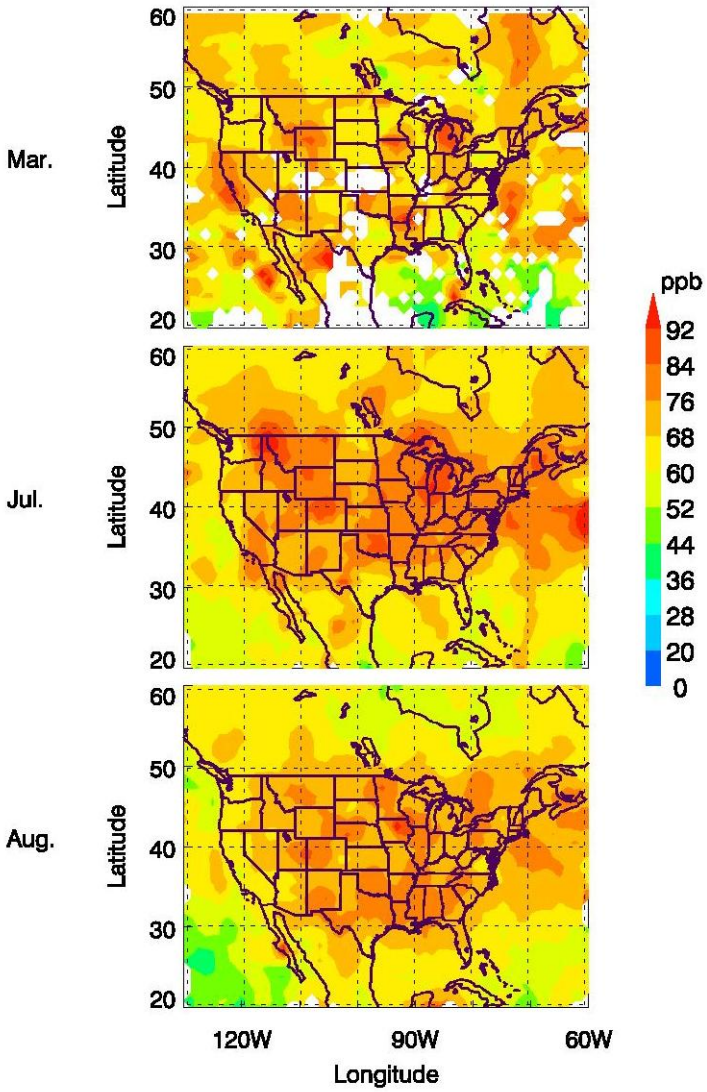

Figure 3.6: Monthly mean TES tropospheric ozone columns (in VMR) over North America for March (top), July (middle), and August (bottom) 2005. A Barnes smoothing routine with a 250 km influencing distance was used to bin the data into $1^{o} \times 1.25^{o}$ latitude by longitude grids.

spreading in the enhancement regions as indicated by model and the other two types of OMI/MLS. Comparisons of monthly means between OMI/MLS and REAM TCOs indicate that relative to REAM the standard deviations of the differences are ~5 DU for OMI/MLS mapped and ~ 8 DU for 2D interpolated TCOs. These standard deviations of the differences are smaller than those calculated based on daily values (Table 3.1). The larger standard deviation (~8 DU versus ~5 DU) of the differences for coincident TCOs is due to their averaging over a smaller number of data. The monthly means of the OMI/MLS mapped, 2-D interpolated, and coincident TCOs were computed by averaging over, on average, 16, 14, and 4 (represented as N) daily values, respectively, in each data grid; hence, the uncertainties of the monthly means are expected to be reduced by a factor of $\frac{1}{\sqrt{N}}$ from those of daily values (see satellite/sonde comparisons in Table 3.1).

Mapping of MLS data produces slightly better quality TCOs than the 2-D interpolation since OMI/MLS mapped TCOs were calculated from OMI and mapped MLS data having the exactly the same times and locations, while 2-D interpolated TCOs resulted from OMI and interpolated MLS data corresponding to different times in a day. Since OMI/MLS mapped TCOs could have as high a spatial resolution as level-II ungridded OMI measurements, the OMI/MLS mapped TCOs tend to be spatially more variable compared with the 2D-interpolated TCOs. On the other hand, the 2-D interpolation technique preserves the observed MLS data, and as a result its TCOs may be more accurate near the MLS measurement locations.

The TES monthly mean TCOs in March (no enough data in April and May) 2005 are presented in the top panels of Figures 3.5 (in DU) and 3.6 (in VMR). Despite the relatively high bias, TES data also show small patchy high values around the TCO

enhancement regions (i.e., around the Baja Peninsula, near the West Coast of California, and over the southeastern United States) that are indicated by the REAM and OMI/MLS.

3.3.2 Summer

The monthly mean TCOs from REAM and OMI/MLS in June, July, and August 2005 are shown in Figures 3.7 (in DU) and 3.8 (in VMR). Similar to what was found for spring, satellite data and model simulations both show two distinct TCO maxima. The locations of the enhancement regions shifted northward relative to those in spring. The TCO high over the Eastern Pacific Ocean elongates northward to the West Coast of California. The OMI/MLS shows some enhancements extending farther north to the southeastern Pacific Ocean which is west of Washington State. In general, Model and OMI/MLS TCOs agree well in the locations of the enhancements over the Eastern States, although they disagree in the relative enhancement intensity in June. The strongest TCO enhancement occurs in June based on OMI/MLS; while it is in July based on REAM. In June, OMI/MLS TCOs are approximately 5-6 DU higher than the REAM TCOs in daily values between 30-50^{o}N, and the monthly mean maps reflect this offset. In July and August, satellite TCOs are approximately 1 DU lower at 20^{o}-40^{o}N and approximately 3-5 DU higher at 40^{o}-50^{o}N compared with REAM. Even though the statistics based on daily values do not indicate significant differences among the three types of OMI/MLS TCOs, monthly mean maps of 2-D interpolated TCOs show lower TCOs in the regions of TCO enhancement over the Eastern States. A possible explanation for the relatively low 2-D interpolated TCOs is the non-linear behavior of the ozone distributions between two

orbits (e.g., a TCO high occurring between two orbits), which could have effects on the interpolation results especially at areas with local TCO maxima.

The TES monthly mean TCOs for July and August are shown in the middle and bottom panels of Figures 3.5 (in DU) and 3.6 (in VMR). TES monthly mean TCOs agree well with those from OMI/MLS and REAM in the locations of enhancements. TES data also show a similar monthly TCO trend as those seen in OMI/MLS and REAM, with the intensity of TCO enhancements decreasing slightly from July to August.

OMI/MLS indicate that the tropospheric ozone columns peak in June, which is probably the result of a dramatic increase in the photochemical production in this month in addition to the still active stratosphere-tropospheric exchange at this time of the year. However, the June TCO maximum is lacking in the model simulations. Tropospheric ozone variation is determined by the stratospheric-tropospheric exchange, horizontal ozone transport, and local ozone chemistry production associated with lightning, surface NOx emission, and so on. Since the model simulations have a low bias (above 350 hPa) due to the strong dependence on the upper boundary conditions [Choi et al., 2007], a more pronounced underestimation of the stratospheric contribution in this month is the possible cause of the underestimation of the TCOs in June. It might also be possible for REAM to over-predict the decreases from spring into summer in surface CO and NO_x concentration or the lightning and soil emissions produce slightly too much NO_x in July and August and/or not enough NOx in June. The monthly variations of REAM simulations have also been suggested by Figure 3.1 in Huntsville and Rhode Island stations the offsets between REAM and sondes changed from negative to positive in July, which indicates the possible increase of ozone concentration in REAM relative to

ozonesonde over the Eastern United States (the TCO enhancement region) in this month. This REAM TCO increase relative to sonde in July is not consistent with the other months studied. Nevertheless, further investigation is needed to determine the discrepancy in the monthly variations between OMI/MLS and REAM during summer.

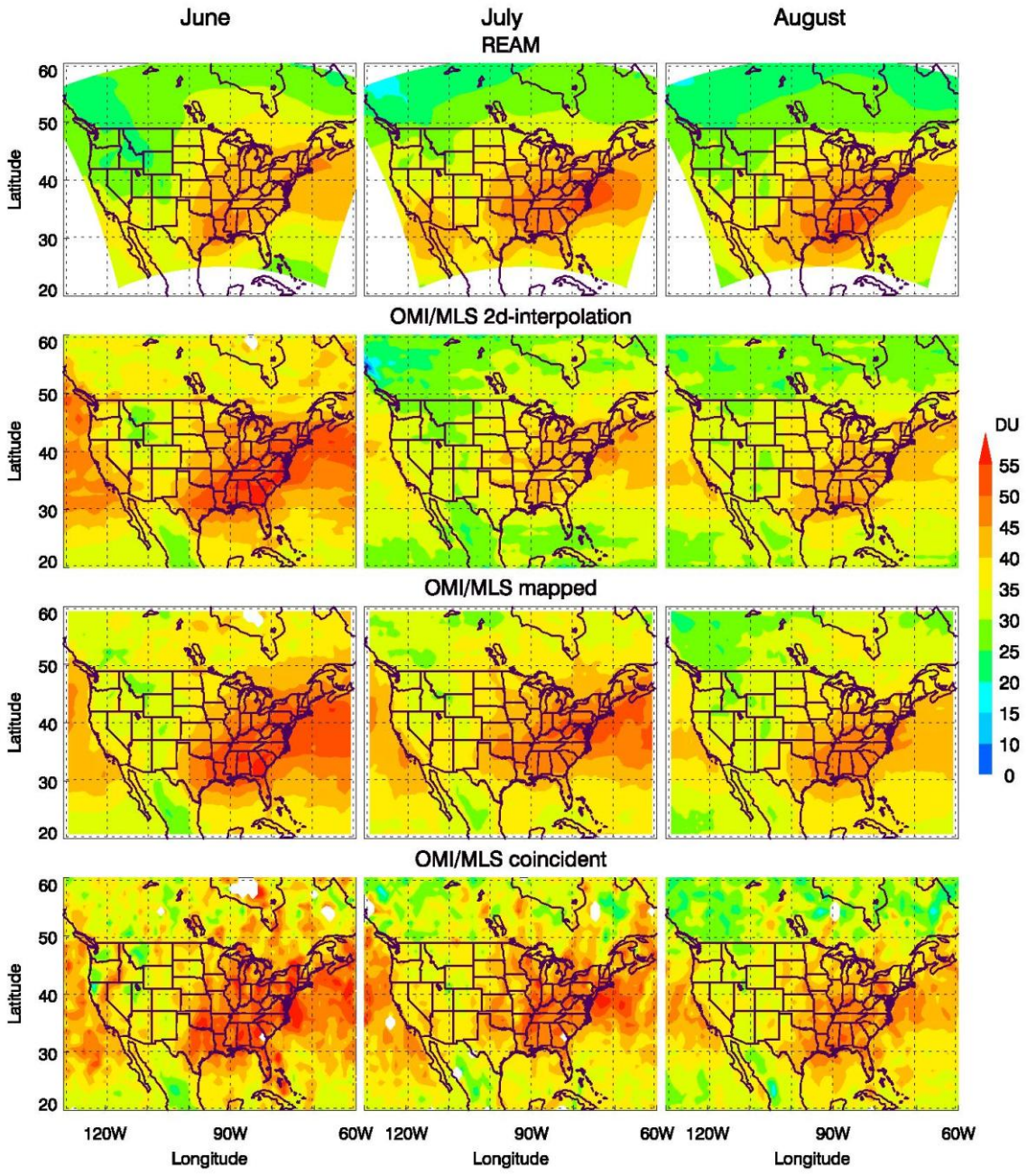

Figure 3.7: Monthly mean tropospheric ozone columns (in DU) based on REAM and OMI/MLS 2D interpolated, OMI/MLS mapped, and OMI/MLS coincident columns (left to right) from June to August (top down) 2005. REAM data are in their original model grids of 70 km × 70 km, and OMI/MLS are in $1.25^{o} \times 1.25^{o}$ (latitude by longitude) grids.

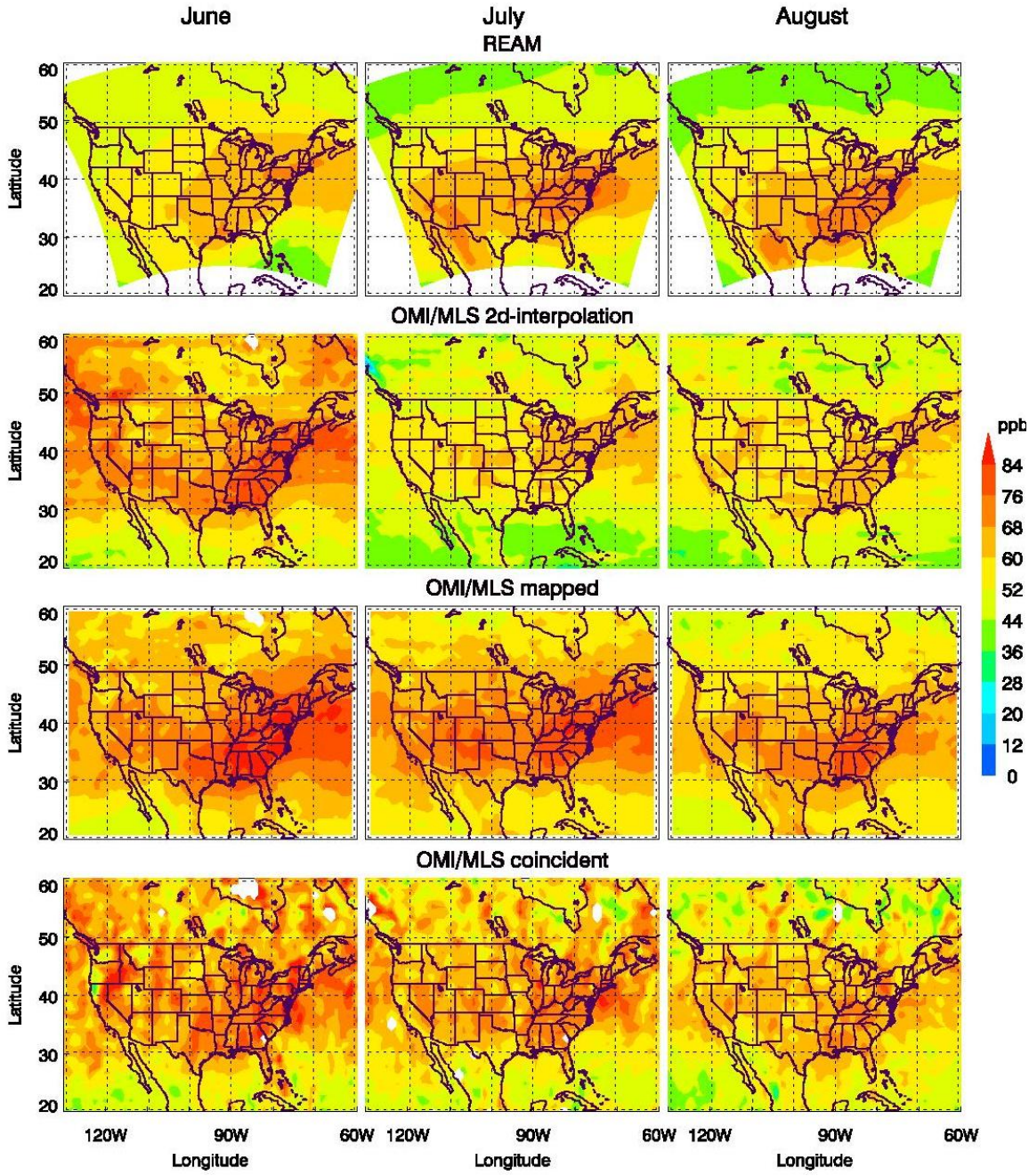

Figure 3.8: Monthly mean tropospheric ozone columns (in VMR) distributions based on REAM and OMI/MLS 2D interpolated, OMI/MLS mapped, and OMI-MLS coincident columns (left to right) from June to August (top down) 2005. REAM data are in their original model grids of 70 km × 70 km, and OMI/MLS are in $1.25^{o} \times 1.25^{o}$ (latitude by longitude) grids.

3.4 A Spring Case Study

To illustrate the evolution of the TCO enhancement over the Baja peninsula, time series of REAM and OMI/MLS TCOs averaged over a $5^o \times 5^o$ (longitude by latitude) area (23-28^{o}N and 114-109^{o}W) over the Baja peninsula (Mexico) are presented in Figure 3.9 for spring 2005. OMI/MLS mapped TCOs follow the variations of model TCOs reasonably well with a correlation coefficient of 0.86 between the two time series during spring. OMI/MLS 2-D interpolated and OMI/MLS coincident TCOs have lower correlation coefficients of 0.45 and 0.2, respectively, with REAM TCOs. Model and OMI/MLS mapped TCOs have a relatively high correlation coefficient maybe because they correspond better in terms of timing than 2-D and coincident products since model daily averages were obtained from averaging of hourly data and an OMI/MLS mapped value in the time series was obtained by averaging TCOs corresponding to different times in a day. The uncertainties of the daily area mean values are 1.82 ± 1 DU, 4.05 ± 2.77 DU, 4.40 ± 2.06 DU, and 4.88 ± 2.33 DU, respectively, for REAM, OMI/MLS coincident, OMI/MLS interpolated, and OMI/MLS mapped TCOs. The uncertainty of each daily area mean datum is represented by one standard deviation of the data used for the averaging. The relatively large uncertainties in the OMI/MLS data in the time series may be mainly associated with the large uncertainties in the derived individual TCO values. Model and OMI/MLS results indicate a high TCO event occurring over the BAJA peninsula in every 5 to 10 days with the high values typically persisting for 2 to 3 days. In REAM simulations, at the second week of March, there was a pronounced TCO maximum over the Baja peninsula with the daily mean TCO values approaching 50 DU, and the TCO high persisted for a few days. Daily mean REAM TCOs on the day of peak

TCO values (March 08, 2005) are shown in Figure 3.10. This TCO enhancement is the strongest of all in the spring enhancement in 2005 in REAM over North America. According to Figure 3.9, OMI/MLS mapped and 2-D interpolated TCOs also captured the enhancement tendency, although this TCO enhancement is not the strongest in the OMI/MLS data during spring 2005. A six-day period was chosen for the spring case study with the first six days (Period 1: March 8-13, 2005) associated with the unusually high TCO event in REAM over the Baja peninsula. The following six-day period (Period 2: March 14-19, 2005) was chosen for comparison purposes based on the REAM TCOs. Note that the case study period selections were constrained by a limitation that data from about six days are required to have a complete OMI/MLS TCO coverage over the North America due to the clear sky constraint.

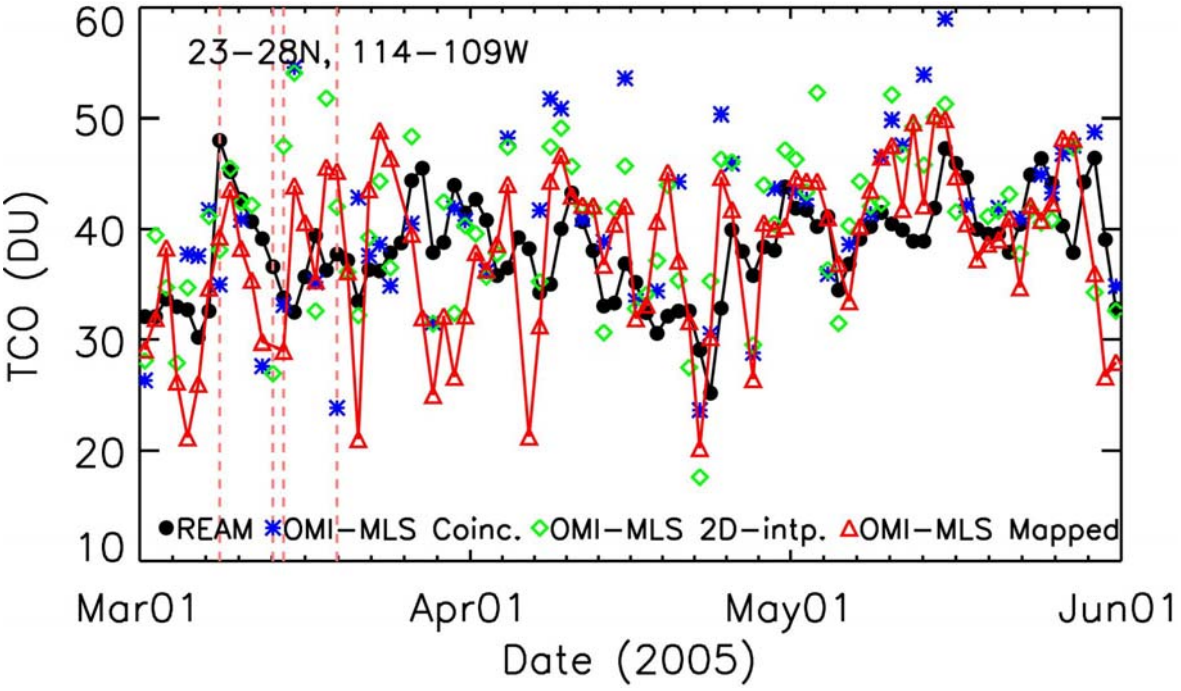

Figure 3.9: Time series of area averaged tropospheric ozone columns for a $5^{o}\times5^{o}$ longitude by latitude area (23-28^{o}N and 114-109^{o}W) based on REAM (black circles), OMI/MLS mapped (red triangles), OMI/MLS 2D interpolated (green diamonds), and OMI/MLS coincident (green stars) columns for spring 2005. Data with center of their grids locating within the averaging area were included in the averaging. The ungridded OMI/MLS mapped TCOs were used in this calculation.

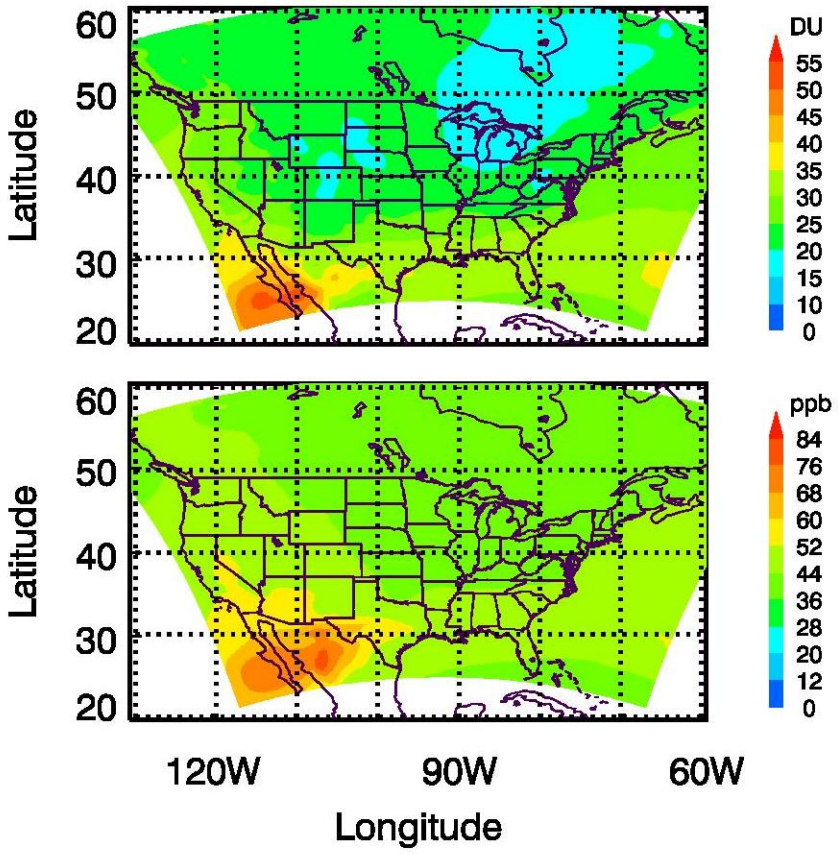

Figure 3.10: The daily mean tropospheric ozone columns from REAM in Dobson units (top panel) and in volume mixing ratios (bottom panel) for March 8, 2005.

3.4.1 Period Mean Column Distributions

The averaged TCOs for periods 1 and 2 based on REAM, OMI/MLS, and TES data are presented in Figures 3.11 (in DU) and 3.12 (in VMR). OMI/MLS, TES, and REAM all show TCO enhancements over the south of the Baja peninsula and over the West Coast of California with the enhancements over the West Coast of California clearly stronger in periods 1 than in period 2. The less consistent changing tendency between OMI/MLS and REAM over the Baja is associated with that the enhancement over Baja is located slightly east of the REAM enhancement location. The statistics based on the daily value comparisons in March show that OMI/MLS mapped and 2-D interpolated TCOs are higher than REAM TCOs by ~ 1 DU for 20-30^{o}N, and ~ 4 DU (~5.5 DU for mapped and ~ 3.5 DU for 2-D interpolated) for 30-40^{o}N. Figure 3.11 indicates ~5 DU higher OMI/MLS TCOs relative to REAM in the enhancement regions, which is consistent with the statistics obtained from the daily value comparisons in March. The ~ 6 DU high biases in TES TCOs relative to OMI/MLS are not very obvious in Figure 3.11; this might be because the large offset is mostly contributed by the discrepancy between TES and OMI/MLS when OMI/MLS TCOs values are lower, this might be related to the upper tropospheric contributions from the stratosphere in the TES retrievals.

Although satellite and model data agree reasonably well in period 1, large disagreements between REAM and OMI/MLS TCOs were found over the High Plains region (UTAH, Colorado, Wyoming, Northern New Mexico, and northern Arizona) in period 2. Model and TES indicate no TCO enhancement tendency from periods 1 to 2 in this region; however, the OMI/MLS shows a strong increase from periods 1 to 2. Figure

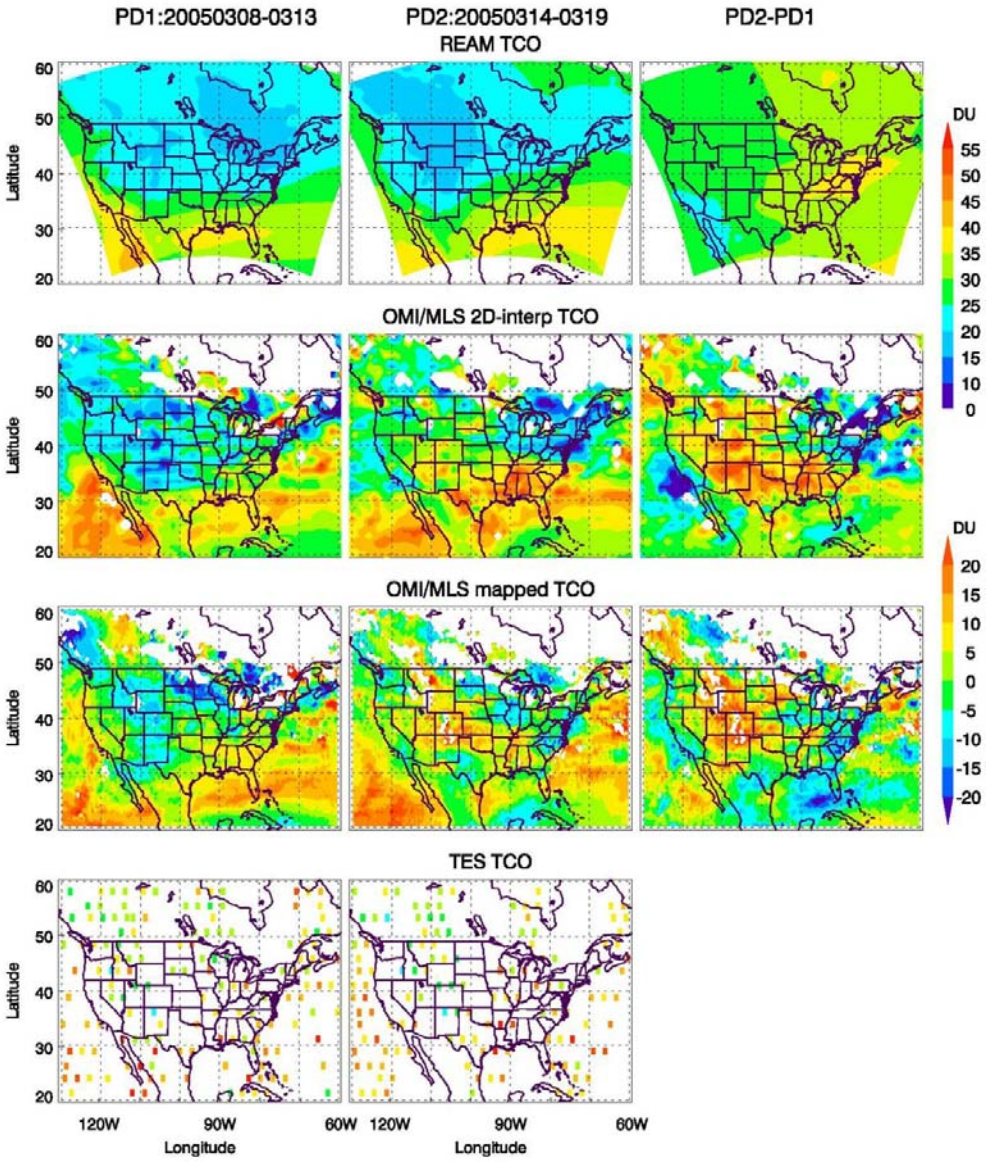

Figure 3.11: Six-day mean tropospheric ozone columns (in DU) during period 1 (PD1: March 8-13, 2005; left) and period 2 (PD2: March 14-19, 2005; middle), and the changes of TCOs from period 1 to period 2 (PD2-PD1, right) based on REAM, OMI/MLS, and TES (top down). The OMI/MLS mapped TCOs were binned into $0.5^{o} \times 0.5^{o}$ (latitude by longitude) grid.

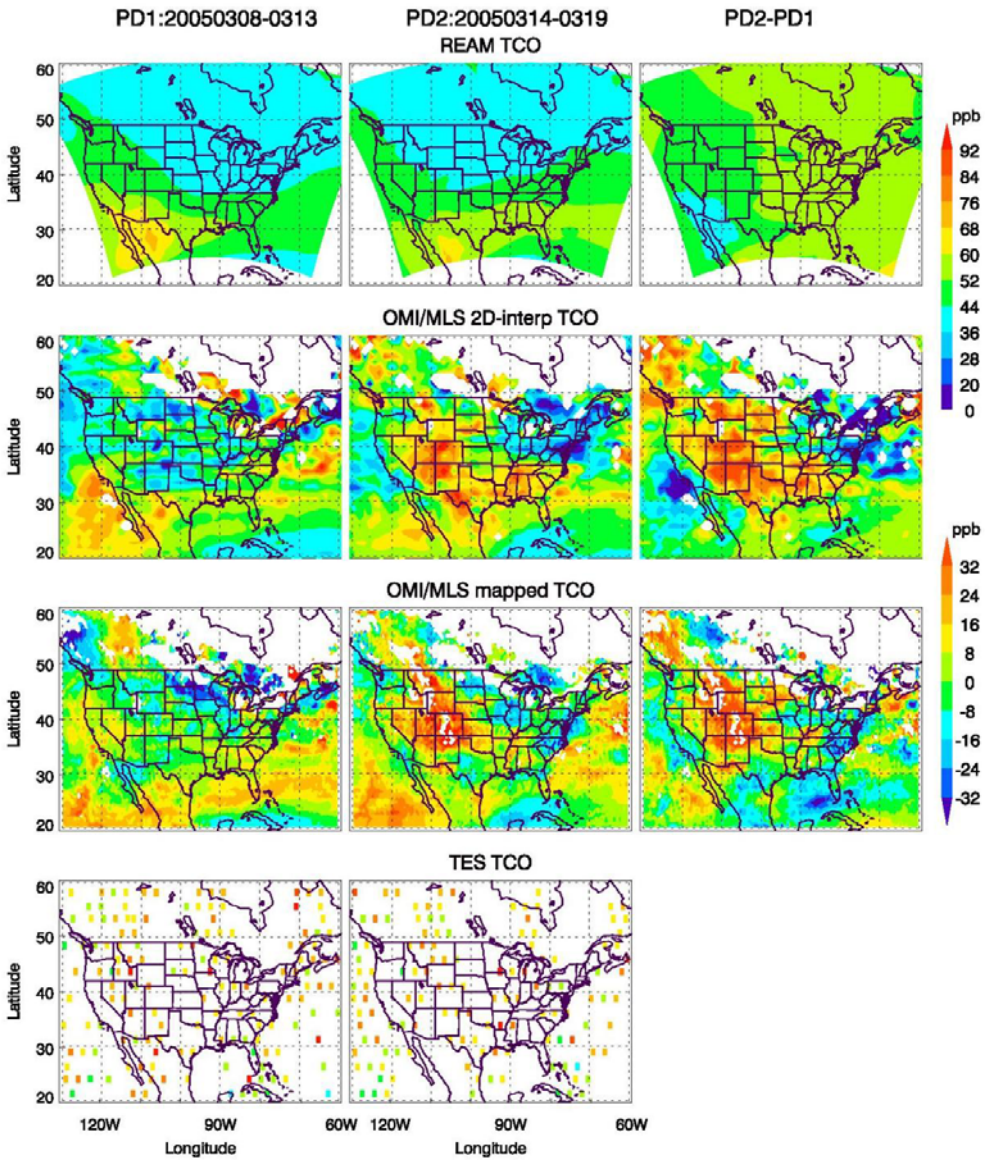

Figure 3.12: Six-day mean tropospheric ozone columns (in VMR) during period 1 (PD1: March 8-13, 2005; left) and period 2 (PD2: March 14-19, 2005; middle), and the change of TCOs from period 1 to period 2 (PD2-PD1, right) based on REAM, OMI/MLS, and TES (top down). The OMI/MLS mapped TCOs were binned into $0.5^{o} \times 0.5^{o}$ (latitude by longitude) grid.

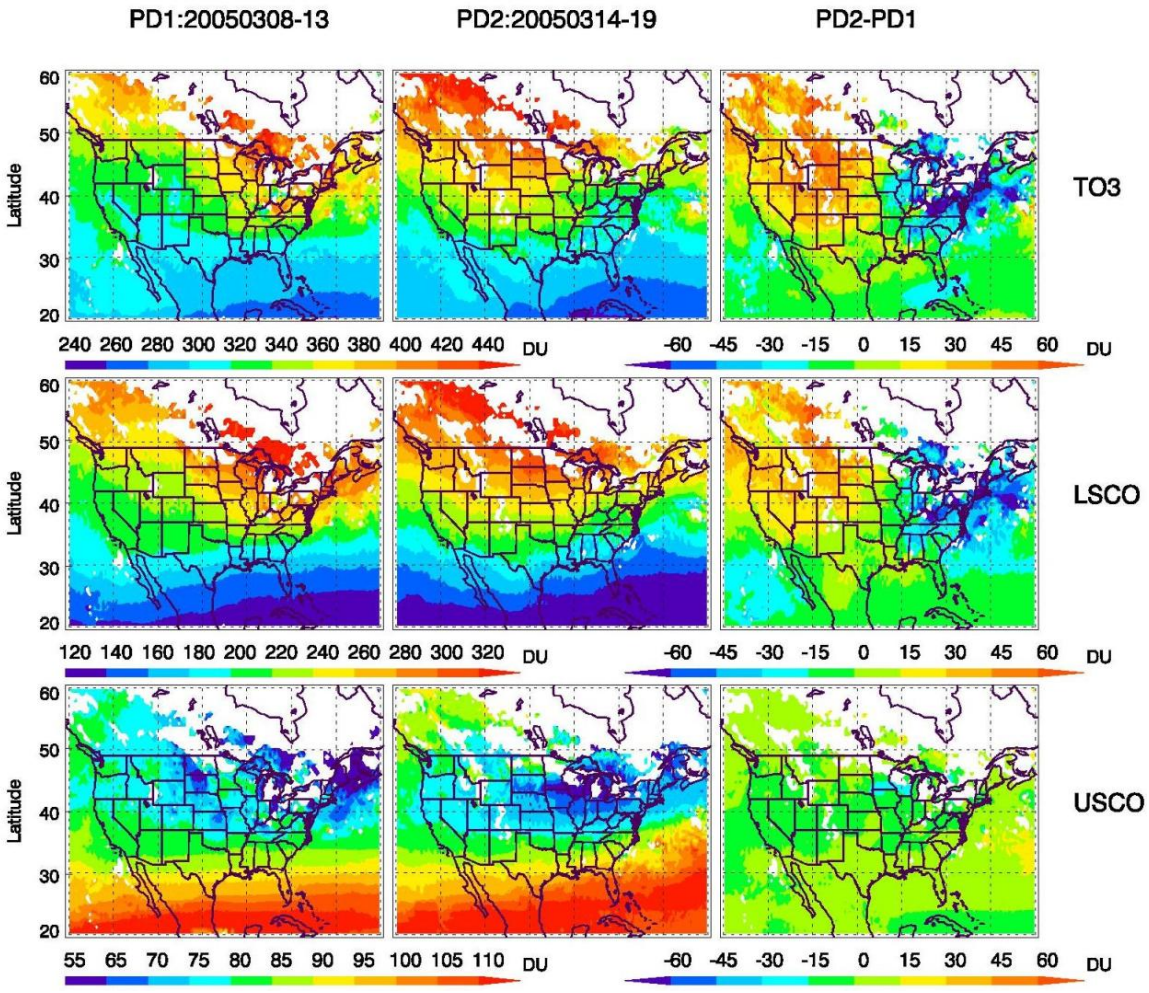

Figure 3.13: The OMI total ozone (TO3, top), lower stratospheric ozone column (LSCO, tropopause - ~18mb) (middle), and stratospheric ozone column above ~18 mb (USCO, bottom) corresponding to the OMI/MLS mapped TCOs shown in Figure 3.11. Data in period 1 (PD1: March 8-13, 2005), period 2 (PD2: March 14-19, 2005) and the changes from period 1 to period 2 (PD2-PD1), respectively, are presented in panels from left to right.

3.13 excludes the possibility that the OMI/MLS TCO enhancement over the mid-western US is due to abnormally high values in OMI or abnormally low values in MLS data alone. A couple of ozonesonde profiles measured at Boulder agree with OMI/MLS by showing a large increase of ozone from March 11 to March 18 for pressure < ~700 mb (Figures not shown). In addition, the tropopause pressure gradients presented in the mid-western U.S. during period 2 but not period 1 suggest that near tropopause dynamics might be responsible for the TCO enhancement. It is possible for REAM to underestimate over this region in period 2 due to its relatively large uncertainty in the upper troposphere in the presence of active dynamics. Further investigation is necessary to determine the cause of the disagreement between OMI/MLS and REAM TCOs over the High Plains region.

The contribution of ozone from different vertical layers to the TCO enhancements was analyzed using REAM and TES ozone on a pressure surface and REAM ozone column amounts in four tropospheric layers. Typical TES averaging kernels indicate that the retrieved TES mean ozone mixing ratios on the 750 mb pressure surface receive most weight from in the lower and mid troposphere. Therefore, the ozone in the lower and mid troposphere can be explicitly estimated by the TES and REAM (after applying TES averaging kernels) ozone on 750 mb (see Figure 3.14). An enhancement of ozone is evident over the Baja peninsula and Northern Mexico. This suggests that a TCO enhancement is resulting from the high ozone concentrations in the lower and/or mid troposphere. The enhancement in period 1 indicated by TES is stronger than that indicated by REAM on the 750 mb pressure surface due to the positive relative bias of TES data.

Ozone column amounts in four tropospheric layers (surface-750 mb, 600-750 mb, 400-600 mb, and 400 mb-tropopause) were calculated using REAM and the six-day mean values are presented in Figures 3.15 (in DU) and 3.16 (in VMR). Both figures indicate that the TCO enhancement over the Baja peninsula is dominated by the high ozone in the near tropopause layer (400 mb –tropopause). The ozone column maximum in the near tropopause layer is located over the Northern Mexico which is west of where the TCO maximum appears. The shifting of the TCO maximum location from the upper layer column maximum location is associated with topography effects (high elevation lead to less air below 750 mb) over Northern Mexico. Figure 3.17 shows the correlations between TCOs and surface-750 mb ozone columns based on REAM hourly data. Strong negative correlations were found between the surface layer ozone and TCOs over the southeast of the Baja peninsula where the TCO maximum is located, indicating that the maximum is largely contributed by the high ozone in the mid and/or upper troposphere.

As shown in Figure 3.16, the enhancements over the West Coast of California are most pronounced in the surface layer (surface -750mb) and in the near tropopause layer in period 1. The strong correlations ($R>0.6$) between TCOs and surface-750 mb ozone columns over the West Coast of California (Figure 3.17) suggest that the TCO enhancement in this region is largely contributed by ozone in the lower troposphere.

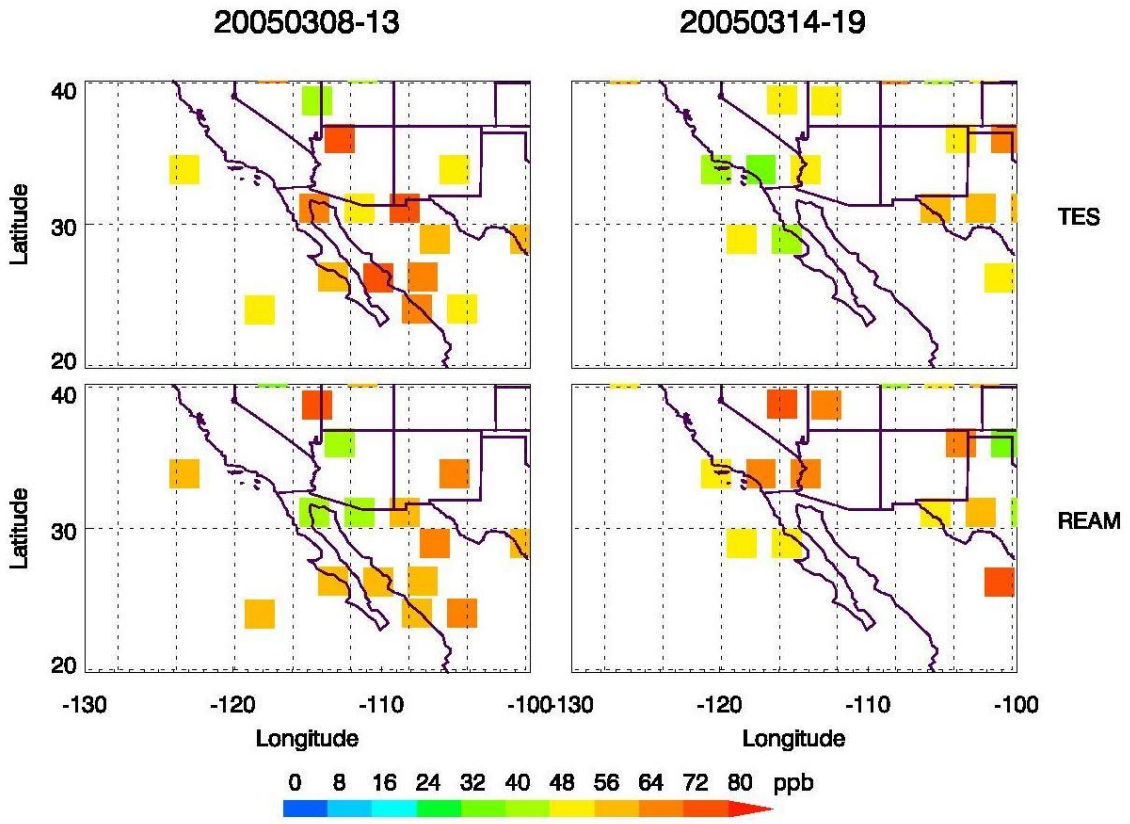

Figure 3.14: TES and REAM mean volume mixing ratios on 750 mb pressure surface during periods 1 (March 8-13, 2005; left) and 2 (March 14-19, 2005; right). TES averaging kernels were applied to REAM data. Each TES datum was assigned a pixel size of $2.5^{o} \times 2.5^{o}$ (longitude by latitude) to enhance the visibility of the figure.

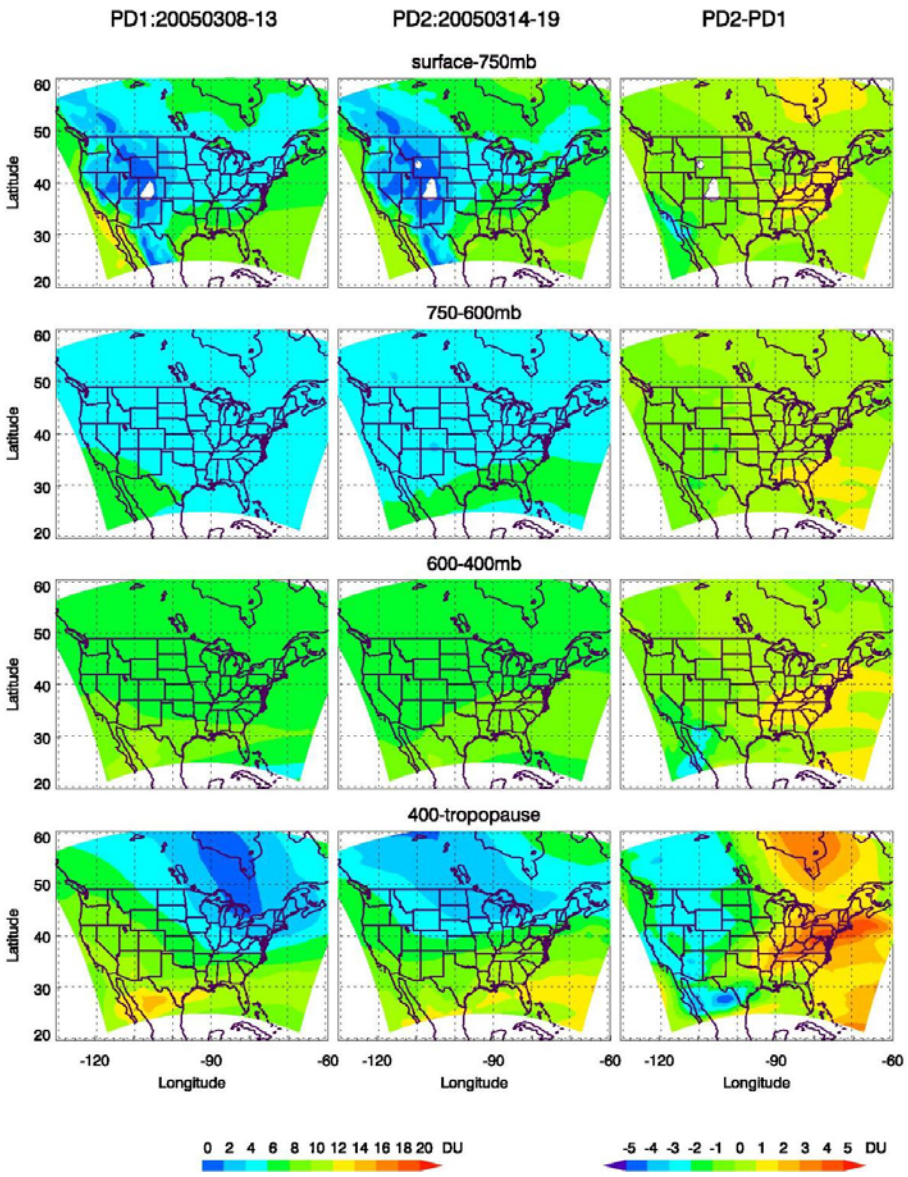

Figure 3.15: The ozone columns (in DU) in four tropospheric layers: surface-750mb, 600-750 mb, 400-600 mb, and 400 mb-tropopause (top down) based on REAM simulations during period 1 (PD 1: March 8-13; 2005; left) and period 2 (PD1 :March 14-19, 2005; middle). The changes in the column amounts from periods 1 to 2 are in the right panels. The color bar on the left corresponds to panels in the first two columns, and the color bar on the right corresponds to the panels in the third column.

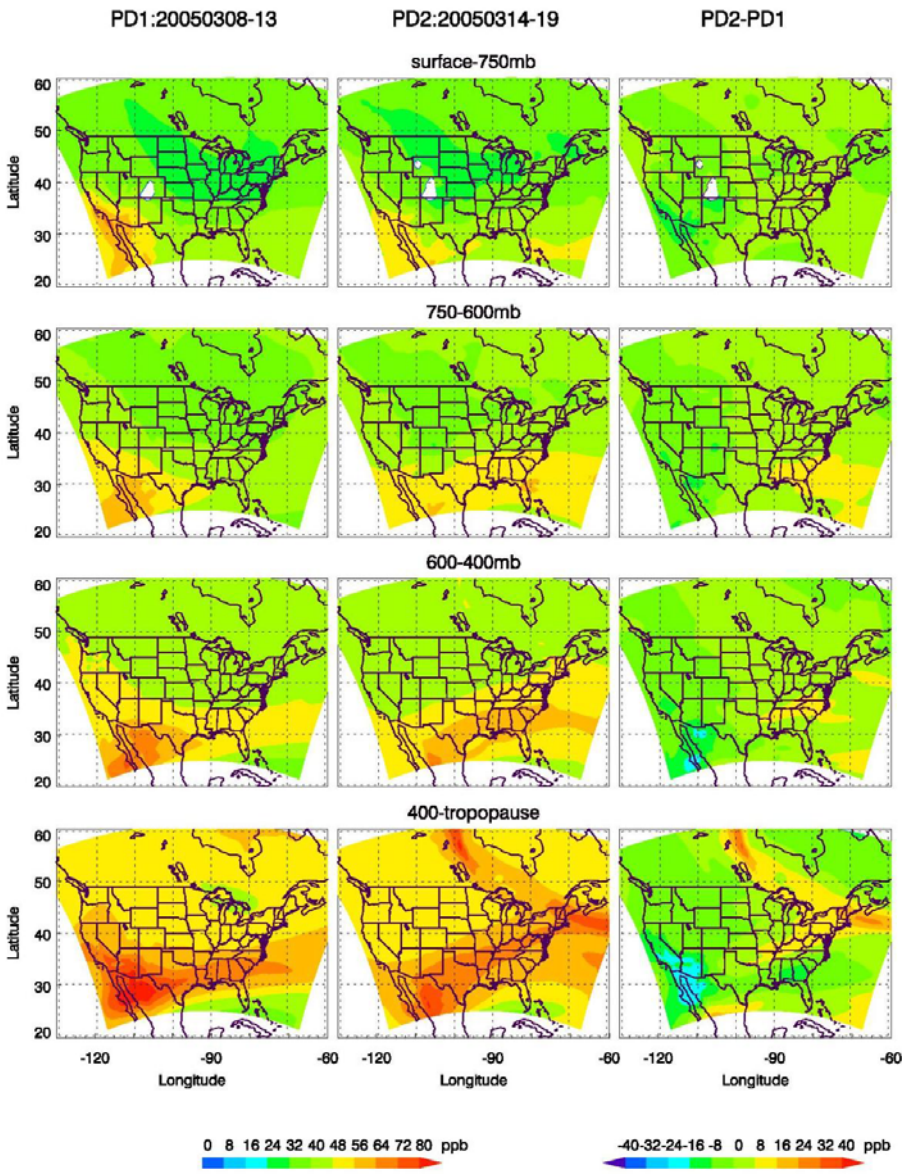

Figure 3.16: The ozone columns (in VMR) in four tropospheric layers: surface-750mb, 600-750 mb, 400-600 mb, and 400 mb-tropopause (top down) based on REAM simulations during period 1 (PD 1: March 8-13; 2005; left) and period 2 (PD1 :March 14-19, 2005; middle). The changes in the column amounts from periods 1 to 2 are in the right panels. The color bar on the left corresponds to panels in the first two columns, and the color bar on the right corresponds to the panels in the third column.

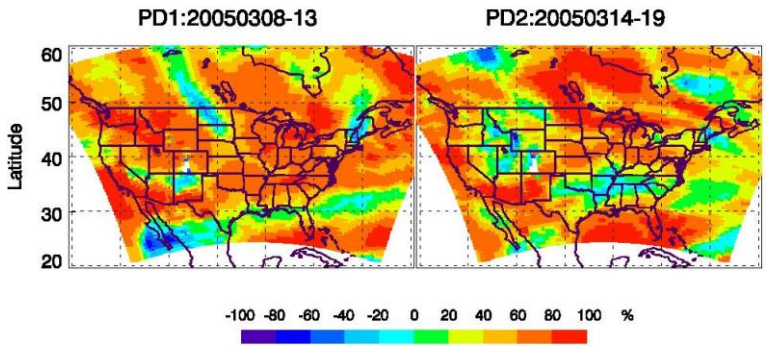

Figure 3.17: Correlation coefficients between TCOs and surface-700 mb ozone columns (in DU) for periods 1 (March 8-13, 2005; left) and 2 (March 14-19, 2005; right).

3.4.2 Stratospheric Intrusions and Wave-breaking

Vertical cross-sections were used to identify the presence of stratospheric intrusions in the regions with TCO enhancements: over the Baja peninsula and over the West Coast. The association of wave breaking with the stratospheric intrusions was investigated using PV on the 350K surface.

Figure 3.18 shows pressure by latitude cross-sections of ozone concentration along the 110^{o}W (which crosses the southern Baja peninsula) and 120^{o}W (which crosses the West Coast of California) meridians in periods 1 and 2 based on REAM simulations. On 110^{o}W meridian, the downward transport of ozone rich air from the stratosphere and the upper troposphere down to the mid and lower troposphere is evident in the subtropical region (20-35^{o}N). In period 1 (Figure 3.18a), a tongue of ozone-rich air (> 60ppb) extends from stratosphere down to ~700 mb causing the TCO elevation over the Baja peninsula region. The same cross section map (Figure 3.19) on the day of peak TCOs (March 08, 2005) more clearly shows the stratospheric air with ozone concentrations higher than 100 ppb extending down to mid-troposphere. In contrast, no substantial

stratospheric intrusions were indicated by REAM during period 2 in the same cross sections for period 2 (Figure 3.18b).

Maps c and d in Figure 3.18 indicate a slight influence of stratospheric transport near the tropopause in both periods across the West Coast of California. Map c of Figure 3.18 shows an ozone enhancement from the surface to 300 mb at latitudes lower than ~35^{o}N during period 1. A small 'cell' of ozone-rich air were trapped on the surface over the West Coast of California in both periods 1 (> 60 ppb) and 2 (> 50ppb). This cell of high ozone locates not far away from LA (about 120 km) and is most likely associated with the air pollution from the surface.

Meteorological conditions were analyzed to investigate the possible association of wave breaking with stratospheric intrusions over the enhancement regions. The TCO enhancement over the Baja peninsula in period 1 is associated with pronounced lowering of tropopause heights (Figure 3.20). In period 1, the 500 mb geopotential heights (upper panel of Figure 3.21) indicate an upper level short wave (also shown on daily maps) over the Northern Mexico with a trough located in an area from the western Texas to the southeast side of the Baja peninsula, and this short wave disappeared in the second period (bottom panel of Figure 3.21). Associated with the short wave, the PV contours on the 330 and 360 K (Figure 3.22) show an area of high PV air extending from Texas to the Baja peninsula, and on the 330 K surface, a small high PV cutoff appearing over the West Coast of California.

Following Postel and Hitchman [1999] and Scott and Cammas [2002], PV on 350 K isentropic surface was used to diagnose wave breaking events. The time evolution

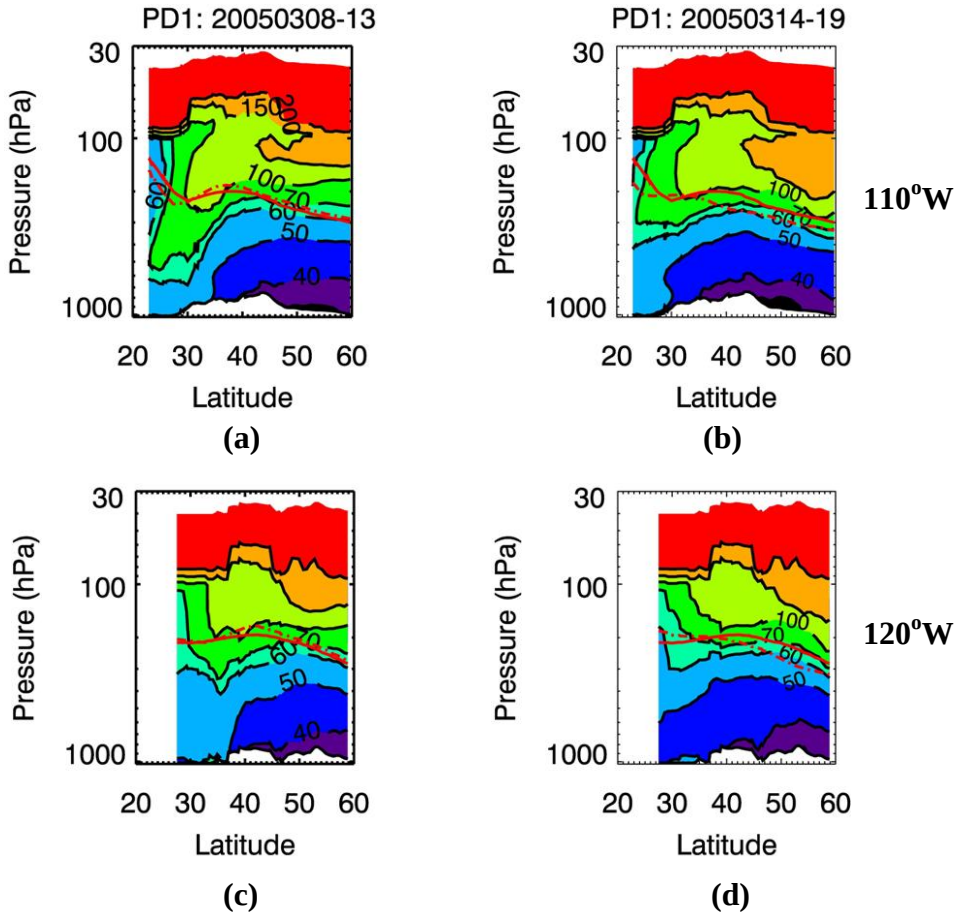

Figure 3.18: Meridional pressure by latitude cross-sections of ozone (in ppb) at 110W (a and b) and 120W (c and d) based on REAM during period 1 (March 8-13, 2005; a and c) and period 2 (March 14-19; b and d). The dash dotted lines and solid lines indicate the locations of the thermal and dynamic tropopause, respectively. The thermal tropopause data are directly obtained from NCEP data and the dynamic tropopause was calculated based on a PV threshold value of 3.5 PVU (1 PVU = 10^{-6} m^2 $Ks^{-1}kg^{-1}$).

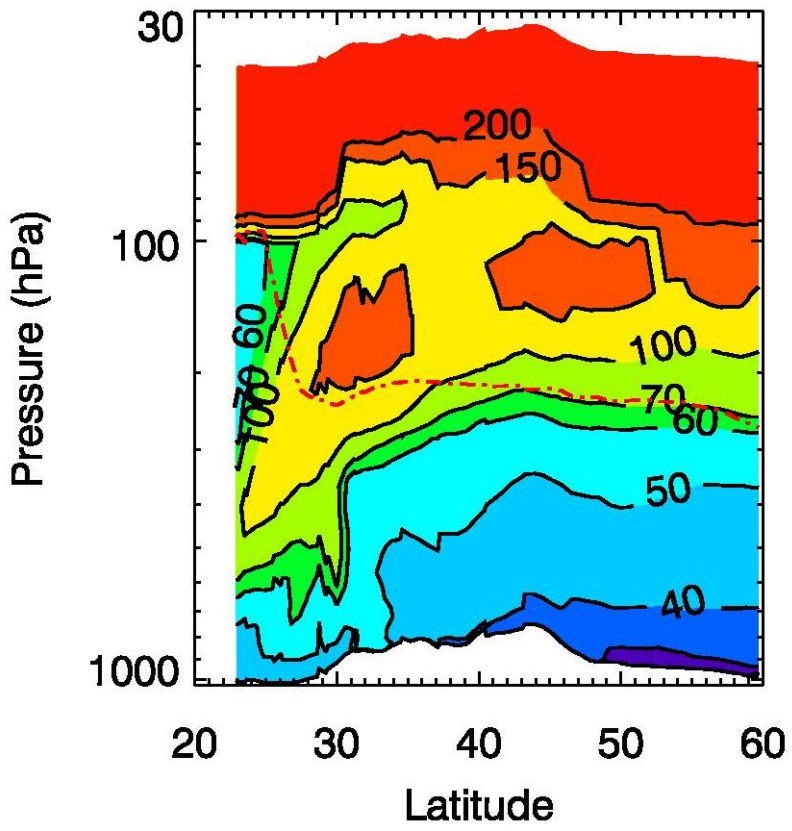

Figure 3.19: Meridional pressure by latitude cross-section of ozone (in ppb) at 110°W based on REAM data for March 08, 2005. The dash dotted line indicates the location of the thermal tropopause.

maps (Figure 3.23) indicate the steepening of the wave crest a couple of days before period 1. On May 08 at 00hr, a tongue of high PV stretches southeast ward, and at 12 hr a high PV cutoff with PV values as high as 6 PV units forms beside the wave crest. Six hours later, a relatively weak cutoff high shows up over the West Coast of the California with center of the PV being 1 PV unit higher than the surroundings. The wave breaking events correspond to the times and locations of the TCO maxima in REAM simulations; therefore, wave breaking is concluded to be associated with the stratospheric intrusions causing the TCO maxima over the Baja peninsula and the West Coast. The day of the wave breaking also corresponds to the unusual upper level deep sinking motion (Figures of Omega in Pa/s not shown) in the region around the Baja peninsula. The relatively deep vertical structure associated with the almost vertically oriented tropopause in the jet region (Figure 3.18) and the location of the event separate this subtropical Rossby wave breaking from the mid-latitude tropopause folding which is associated with the deformation of a relatively horizontally oriented tropopause. Rossby wave breakings in the subtropics are accompanied by quasi-horizontal processes [Scott and Cammas, 2002]. The estimated monthly isentropic stratosphere to troposphere ozone flux for February presented in Ping et al. [2004] indicates an stratospheric flux maximum around the Baja peninsula on 345 K and 355 K.

Clearly, associated with the Rossby wave breaking, the stratospheric ozone-rich air has been transported into troposphere causing the TCO enhancement over the Baja peninsula; the wave breaking is also associated with the upper tropospheric ozone enhancement over the West Coast of the California.

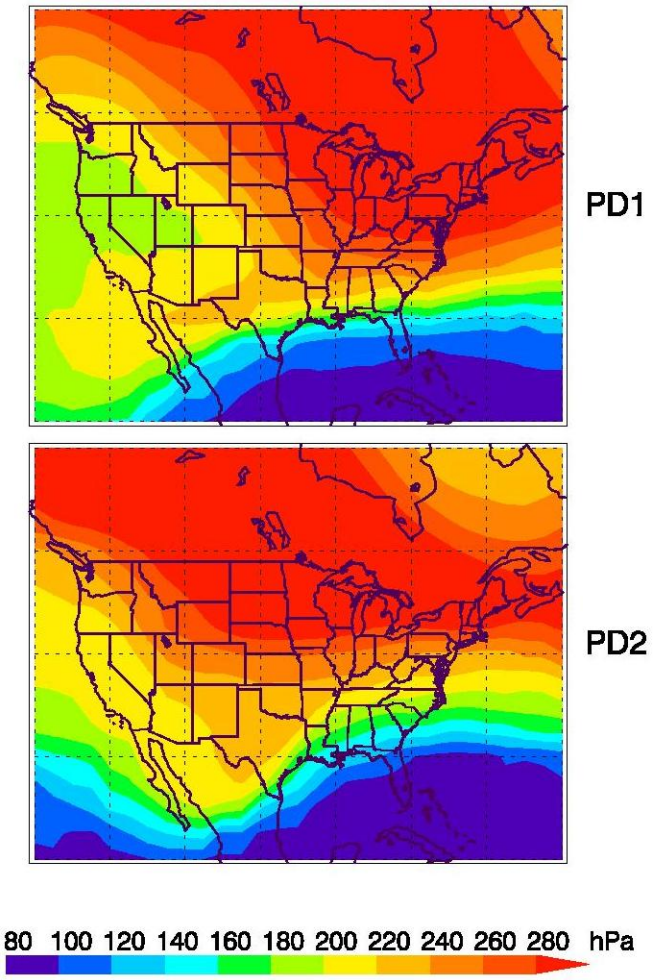

Figure 3.20: The average tropopause pressure during period 1 (PD1: March 8-13, 2005; top) and period 2 (PD2: March 14-19, 2005; bottom). The tropopause pressure was based on six-hourly NCEP reanalysis data.

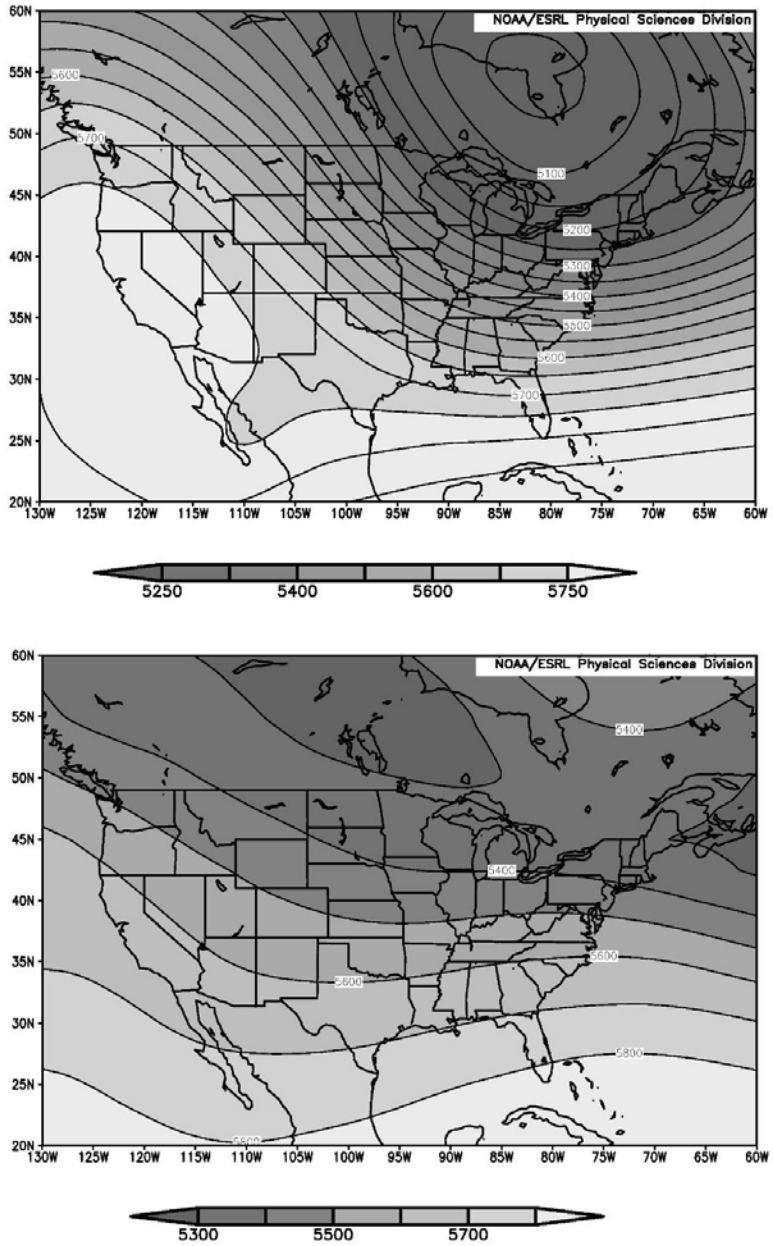

Figure 3.21: Geopotential height (m) on 500 mb for March 8-13 (top) and March 14-19 (bottom), 2005. The contour maps were generated by National Oceanic and Atmospheric Administration/Earth System Research Laboratory (NOAA/ESRL) physical science division using NCEP reanalysis data.

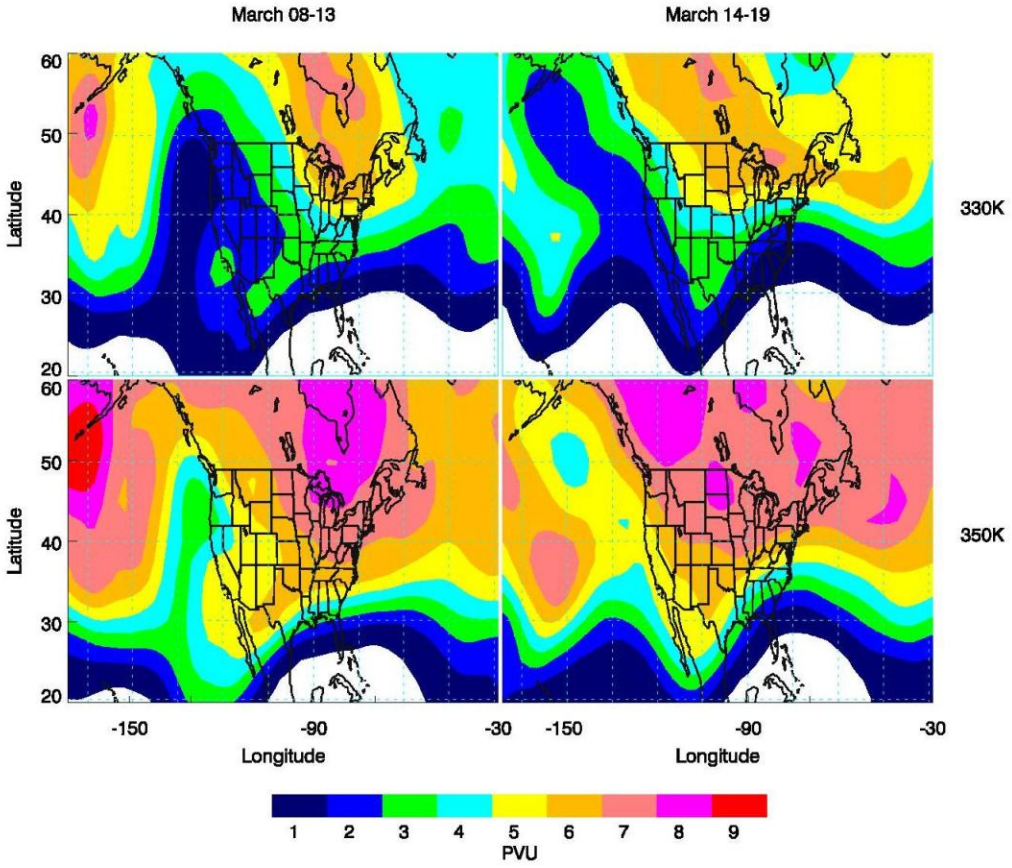

Figure 3.22: Six-day average PV on the 330 K (upper panels) and 350 K (lower panels) isentropic surfaces for March 8-13, 2005 (left panels) and March 14-19, 2005 (right panels). PV values were calculated using six-hourly NCEP reanalysis data.

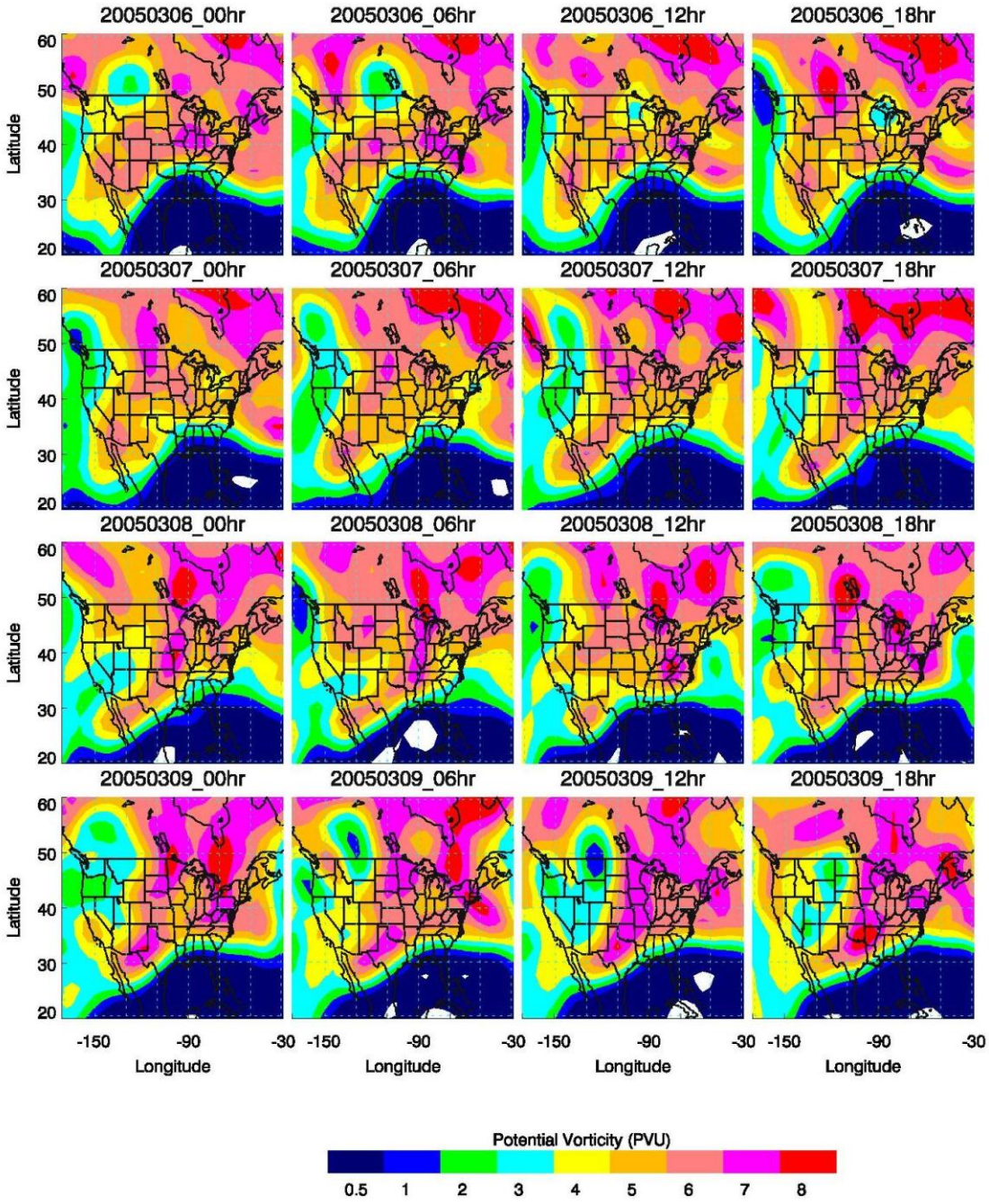

Figure 3.23: Six-hourly PV evolution maps on the 350 K isentropic surface for March 6-11, 2005. PV values were calculated using six-hourly NCEP reanalysis data.

3.4.3 Trans-Pacific Influence

3.4.3.1 Back Trajectories

Relatively high ozone from the surface to ~ 300mb are shown in the previous cross-section maps over the West Coast of the California in period 1; however, cross-section maps do not support the stratospheric influences to the high ozone in the lower and mid troposphere. To investigate the possible influence of cross-Pacific transports on the TCO enhancement over the West Coast of the North America, 315-hours back trajectories were implemented using the Hybrid Single-Particle Lagrangian Integrated Trajectory (HY-SPLIT) model [Draxler and Hess, 1998]. The meteorological data used for HY-SPLIT were from the NCEP-reanalysis data set. A back trajectory time of 315 hours is considered sufficiently long for the purpose of identifying the general features of air mass origins (Wang 2003 and references therein).

A $5^{o}\times5^{o}$ longitude by latitude area (123-118 ^{o}W and 32-37 ^{o}N) was chosen to study the influence of cross-Pacific transport over the West Coast of California. Back trajectories were initialized at the center of the 15 out of 20 $1^{o}\times1.25^{o}$ latitude by longitude grids. Five grids relatively far from the coastline were not included. For each grid, back trajectories were initialized every six hours at heights of 2, 4, and 6 km during periods 1 and 2, respectively. The average time for trajectories initialized at 2, 4, and 6 km to cross the Pacific is 8, 6, and 6 days, respectively, during period 1; and 8, 7, and 7 days, respectively, during period 2. The back trajectories initialized at 4 km were most likely associated with westerlies in spring, and trajectories with an initial height of 2 km mostly originated from higher latitudes (40-60^{o}N).

Table 3.3: The statistics of the trajectories initialized at heights of 2, 4, and 6 km over West Coast of California during period 1 (March 8-13, 2005) and period 2 (March 14-19, 2005). The table is based on a total of 1080 trajectories with 180 trajectories at each initial height in each period.

Periods		Period 1 (Mar. 8-13, 2005)			Period 2 (Mar. 14-19, 2005)		
initial heights		2 km	4 km	6 km	2km	4km	6km
ending heights* (m)	N. Asia***	3.0	0.9	3.4	4.0	5.1	5.9
	S. Asia****	3.4	2.4	2.0	4.8	3.6	6.0
# (%) origin from	N. Asia	51 (28%)	6 (3%)	31 (17%)	34 (19%)	15 (8%)	24 (13%)
	S. Asia	19 (11%)	31 (17%)	42 (23)	1 (1%)	6 (3%)	13 (7%)
# in mixed layer**	N. Asia	32 (18%)	8 (4%)	19 (11%)	8 (4%)	2 (1%)	5 (3%)
	S. Asia	2 (1%)	8 (4%)	23 (13%)	0 (0%)	2 (1%)	0 (0%)

** 'ending heights' refers to the heights of the trajectories at the end of the back trajectory period.*
*** '# in mixed layer' refers to the number of trajectories which crossed the mixed layer over East Asia.*
**** 'N. Asia' refers to Northern East Asia which is defined as 30-50 ^{o}N and 100-145^{o}E.*
***** 'S. Asia' refers to Southern East Asia which is defined as 10-30N and 110-125E.*

Table 3.3 shows the comparison between periods 1 and 2 based on the 540 back trajectories for each period. Among all trajectories, 30% of them were found to originate over East Asia (northern East Asia is defined as 30-50 ^{o}N and 100-145^{o}E; and southern East Asia is defined as 10-30N and 110-125E) in period 1, compared to only 15% in period 2. For the trajectories originating from East Asia, in period 1 the average height at the end of the trajectory period is ~2.5 km, which is significantly lower than the average of ~ 5 km in period 2. In period 1, approximately 50% (92 out of 180) of the trajectories originating from East Asia were within the mixed layer when the trajectories were crossing East Asia, while only 18% (17 out of 93) were found in period 2. The large number of trajectories in period 1 (17%) originating from near surface layer over East Asia compared with period 2 (3%) suggest that the TCO enhancement over the West Coast of California in period 1 may have been influenced by pollutants from East Asia lifted from the boundary layer and transported across the Pacific.

The cross-Pacific influence was further investigated by comparing high REAM TCO (≥45 DU) back trajectories with the periodically initialized back trajectories previously discussed. High TCO values were found only in period 1 over the West Coast of the California.

The back trajectories associated with high TCOs over the West Coast in period 1 are shown in Figure 3.23. Associated with the high pressure system around Washington State, the trajectories had a circular shape crossing higher latitudes (up to ~58^{o}N) before they arrived over the West Coast of California. The GEOS-CHEM model also indicates elevation of CO columns along the trajectory tracks over the North America continent (see Figure 3.27 at the end of this section). Compared with all the trajectories in period 1,

the high TCO trajectories initialized at a height of 6 km have an average passing height about ~1 km lower than all the trajectories in period 1 over East Asia. There was an approximately 20% increase in the number of trajectories within the mixed layer while they passed East Asia. As indicated by the green trajectories in the time-height cross-section map in Figure 3.23, most of the trajectories initialized at 2 km experienced dramatic lifting (probably associated with a front) near the East Coast of Asia. Before being lifted, these trajectories resided at a height of less than 2 km. In addition, Figure 3.24 further indicates that no obvious sinking motions were detected before their arrival over the West Coast of California (Figure 3.24).

Comparisons of trajectories in periods 1 and 2 indicate that the cross-Pacific transport was more likely to occur in periods 1 than 2. Comparisons of high TCO trajectories with all trajectories in period 1 indicate that trans-Pacific influences were likely to be more significant at altitudes of around 2 and 6 km over the West Coast of California.

Even though the stratospheric contribution is dominant over the Baja peninsula in period 1, the possible effect from cross-Pacific transport was investigated over this region using a similar approach. Figure 3.25 shows the distribution of the high TCO trajectories over the Baja peninsula, and Figure 3.26 shows the corresponding time-height cross-section. As indicated by Figure 3.26, most of the trajectories experienced sinking of up to ~3 km a few hours before they reached the Baja peninsula. While the trajectories initialized at 4 and 6 km over the Baja peninsula have high East Asia crossing heights (> 7 km on average), the trajectories initialized at 2 km indicate a possible trans-Pacific influence. For the trajectories initialized at 2 km, 25% of them ended in northern East

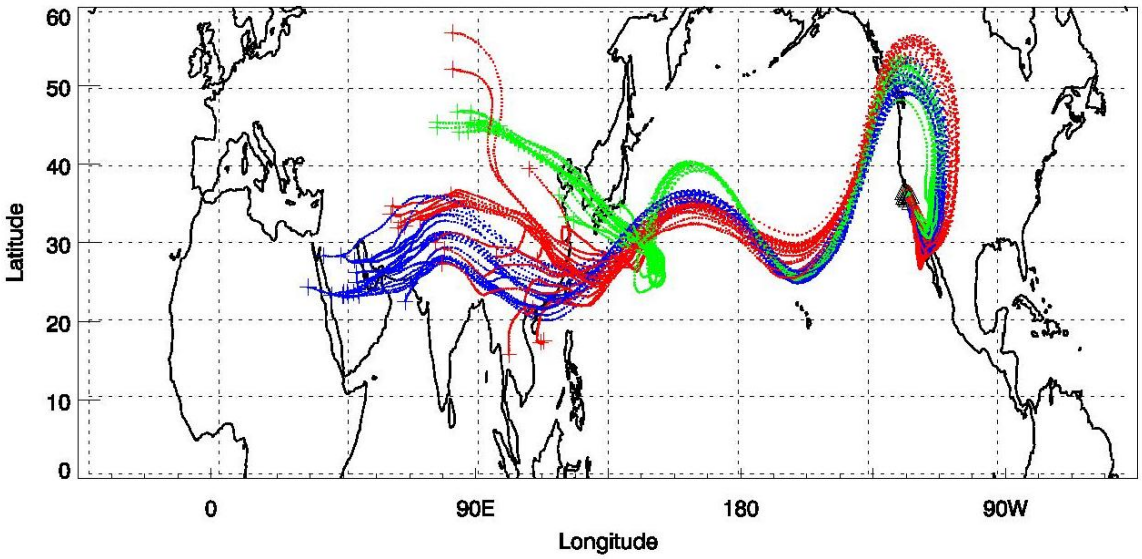

Figure 3.23: High REAM TCO (≥45 DU in six-hourly outputs) back trajectories initialized at 2 (green), 4 (blue), and 6 km (red), respectively, around the West Coast of United States (123-118 ^{o}W and 32-37 ^{o}N).

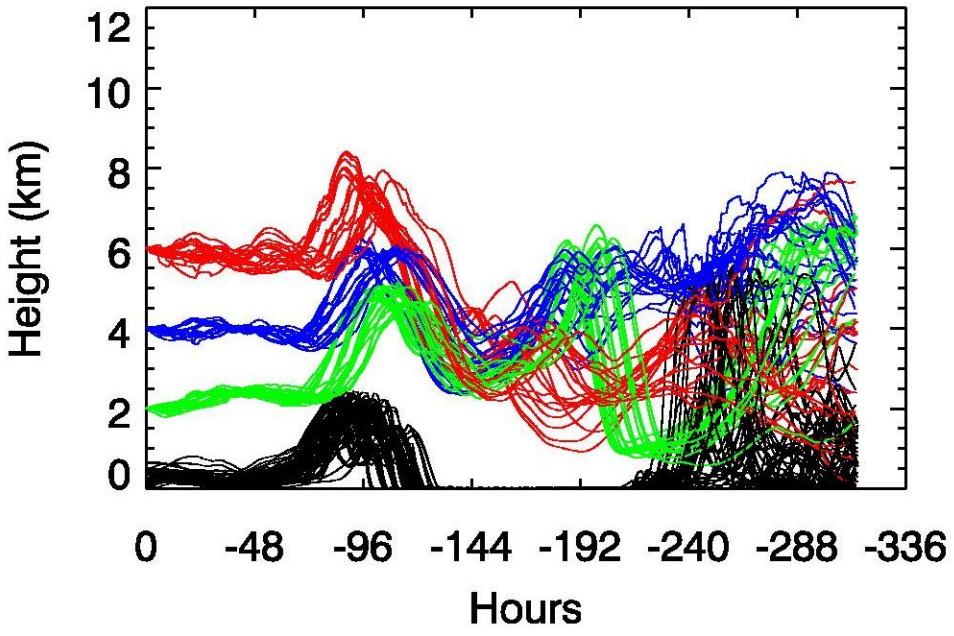

Figure 3.24: The time-height cross-section of the back trajectories as those in Figure 2.23. Green, blue, and red lines correspond to trajectories initialized at heights of 2, 4, and 6 km, respectively. The black lines are topography heights corresponding to the trajectories.

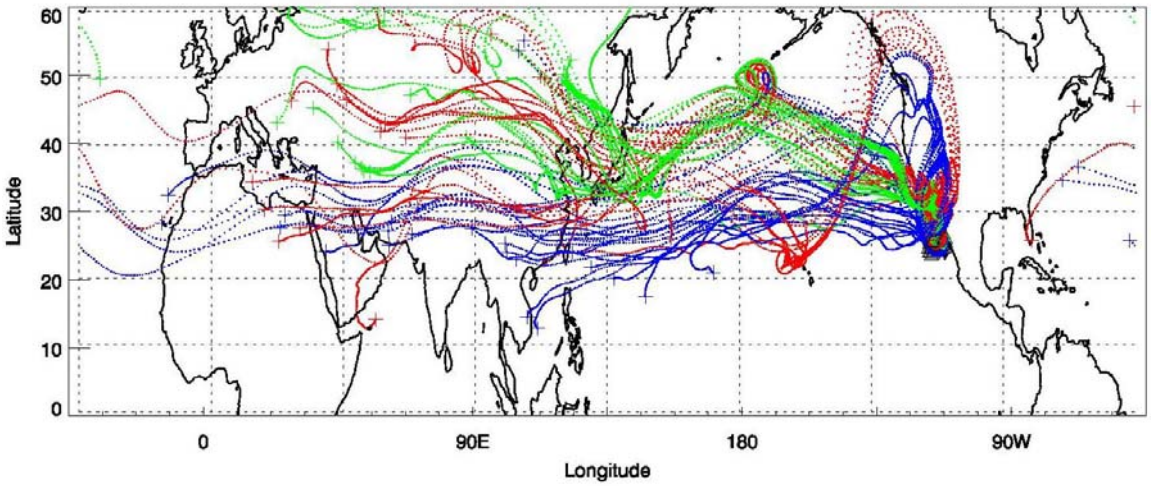

Figure 3.25: High REAM TCO (≥50 DU in six-hourly outputs) back trajectories initialized at 2 (green), 4 (blue), and 6 km (red), respectively, around the BAJA peninsula (114-109 ^{o}W and 22-27^{o}N).

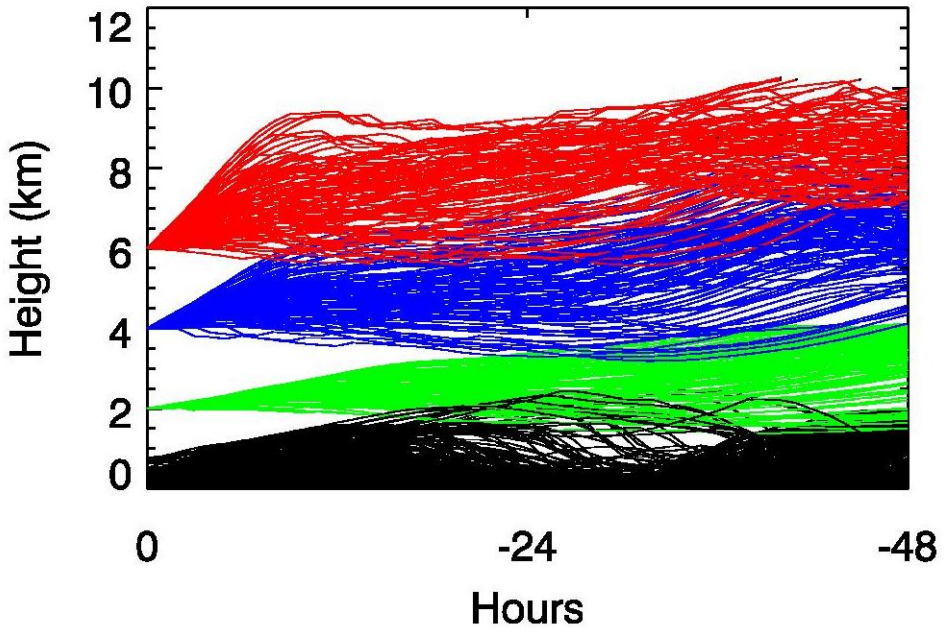

Figure 3.26: The time-height cross-section of the back trajectories as those in Figure 22. Green, blue, and red lines correspond to trajectories initialized at heights of 2, 4, and 6 km, respectively. The black lines are topography heights corresponding to the trajectories.

Asia with an average ending height of ~ 2 km, and 31% of them were in the mixed layer when the trajectories were crossing Northern East Asia.

3.4.3.2 GEOS-CHEM Tropospheric Ozone and CO Columns

To provide some additional evidence for an influence from Asia, Figure 3.27 shows the daily mean ozone and CO tropospheric columns from GEOS_CHEM. TCO daily maps indicate a TCO maximum propagated across the Pacific Ocean a few days before period 1. The corresponding CO maps indicate similar transport activities; however, the CO high dissipated before it reached the North America, though there was a slight elevation of CO at the end of the 7 day period over the West Coast.

OMI/MLS mapped TCOs were binned into $2.5^{o}\times2.5^{o}$ (longitude by latitude) grids with the use of a Barnes smoothing scheme and a 500 km influencing distance. The Barnes smoothing scheme weighted the data points within the influencing distance using the exponential of the normalized distance. The daily maps of OMI/MLS mapped TCOs in Figure 3.28 have better agreement with GEOS_CHEM daily maps in the last three days. During these days OMI/MLS also indicated a TCO high in the middle of the North Pacific propagated to the West Coast of the North America a few days before period 1.

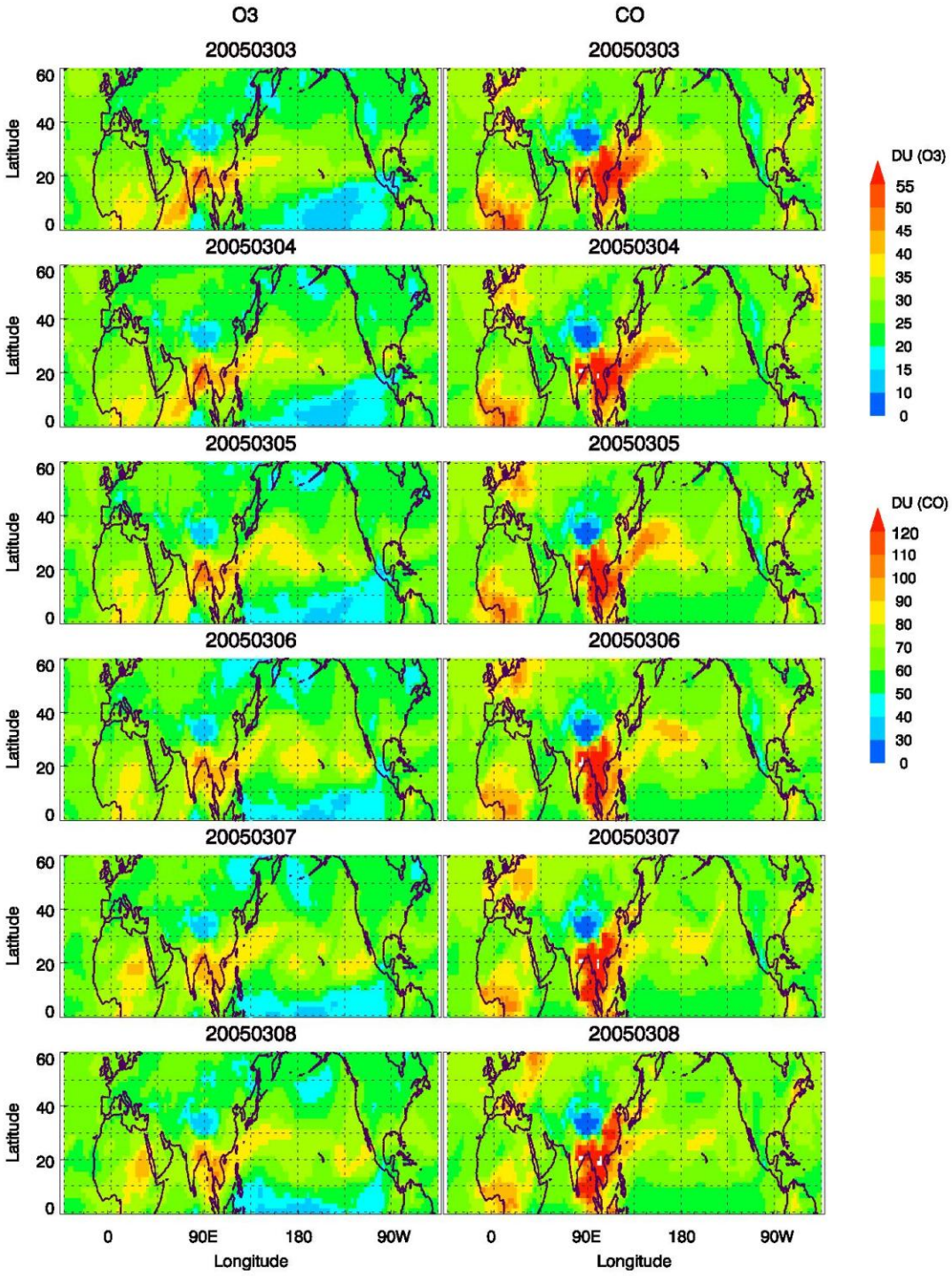

Figure 3.27: GOES-CHEM daily mean tropospheric ozone and carbon oxide (CO) columns for March 3 - 08, 2005. The CO columns can be converted from Dobson units to modelcules/cm^2 by multiplying a constant (2.687E16).

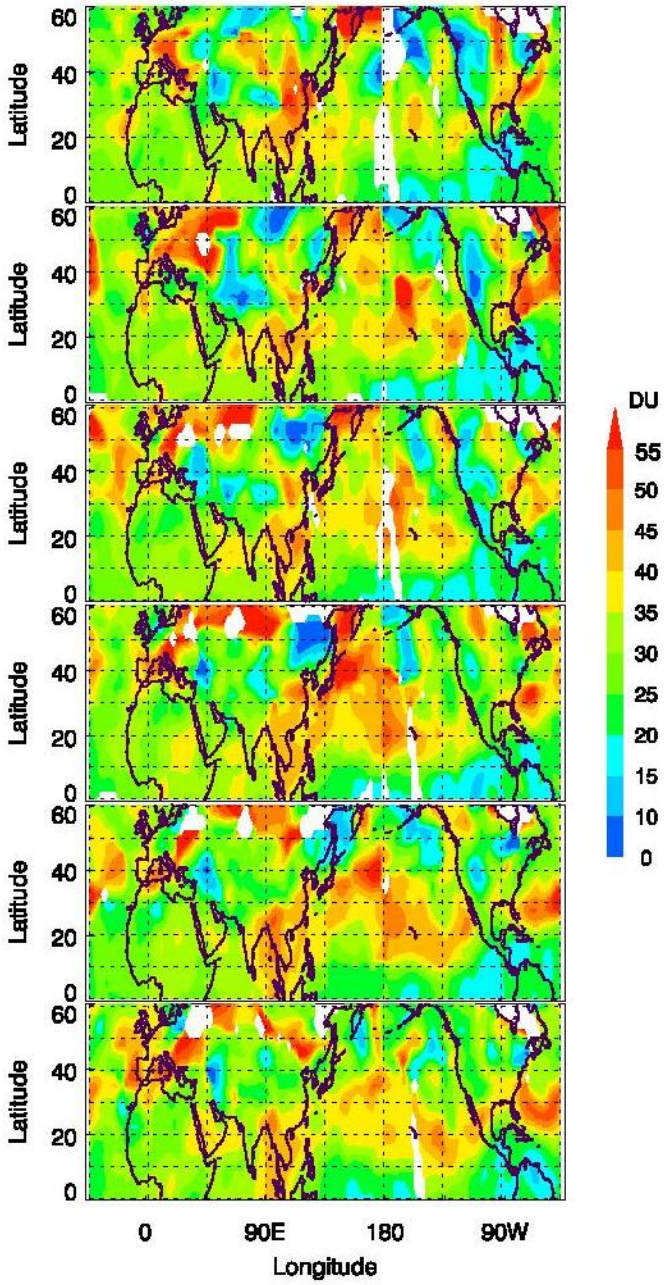

Figure 3.28: The daily mean OMI/MLS mapped tropospheric ozone columns from March 3 – 08, 2005 (from top down). The OMI/MLS mapped TCOs were gridded into $2.5^{o}\times2.5^{o}$ longitude by latitude grids by implementing a Barnes smoothing scheme with a 500 km influencing distance.

3.4.3.3 Meteorological Conditions

The TCO enhancement over the West Coast of California has the pronounced influence from the near surface layer. The 850 mb air temperature map (Figure 3.29) for period 1 shows a tongue of warm air extending from Gulf of California to the West Coast of California indicating the presence of unstable air above 850 mb in this region. Consequently, convective mixing could bring ozone precursors from the mid and lower troposphere down to the lower troposphere and surface. Furthermore, the high temperature in the lower troposphere is in favor of ozone production which could contribute to the ozone enhancements in the mid and lower troposphere. Low humidity is speculated since the air came from inland regions with higher latitudes.

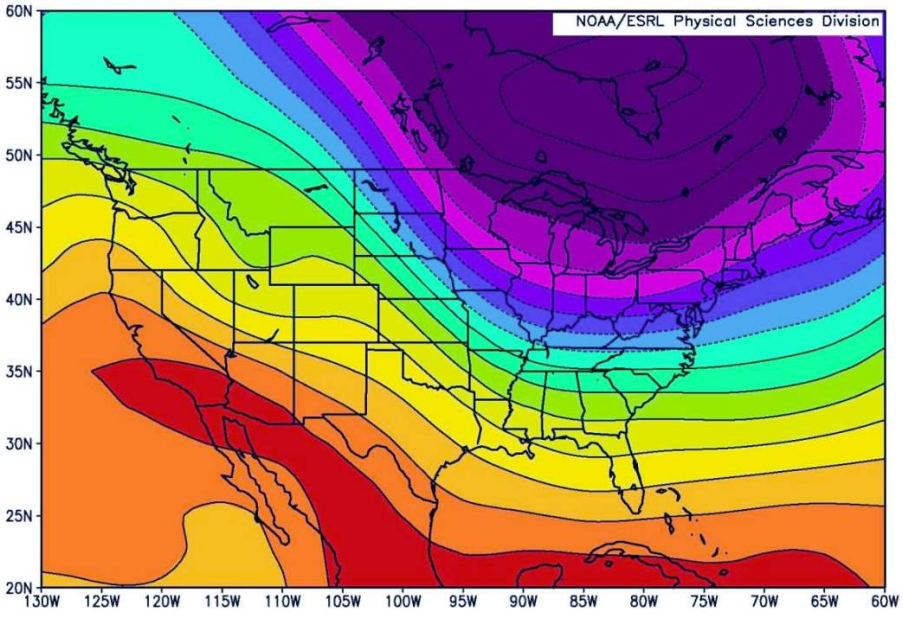

Figure 3.29: Mean temperature on 850 mb during March 8-13, 2005. This plot was generated by NOAA/ESRL physical science division using NCEP reanalysis data.

3.5 Correlation with Meteorological Parameters

REAM TCOs have been correlated with geopotential height, horizontal wind speed, and tropopause pressure using six-hourly NCEP reanalysis meteorological data. The correlations between the meteorological parameters and tropospheric ozone resemble similar features using either TCOs in column amounts (Figure 3.30) or in volume mixing ratios (not shown).

The 500mb geopotential heights are anti-correlated with REAM TCOs over the Baja peninsula and over the West Coast of California. The compression associated with the downward stratospheric flux will cause geopotential height to decrease leading to the anti-correlation between TCOs and geopotential height.

As shown in the middle panels of Figures 3.30, wind speed on 500 mb could be positively or negatively correlated with TCOs. The strong correlations around the Baja peninsula in period 1 suggest that the local dilution by wind is not a dominant process in this region; in contrast, stronger winds at 500 mb are associated with stronger upper level convergence, thus higher TCO values.

During period 1 (the bottom left panel of Figure 3.30), tropopause pressure is highly anti-correlated ($R<-0.6$) with the TCO values over the Baja peninsula. This correlation is not unexpected, since low tropopause pressure means more air in the troposphere, thus more ozone in the troposphere. In contrast, the strong positive correlation ($R>0.6$) between tropopause pressure and TCO were found over the West Coast of the California; this correlation may be caused by the increased photochemical activities since a higher tropopause is associated with warmer air and stronger solar radiation in the upper troposphere.

In a sum, geopotential height on 500 mb is the best parameter, compared with tropopause and wind speed, to identify areas of TCO enhancements over the subtropical and mid-latitude regions. One possible explanation is that variations of geopotential height follow closely with the stratosphere intrusions in the subtropical regions.

3.6 Surface Ozone

Surface ozone measurements from EPA ground network were used to investigate the possible association of TCO enhancements with the increase of surface ozone. As shown in Figure 3.31, surface ozone along the West Coast of California during period 1 is strongly correlated with the hourly TCOs and near surface layer ozone columns, which suggests that the TCO enhancement in this area is associated with an increase of surface ozone. No strong correlations between column ozone and surface ozone were found over the West Coast during the second period.

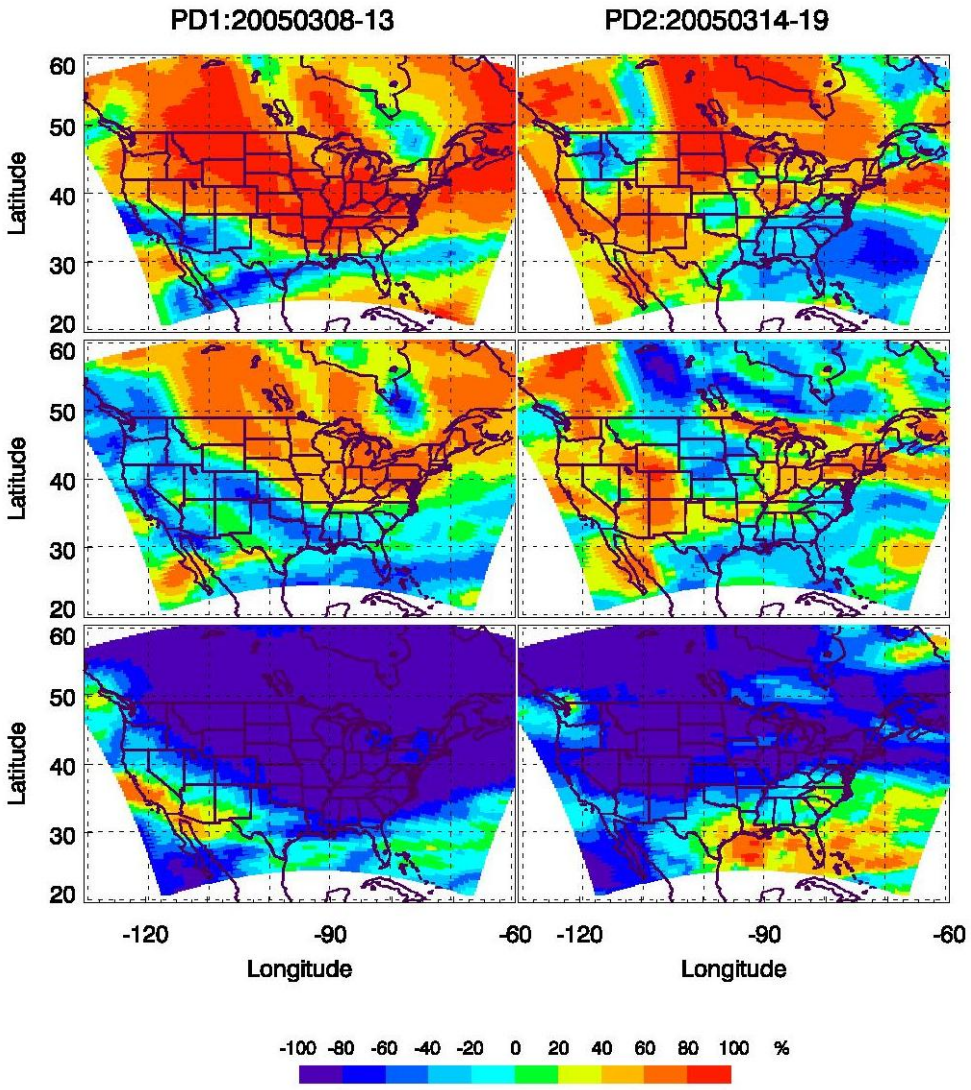

Figure 3:30: Correlation coefficients of TCOs (in DU) with 500 mb geopotential height (top), 500 mb wind speed (middle), and tropopause pressure (bottom), respectively, based on six-hourly REAM and NCEP data for period 1 (March 8-13, 2005) and period 2 (March 14-19, 2005).

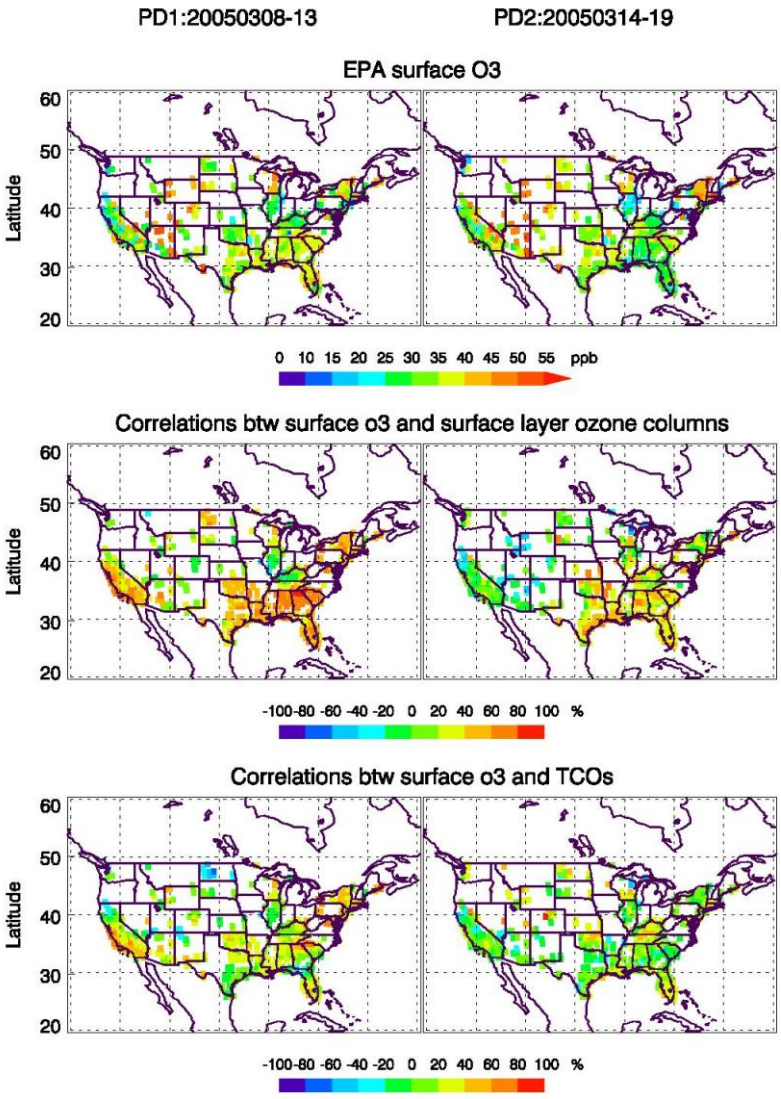

Figure 3.31: Surface ozone from EPA network (top) and their correlations with REAM column amounts in the surface layer (middle) and in the troposphere (bottom), respectively, for period 1 (March 8-13, left) and period 2 (March 14-19, right). Hourly data were used for the calculation of correlations.

3.7 Conclusions

The variability of tropospheric ozone columns have been examined using a regional 3-D chemical transport model, the Tropospheric Emission Spectrometer (TES) measurements and the Aura derived tropospheric ozone for spring and summer 2005. Good agreement has been found between model and satellite data during spring. Monthly mean TCOs from REAM, OMI/MLS, and TES showed two enhancement areas in spring: one around the Eastern Pacific near the Baja peninsula and the other around the Eastern States and the adjacent oceans. The TCO enhancements increased from March to May. The areas TCO enhancements in summer shifted northward compared to spring. Model and OMI/MLS Monthly mean TCOs agreed well in the locations of enhancements in summer, although they disagreed in the enhancement intensity in June. TES monthly mean data agreed well with OMI-MLS and REAM in the locations of enhancements and the monthly variations from July to August.

For the purpose of identifying the mechanisms associated with the TCO enhancements in spring, two six-day periods in March were selected to study the TCO enhancements in two regions, over the West Coast of California and around the Baja peninsula (Mexico).

Over the West Coast of California, both stratospheric intrusions and cross-Pacific transport were indicated to be responsible for the TCO enhancement over this region. As indicated from layer ozone columns and the pressure-latitude ozone cross-section maps from REAM, the high TCOs in period 1 over the West Coast were mainly contributed by the enhancements in the near surface layer as well as in the near tropopause layer. There were some indications of stratospheric influence in the upper troposphere, but there is no

indication that the stratospheric influence could lead to the high ozone in the mid and lower troposphere over this region. Cross-Pacific influences were investigated using back trajectories. Compared with period 2, the West Coast of California during period 1 is more likely under the influence of cross-pacific transports due to a larger number of trajectories passing through the near surface layer of East Asia. Meteorological conditions are in favor of ozone production in the lower troposphere over this region: high temperature and relatively static surface air; low humidity is speculated since the air came from inland regions with higher latitudes. In addition, convective mixing could bring the ozone precursors down to the lower troposphere. Daily maps of tropospheric carbon monoxide and ozone columns from GEOS-CHEM and OMI/MLS mapped TCOs indicate the propagation of high tropospheric CO and ozone columns across the Pacific a week before the time of the TCO enhancements over the West Coast of the North American. Correlations with the hourly surface ozone from the EPA ground ozone measurements indicate that the TCO enhancement in REAM over the West Coast of California is associated with a surface ozone enhancement.

A stratospheric air intrusion associated with Rossby wave breaking was found to mainly contribute to the TCO maximum over the Baja peninsula in period 1. Tropospheric layer ozone columns over the Baja peninsula indicate that the TCO maximum in period 1 is most pronounced in the near tropopause layer. Ozone cross-section maps showed high ozone concentrations typically found in the lower stratosphere present in the upper and middle troposphere indicating the effect of stratospheric intrusions. The PV evolutions on 350 K isentropic surface were used to diagnose wave breaking. The wave breaking is concurrent with the times and locations of the peak TCO

values in REAM. Therefore, it is concluded that deep wave breaking associated with sinking motion and tropopause deformation causing stratospheric air intrusions led to the TCO enhancement over the Baja peninsula.

CHAPTER 4

CONCLUSION

The first objective of this study was to estimate tropospheric ozone columns from Ozone Monitoring Instrument (OMI) and Microwave Limb Sounder (MLS) and to access the data quality of the derived Tropospheric Ozone Columns (TCOs). The second objective was to study the TCO distributions over North America, and to illustrate the mechanisms associated with TCO enhancements through the study of one spring enhancement event over North America.

Despite the improved global coverage of the Aura satellite, the direct implementation of TOR techniques on OMI and MLS produces TCOs (referred to in this paper as OMI/MLS coincident TCOs) with large data gaps due to a ~ 24^{o} longitude separation between orbits and a clear sky constraint on OMI measurements. PV mapping and 2-D interpolation techniques were applied to MLS profiles to improve the resolutions of the OMI/MLS TCOs. The mapping of the MLS stratospheric columns to the locations and times of the OMI measurements using relationships between ozone, potential vorticities (PV), and geopotential heights on isentropic surfaces over three day periods were emphasized. Using this procedure with the NCEP/NCAR reanalysis meteorological data set, we found that the resulting tropospheric ozone columns (referred to in this paper as OMI/MLS mapped TCOs) are 4 DU low on average from August 2004 to November 2005 relative to measurements from eight Northern Hemisphere mid-latitude ozonesonde sites. The same results were found in the OMI/MLS coincident and OMI/MLS 2-D interpolated TCOs. The 4 DU offset between OMI/MLS TCOs and ozonesonde is

consistent with the MLS (version 1.5) stratospheric columns above 215 mb being high relative to Stratospheric Aerosol and Gas Experiment (SAGE II) columns by approximately 3 DU. The low bias in the tropospheric ozone columns is related to the high bias in the MLS v1.5 stratospheric columns (biased high by about 11 ± 11 DU in lower stratosphere and possibly biased low by about 7 DU in the middle and upper stratosphere). The influence of OMI is negligible since OMI values are only slightly higher (0.4 ±0.5% [Yang et al., 2007]) as compared to the ground based total column Dobson measurements.

Mapped MLS ozone columns between approximately 18 and 215 mb (or the tropopause if it is above the 215 mb level) in the lower stratosphere have a standard deviation in the differences from the sonde measurements over the entire period of approximately 11 DU. Based on comparisons against other satellite measurements, as well as differences between mapped and individual coincident MLS profiles, uncertainties in the interpolated MLS measurements are most likely the principal contributors to these standard deviations. The standard deviations in the lower stratospheric column differences are mirrored in standard deviations in the differences between ozonesondes and OMI/MLS derived tropospheric columns of, for example, 12 DU in winter/spring and 6 DU in summer. The largest variations of the mean differences in tropospheric ozone columns with respect to ozonesondes occur in winter and spring.

A preliminary study using MLS version 2.2 provisional profiles indicates that the 4 DU offset of the OMI/MLS derived tropospheric columns relative to ozonesondes will essentially disappear when version 2.2 MLS retrievals become generally available. The vertical integration procedure supplied by the MLS team should be used for obtaining

stratospheric ozone columns from the MLS measurements. Other integration algorithms which are often used for the vertical integration result in column differences of approximately ±1% because of the MLS layer thickness of approximately 2.7 km.

PV mapping of MLS columns has been shown to be especially effective for spatially interpolating over 24^{o} of longitude, and it reduces the standard deviations of the lower stratospheric differences from ozonesonde measurements somewhat during winter compared to linear interpolation between MLS measurements or just using the nearest MLS measurement to the sonde location.

The uncertainties (one sigma) in the individual OMI/MLS derived tropospheric columns, based on the ozonesonde comparisons, are approximately 35% and 15% in winter and summer, respectively. Therefore, for many applications, it may be best to use spatially or temporally averaged columns [e.g., Jing et al., 2006]. A significant advantage of the mapping and 2-D interpolation procedures is that they produce an increased number of averagable observations. The mapping procedure has the special strength in being less affected by missing MLS data. It is shown that this PV mapping procedure produces somewhat better agreement in comparisons with ozonesonde measurements, particularly in winter, than does simple linear interpolation of the MLS stratospheric columns or the use of typical coincidence criteria.

In addition, increasing reflectivity threshold from 10% to 30% as the condition for clear sky OMI measurements produced approximately 40% more tropospheric ozone column measurements without any significant increase in their mean differences and their standard deviations relative to the sondes.

The Tropospheric Emission Spectrometer (TES) measurements and a 3-D Regional chEmical trAnsport Model (REAM) have been integrated with the OMI/MLS derived tropospheric ozone columns to examine the variability of tropospheric ozone columns for spring and summer 2005. Comparisons of monthly mean distributions show good agreements between OMI/MLS tropospheric ozone column, REAM column, and TES column. Monthly mean TCOs from REAM, OMI/MLS, and TES show two areas of high ozone columns in spring: one around the Eastern Pacific near the Baja peninsula and the other around the Eastern States and the adjacent oceans. The TCO enhancements increase from March to May. The areas of TCO enhancements in summer shift northward compared to the spring. Model and OMI/MLS monthly mean TCOs agree well in the locations of enhancements in summer although they disagree in the enhancement intensity in June. TES monthly mean data agree with OMI-MLS and REAM in the locations of enhancements and the monthly variations from July to August.

A six-day period in March has been chosen for the spring case study due to its association with the strongest TCO enhancement event in spring 2005 in REAM. The following six-day period has been chosen for comparison purposes. The case study focuses on the TCO enhancements in two regions, over the West Coast of California and around the Baja peninsula (Mexico).

Over the West Coast of California, stratospheric intrusions are responsible for the high ozone in the near tropopause layer. The high ozone concentrations in mid and lower troposphere may well have been under the influence by cross-Pacific transport over this region. As indicated from tropospheric layer ozone columns from REAM, the high TCOs in period 1 over the West Coast are due to the enhancement in the near surface layer as

well as in the near tropopause layer. The pressure-latitude ozone cross-section maps from REAM provide some indication of stratospheric influences on the upper tropospheric ozone, however there is no evidence that stratospheric influences could lead to the high ozone in the lower and mid troposphere over this region. Thirteen-day back trajectories and daily mean maps of carbon monoxide (CO) and ozone from GEOS-CHEM and OMI/MLS have been integrated to investigate the influence of cross-Pacific transport. Back trajectories suggest that compared with period 2, the West Coast of California during period 1 is more likely to have been under the influence of cross-pacific transports due to a larger number of trajectories (15% in period 1 vs. <1% in period 2) passing through the near surface layer over East Asia. Daily mean tropospheric carbon monoxide and ozone columns from GEOS-CHEM and OMI/MLS indicate high tropospheric CO and ozone columns propagate across the pacific a few days before the enhancement event. Meteorological conditions are in favor of ozone production in the lower troposphere over this region due to the presence of high temperature and low humidity. In addition, convective mixing could bring the ozone precursors down to the lower troposphere. The correlations between REAM TCOs and surface ozone from Environmental Protection Agency ground network measurements indicate that the TCO enhancement over the West Coast of California is associated with an increase of surface ozone in period 1.

A stratosphere air intrusion associated with Rossby wave breaking is found to mainly contribute to the TCO maximum over the Baja peninsula in period 1. Tropospheric layer ozone columns indicate that the TCO maximum over the Baja peninsula in period 1 is most pronounced in the near tropopause layer. Ozone cross-

section maps show high ozone mixing ratios typically found in the near tropopause levels present at the middle and lower troposphere. The PV evolutions on 350 K isentropic surface have been used to diagnose wave breaking. The diagnosed wave breaking is concurrent with the times and locations of peak TCO values in REAM. Therefore, it is concluded that deep wave breaking associated with sinking motion and tropopause deformation causing stratospheric air intrusions leading to the TCO enhancement over the Baja peninsula.

The correlations of TCOs with geopotential height, wind speed, and tropopause pressure suggest that TCO enhancements over extra-tropical region are best characterized in springtime by decreases of geopotential height on the 500 mb surface.

Future work includes the update and further validation of the OMI/MLS TCOs with the soon to be released new version MLS and OMI data, and the study of one summer TCO enhancement events on a several day span.

REFERENCES

Bhartia, P. K., and C. Wellemeyer (2004), TOMS version 8 algorithm theoretical basis document, http://toms.gsfc.nasa.gov.

Bhartia, P. K., "TOMS-like" total O_3 Algorithm (OMTO3) – a status report. An oral talk presented at the Aura science and validation team meeting, NCAR center green facility, Boulder, CO, September 11-15, 2006.

Chandra, S., J. R. Ziemke, P. K. Bhartia, and R. V. Martin (2002), Tropical tropospheric ozone: implications for dynamics and biomass burning, *J. Geophys. Res.*, *107*(D14), 4188, doi:10.1029/2001JD000447.

Chandra, S., J. R. Ziemke, and R. V. Martin (2003), Tropospheric ozone at tropical and middle latitudes derived from TOMS/MLS residual: Comparison with a global model, *J. Geophys. Res.*, *108*(D9), 4291, doi:10.1029/2002JD002912.

Choi, Y., Y. Wang, T. Zeng, D. Cunnold, E. Yang, R. V. Martin, K. Chance, and V. Thouret (2007), Modeling analysis of springtime transition of NO_2, CO, and O_3 over North America on the basis of in situ and satellite measurements, to be submitted to J. Geophys. Res..

Choi, Y., Y. Wang, T. Zeng, R. Martin, T. Kurosu, and K. Chance (2005), Evidence of lightning NO_x and convective transport of pollutants in satellite observations over North America, *Geophys. Res. Lett. 32*, L02805, doi: 10.1029/2004GL021436.

Draxler, R. R., and G. D. Hess (1998), An overview of the HY-SPLIT 4 Modeling System for trajectories, dispersion, and deposition, *Aust. Meterol. Mag., 47*, 295-308.

Edouard, S., R. Vautard, and G. Brunet (1997), On the maintenance of potential vorticity in isentropic coordinates, *Q. J. R. Meteorol. Soc.*, *123*, 2069-2094.

Fishman, J., and J. C. Larsen (1987), Distribution of total ozone and stratospheric ozone in the tropics: implications for the distribution of tropospheric ozone, *J. Geophys. Res.*, *92*, 6627-6634.

Fishman, J., C. E. Watson, J. C. Larsen, and J. A. Logan (1990), Distribution of tropospheric ozone determined from satellite data, *J. Geophys. Res.*, *95*, 3599-3617.

Fishman, J., V. G. Brackett, E. V. Browell, and W. B. Grant (1996), Tropospheric ozone derived from TOMS/SBUV measurements during TRACE A, J. *Geophys. Res.*, *101*, 24,069-24,082.

Fishman, J., and V. G. Brackett (1997), The climatological distribution of tropospheric ozone derived from satellite measurements using version 7 Total Ozone Mapping Spectrometer and Stratospheric Aerosol and Gas Experiment data sets, *J. Geophys. Res.*, *102*, 19,275-19,278.

Froidevaux, L., et al. (2006), Early validation analyses of atmospheric profiles from EOS MLS on the Aura satellite, *IEEE Trans. Geosci. Remote Sens.*, *44,* 1106-1121.

Froidevaux, L., et al. (2007), Validation of Aura Microwave Limb Sounder stratospheric ozone measurements, submitted to *J. Geophy. Res*..

Heald, C. L., D. J. Jacob, A. M. Fiore, L. K. Emmons, J. C. Gille, M. N. Deeter, J. Warner, D. P. Edwards, J. H. Crawford, A. J. Hamlin, G. W. Sachse, E. V. Browell, M. A. Avery, S. A. Vay, D. J. Westberg, D. R. Blake, H. B. Singh, S. T. Sandholm, R. W. Talbot, and H. E. Fuelberg (2003), Asian outflow and trans-Pacific transport of carbon monoxide and ozone pollution: A integrated satellite, aircraft, and model perspective, *J. Geophys. Res., 108*, D24, 4804, doi: 10.1029/2003JD003507.

Heald, C. L., D. Jacob, R. J. Park, B. Alexander, T. D. Farelie, R. M. Yantosca, and D. A. Chu (2006), *J. Geophys. Res., 111*, D14310, doi: 10.1029/2005JD006847.

Holton, J. R., P. H. Hayns, M. E. McIntyre, A. R. Douglass, R. B. Rood, and L. Pfister (1995). Stratosphere-troposphere exchange. *Rev. of Geophys*., *33*, 403-439.

Hudman, R. C., D. J. Jacob, O. R. Cooper, M. J. Evans, C. L. Heald, R. J. Park, F. Fehsenfeld, F. Flocke, J. Holloway, G. Hubler, K. Kita, M. Koike, Y. Kondo, A. Newman, J. Nowak, S. Oltmans, D. Parrish, J. M. Roberts, and T. Ryerson (2004), Ozone production in trans-Pacific Asian pollution plumes and implications for ozone air quality in California, *J. Geophys. Res., 109*, D23S10, doi: 10.1029/2004JD004974.

Hudson, R. D., J. Kim, and A. M. Thompson (1995), On the derivation of tropospheric column ozone from radiances measured by the total ozone mapping spectrometer, *J. Geophys. Res.*, *100*, 11,137-11,145.

Hudson, R. D., and A. M. Thompson (1998), Tropical tropospheric ozone from total ozone mapping spectrometer by a modified residual method, *J. Geophys. Res.*, *103*, 22,129-22,145.

Hudson, R. D., A. D. Frolov, M. F. Andrade, and M. B. Follette (2003), The total ozone field separated into meteorological regimes. Part I: defining the regimes, *J. Atmos. Sci.*, *60*, 1669-1677.

Jing, P., D. M. Cunnold, H.-J. Wang, and E.-S. Yang (2004), Isentropic cross-tropopause ozone transport in the northern hemisphere, *J. Atmos. Sci.*, *61*, 1068-1078.

Jing, P., D. M. Cunnold, Y. Choi, and Y. Wang (2006), Summertime tropospheric ozone columns from Aura OMI/MLS measurements versus regional model results over the United States, *Geophys. Res. Lett.*, *33*, L17817, doi:10.1029/2006GL026473.

Kim, J. H., R. D. Hudson, and A. M. Thompson (1996), A new method of deriving time-averaged tropospheric column ozone over the tropics using total ozone mapping spectrometer (TOMS) radiances: Intercomparison and analysis using TRACE A data, *J. Geophys. Res.*, *101*, 24,317-24,330.

Kley, D. (1997), Tropospheric chemistry and transport, *Science, 276*, 1043-1045.

Levelt, P. F., E. Hilsenrath, G. W. Leppelmeier, G. H. J. van den Oord, P. K. Bhartia, J. Taminnen, J. F. de Haan, and J. P. Veefkind (2006a), Science objectives of the ozone monitoring instrument, *IEEE Trans. Geo. Rem. Sens., Special Issue on the EOS-Aura mission*, *44*, 1093-1101.

Levelt, P. F., G. H. J. van den Oord, M. R. Dobber, A. Malkki, H. Visser, J. de Vries, P. Stammes, J. Lundell, and H. Saari (2006b), The ozone monitoring instrument, *IEEE Trans. Geo. Rem. Sens., Special Issue on the EOS-Aura mission, 44*, 1199-1208.

Liang, Q., L. Jaegle, D. A. Jaffe, P. Weiss-Penzias, A. Heckman, and J. A. Snow (2004), Long-range transport of Asian pollutin to the northeast Pacific: Seasonal variations and transport pathways of carbon monoxide., *J. Geophys. Res., 109*, D23S07, doi:10.1029/2003JD004402.

Livesey, N. J., et al. (2005), Version 1.5 Level 2 data quality and description document, 91-94pp, Jet Propulsion Laboratory, California Institute of Technology, Pasadena, California.

Logan, J. A. (1999), An analysis of ozonesonde data for the troposphere: Recommendations for testing 3-D models and development of a gridded climatology for tropospheric ozone, *J. Geophys. Res.*, *104*, D13, 16,115-16,150.

Mahlman, J. D. (1997), Dynamics of Transport Processes in the upper troposphere, *Science*, *276*, Doi:10.1126/science.276.5315.1079.

Morgenstern, O., and A. Marenco (2000), Wintertime climatology of MOZAIC ozone based on the potential vorticity and ozone analogy. *J. Geophys. Res.*, *105*, 15,481-15,493.

Osterman (editor) (2007), Earth observing system (EOS) tropospheric emission spectrometer (TES) Level 2 (L2) data user's Guide), JPL, Pasadena, California.

Postel, G. A., and M. H. Hitchman, (1999), A climatology of Rossby waves breaking along the subtropical tropopause. J. Atmos. Sci., 56, 359-373.

Roelofs, G.-J., and J. Lelieveld (1997), Model study of the influence of cross tropopause O_3 transports on tropospheric O_3 levels, *Tellus, Ser. B, 49*, 38-55.

Schoeberl, M. R., et al. (2007), A trajectory based estimate of the tropospheric ozone column using the residual method, submitted to J. Geophy. Res..

Scott R. K., and J.-P. Cammas (2002), Wave breaking and mixing at the subtropical tropopause, *J. Atmos. Sci., 50*, 2347-2361.

Shalamyanskiy, A. M., and A. K. Romashkina (1980), Distribution and variation in the total ozone concentration in various air masses. *Izv. Atmos. Oceanic Phys.*, *16*, 931-937.

Tang, Y., et al. (2003), Influences of biomass burning during the Transport and Chemical Evolution Over the Pacific (TRACE-P) experiment identified by the regional chemical transport model, *J. Geophys. Res.*, *108* (D21), 8824, doi:10.1029/2002JD003110.

Thompson A.M., et al. (2003), Southern Hemisphere Additional Ozonesondes (SHADOZ) 1998-2000 tropical ozone climatology 1. Comparison with Total Ozone Mapping Spectrometer (TOMS) and ground based measurements, *J. Geophys. Res*., *108* (D2), 8238, doi: 10.1029/2002JD000967.

Veefkind, J. P., J. F. de Haan, E. J. Brinksma, M. Kroon, and P. F. Levelt (2006), Total ozone from the ozone monitoring instrument (OMI) using the DOAS technique, *IEEE Trans, Geo. Rem. Sens*., *Special issue on the EOS-Aura mission*, *44*, 1239-1244.

Visconti, G., P. D. Carlo, W. Brune, M. Schoeberl, and A. Wahner (editors) (2007), Observing systems for atmospheric composition: satellite, aircraft, sensor web, and ground-based observational methods and strategies, Page 61, Springer, New York, 244pp.

Vukovich, F. M., V. Brackett, J. Fishman, and J. E. Sickles II (1996), On the feasibility of using the tropospheric ozone residual for nonclimatological studies on a quasi-global scale, *J. Geophys. Res.*, *101*, 9093-9105.

Wang, H.-J., D. M. Cunnold, L. W. Thomason, J. M. Zawodny, and G. E. Bodeker (2002), Assessment of SAGE version 6.1 ozone data quality, *J. Geophys. Res.*, *107*(D23), 4691, doi:10.1029/2002JD002418.

Wang, H.-J., D. M. Cunnold, C. Trepte, L. W. Thomason, and J. M. Zawodny (2006), SAGE III solar ozone measurements: Initial results, *Geophys. Res. Lett*., *33*, L03805, doi:10.1029/2005GL025099.

Wang, Yuhang, Y. Choi, T. Zeng, B. Ridley, N. Blake, D. Blake, and F. Flocke (2006), Late-spring increase of trans-pacific pollution transport in the upper troposphere, *Geopys. Res. Lett., 33*, L01811, doi:10.1029/2005GL024975.

Waters, J. W., et al. (2006), The Earth Observing System Microwave Limb Sounder (EOS MLS) on the Aura satellite, *IEEE Trans. Geosci. Remote Sens.*, *44*, 1075-1092.

Worden, J., K. Bowman, R. Beer, A. Eldering, M. Gunson, and H. Worden (2007), Improved tropospheric ozone profile retrievals using OMI and TES radiances, *Geophys. Res. Lett, 34*, L01809, doi:10.1029/2006GL027806.

Yienger, J. J., M. Galanter, T. A. Holloway, M. J. Phadnis, S. K. Guttikunda, G. R. Carmichael, W. J. Moxim, and H. Levy II (2000), The episodic nature of air pollution transport from Asia to North America, *J. Geophys. Res., 105*, 26,931-26,945.

Zanis, P., E. Gerasopoulos, A. Priller, C. Schnabel, A. Stohl, C. Zerefos, H. W. Gaggeler, L. Tobler, P. W. Kubik, H. J. Kanter, H. E. Scheel, J. Luterbacher, and M. Berger (2003), An estimate of the impact of stratosphere-to-troposphere transport (SST) on the lower free tropospheric ozone over the Alps using ^{10}Be and ^{7}Be measurements, 108, *J. Geophys. Res., 108*, D12, 8520, doi:10.1029/2002JD002604.

Zeng, T., et al. (2006), Halogen-driven low altitude O3 and hydrocarbon losses in spring in northern high latitudes, *J. Geophys. Res, 111*, D17313, doi: 10.1029/2005JD006706.

Ziemke, J. R., and S. Chandra (1998), Comment on "Tropospheric ozone derived from TOMS/SBUV measurements during TRACE A" by J. Fishman et al., *J. Geophys. Res.*, *103*, 13,903-13,906.

Ziemke, J. R., S. Chandra, and P. K. Bhartia (1998), Two new methods for deriving tropospheric column ozone from TOMS measurements: assimilated UARS MLS/HALOE and convective-cloud differential techniques, *J. Geophys. Res.*, *103*, 22,115-22,127.

Ziemke, J. R., and S. Chandra (1999), Seasonal and interannual variabilities in tropical tropospheric ozone, *J. Geophys. Res.*, *104*, 21,425-21,442.

Ziemke, J. R., S. Chandra, and P. K. Bhartia (2005), A 25-year data record of atmospheric ozone in the Pacific from Total Ozone Mapping Spectrometer (TOMS) cloud slicing: implications for ozone trends in the stratosphere and troposphere, *J. Geophys. Res.*, *110*, D15105, doi:10.1029/2004JD005687.

Ziemke, J. R., S. Chandra, B. N. Duncan, L. Froidevaux, P. K., Bhartia, P. F. Levelt, and J. W. Waters (2006), Tropospheric ozone determined from Aura OMI and MLS: Evaluation of measurements and comparison with the Global Modeling Initiative's Chemical Transport Model, *J. Geophys. Res.*, *111*, D19303, doi:10.1029/2006JD007089

VITA

Qing Yang

Qing Yang was born in Xiamen, China. She attended the Lanzhou University in 1993 where she received a Bachelors degree in atmospheric physics and atmospheric environment in 1997. After working in Environmental Protection Agency in Xiamen, China, for three years, she entered a master program in atmospheric science at the University of Wyoming in August 2000. Upon graduation with her master degree, she came to Georgia Institute of Technology to pursue a doctorate degree in atmospheric science in August 2002.